# CHARACTERIZATION OF UNDER-HOOD AIRFLOW IN CONSTRUCTION EQUIPMENT USING EXPERIMENTAL TECHNIQUES

YUNUS ORHUN SUBAŞIOĞLU

JULY 2025

**ÇANKAYA UNIVERSITY**

**GRADUATE SCHOOL**

**MECHANICAL ENGINEERING DEPARTMENT**
**MECHANICAL ENGINEERING MASTER'S THESIS**

# CHARACTERIZATION OF UNDER-HOOD AIRFLOW IN CONSTRUCTION EQUIPMENT USING EXPERIMENTAL TECHNIQUES

**YUNUS ORHUN SUBAŞIOĞLU**

**JULY 2025**

## ABSTRACT

**CHARACTERIZATION OF UNDER-HOOD AIRFLOW IN CONSTRUCTION EQUIPMENT USING EXPERIMENTAL TECHNIQUES**

**SUBAŞIOĞLU, YUNUS ORHUN**
**MECHANICAL ENGINEERING MASTER'S THESIS**

Supervisor**:** Assoc. Prof. Dr. Ulku Ece AYLI
Co-Supervisor**:** Assist. Prof. Dr. Eyup KOCAK
July 2025, 125 pages

This thesis investigates the effects of hot air accumulation beneath the hood in excavator-type construction machinery during engine operation and proposes a practical design solution to improve airflow. Accumulated thermal energy under the hood negatively impacts the operational efficiency of the engine and surrounding components, potentially leading to reduced performance and shorter component lifespan over time. To address this issue, ventilation openings were strategically added to the hood structure, allowing heated air to be directed outward more effectively.The study not only evaluates the thermal improvement achieved through these modifications but also considers the impact on noise emission.Noise measurements were conducted according to relevant standards, and the results were analyzed to determine whether the values remained within legally acceptable thresholds.The findings demonstrate that the addition of ventilation vents effectively reduced the under-hood temperature, contributing to better thermal management. At the same time, the noise levels recorded after the modification were observed to remain within permissible limits. These results suggest that it is possible to enhance thermal flow characteristics without compromising compliance with environmental noise regulations.



**Keywords:** Under-Hood Flow, Thermal Management, Noise Measurement, Thermal Analysis, Construction Machinery,

# ÖZET

## CHARACTERIZATION OF UNDER-HOOD AIRFLOW IN CONSTRUCTION EQUIPMENT USING EXPERIMENTAL TECHNIQUES

**SUBAŞIOĞLU, YUNUS ORHUN**
**MAKİNE MÜHENDİSLİĞİ YÜKSEK LİSANS TEZİ**

Danışman: Assoc. Prof. Dr. Ulku Ece AYLI
Ortak Danışman: Assist. Prof. Dr. Eyup KOCAK
Temmuz 2025, 125 pages

Bu tez çalışmasında, ekskavatör tipi iş makinelerinde motor çalışması sırasında kaput altında oluşan sıcak havanın etkileri incelenmiş ve bu sıcak havanın tahliyesine yönelik iyileştirici bir çözüm önerilmiştir. Yoğun ısıl birikim, motor ve diğer önemli bileşenlerin çalışma verimliliğini düşürmekte, uzun vadede ise performans kayıplarına ve parça ömrünün kısalmasına neden olabilmektedir. Bu sorunu azaltmak amacıyla, kaput yüzeyine belirli bölgelere menfezler açılmış ve bu açıklıklar sayesinde sıcak havanın dış ortama aktarılması sağlanmıştır.Yapılan bu yapısal değişikliğin yalnızca ısıl performans üzerindeki etkileri değil, aynı zamanda gürültü yayılımı üzerindeki etkileri de değerlendirilmiştir.Bu kapsamda, belirlenen standartlara uygun olarak gürültü ölçümleri yapılmış, elde edilen değerlerin yönetmeliklerde belirtilen sınırlar içerisinde kalıp kalmadığı kontrol edilmiştir.Çalışma sonucunda, menfezlerin kaput altındaki sıcak hava akışını olumlu yönde etkilediği, motor bölmesinde sıcaklık değerlerinin düşürüldüğü ve buna rağmen gürültü seviyelerinin kabul edilebilir sınırlar içerisinde kaldığı gözlemlenmiştir. Böylece, hem ısıl yönetimin iyileştirilmesi hem de çevresel gürültü standartlarına uyumun aynı anda sağlanabileceği gösterilmiştir.

**Anahtar Kelimeler:** Kaput Altı Akışı, Sıcaklık Yönetimi, Gürültü Ölçümü, Termal Analiz, İş Makineleri

## ACKNOWLEDGEMENT

I would like to express my sincere gratitude to the esteemed jury members, Assist. Prof. Dr. Salih KARAASLAN, Assoc. Prof. Dr. Ekin Özgirgin YAPICI, and for their valuable contributions during the thesis defense process. Their insightful feedback and constructive criticisms have significantly enhanced the academic quality of this study. I am truly thankful for the time and attention they dedicated to my work.

I would like to express my deepest gratitude to my esteemed advisor, Assoc. Prof. Dr. Ulku Ece AYLI and Asist Prof.Dr. Eyup KOCAK whose genuine approach and guiding support played a major role in the completion of this thesis, and who generously shared her knowledge and experience with me throughout my graduate studies.

From the very first day I started at the Faculty of Engineering, it was my beloved father, Süleyman Subaşıoğlu—who, sadly, is no longer with us to read these words—who instilled in me the dream of becoming a "senior engineer" and constantly encouraged me to aim higher. I am deeply grateful to him for his unwavering material and emotional support, and I remember him with heartfelt gratitude and longing.

I also owe a special debt of thanks to my precious mother, Nermin Subaşıoğlu, who has always stood firmly behind me at every step of my life, silently but with great patience and sacrifice, and whose love has been a constant source of strength.

My sincere thanks go to my dear wife, Fatma Subaşıoğlu, who has been by my side through good times and bad, uplifted me when I was weary, shared in my joys first, believed in me throughout my academic journey, and supported me unconditionally.

Finally, I offer my heartfelt thanks to my beloved daughter, Nermin Ayçıl Subaşıoğlu, who joined our lives in 2024, bringing indescribable joy and meaning to our family, and who has become a daily source of hope and inspiration. I hope that when she holds this thesis in her hands one day, it will inspire her through the determination and love with which her father wrote it, and that it will encourage her to reach great success in her own journey.

## TABLE OF CONTENTS

## LIST OF TABLE

## LIST OF FIGURES

## LIST OF SYMBOLS AND ABBREVIATIONS

### SYMBOLS

| | |
|---|---|
| Ni-Cr | :Nickel-Chromium |
| Ni-Al | :Nickel-Aluminum |
| Fe-CuN | :Iron-Copper-Nickel |
| dB(A) | :Decibel |
| $L_WA$ | :The A-weighted sound power level |
| $L_pA,T$ | :The energy-average of the time-averaged |
| $K_1A$ | : The background noise correction factor |
| $K_2A$ | : The environmental correction factor |
| S | : The area of the hemispherical measurement surface |
| $L_pA,I$ | : Time-averaged A-weighted sound pressure level |
| NOx | : Nitrogen oxides |

### ABBREVIATIONS

| | |
|---|---|
| EGR | :Exhaust Gas Recirculation |
| SCR | :Selective Catalytic Reduction |
| LPG | :Liquid Pressured Gas |
| ECU | :Engine Control Unit |
| ECM | :Engine Control Module |
| DEF | :Diesel Exhaust Fluid |
| NRMM | :Non-road mobile machinery |
| PM | :Particulate Matter |
| HC | :Hydrocarbons |
| CO | :Carbon monoxide |
| kW | :kilowatt |
| PN | :Particulate Number |
| DPFs | :Diesel Particulate Filters |

| | |
|---|---|
| MCV | :Main Control Valve |
| CFD | :Computational Fluid Dynamics |
| RANS | : Reynolds-Averaged Navier–Stokes |
| FEA | : Finite Element Analysis |
| PG | : Propylene Glyco |
| EG | : Ethylene Glycol |
| K | : Thermal conductivity coefficient |
| PTO | : Power Take-Off |
| P-Q | :Pressure-Flow |
| RPM | :Engine Speed |
| HP Mod | :High Power |
| ATB | :Air to Boil |
| TBP | :Temperature of Boiling Point |
| TCI | :Coolant radiator inlet temperature |
| TAI | :Ambient Temperature |
| HVAC | :Heating, Ventilating and Air Conditioning |
| T | :Temperature |
| V | :Voltage |
| Emf | :Electromotive force |
| L | :Length |
| Etc | :Et cetera |
| Eg. | :Exempli gratia |
| Cm | :centimeter |
| M | :meter |
| Mm | :milimeter |
| Kpa | :kilopascal |

# CHAPTER I
# INTRODUCTION

## 1.1. OVERVIEW OF CONSTRUCTION MACHINERY

Today, the demand for machine power is rapidly increasing across various sectors such as construction, mining, agriculture, and infrastructure development. In response to this demand, construction equipment has evolved to incorporate numerous mechanical and electronic components, each designed for specific tasks. Excavators, in particular, are widely used for heavy-duty operations such as excavation, loading, and demolition. The performance of these machines depends on the seamless interaction between essential systems including the engine, hydraulic system, transmission, differential, axle, braking system, and control units. Since such machines are expected to deliver continuous power and high torque, it is essential that each component is thoroughly tested and their integration within the system is optimized.

One of the key factors affecting the efficiency and lifespan of construction machinery is thermal management. In particular, the high temperatures generated within the engine compartment can significantly reduce performance and lead to mechanical failures over time. Proper underhood airflow management plays a critical role in preventing overheating of engine and hydraulic components. Inadequate airflow can result in heat accumulation in the radiator, charge air cooler (intercooler), engine block, and surrounding parts, whereas a well-designed airflow system ensures these components operate within safe temperature ranges—ultimately reducing fuel consumption and maintenance costs. Therefore, in machines like excavators that generate substantial heat, underhood airflow design is not merely a cooling issue, but a matter of operational efficiency and system reliability.[1]

In recent years, tightening emissions regulations and growing customer expectations have driven significant changes in the design of cooling systems and airflow layouts in construction machinery. Particularly in engines compliant with emission standards such as Stage 4 and Stage 5, additional systems like Exhaust Gas

Recirculation (EGR), Selective Catalytic Reduction (SCR), and AdBlue have become standard. As a result,the engine compartment has become more crowded with components, leading to increasingly complex airflow dynamics. This study aims to experimentally analyze underhood airflow behavior in excavators, identify regions prone to excessive heat accumulation, and develop improvement strategies to reduce thermal stress. By comparing pre- and post-modification conditions, the effectiveness of the implemented enhancements will be evaluated, and recommendations will be provided to support better system performance.[1]

## 1.2. ENGINE SYSTEMS & EMISSION STANDARDS

Engines are the core components of construction machinery, providing the necessary power to perform demanding tasks. These engines typically run on fuel sources such as diesel, gasoline, or LPG. However, due to the high power output and efficiency required in construction applications, diesel engines are predominantly used. In diesel engines, fuel is directly injected into the combustion chamber, where it ignites under high compression. This combustion process, driven by the chemical properties of diesel fuel, results in superior performance and lower fuel consumption, making it ideal for heavy-duty machinery operating under continuous and strenuous conditions. - The view of the Diesel Engine is shown in Figure 1.

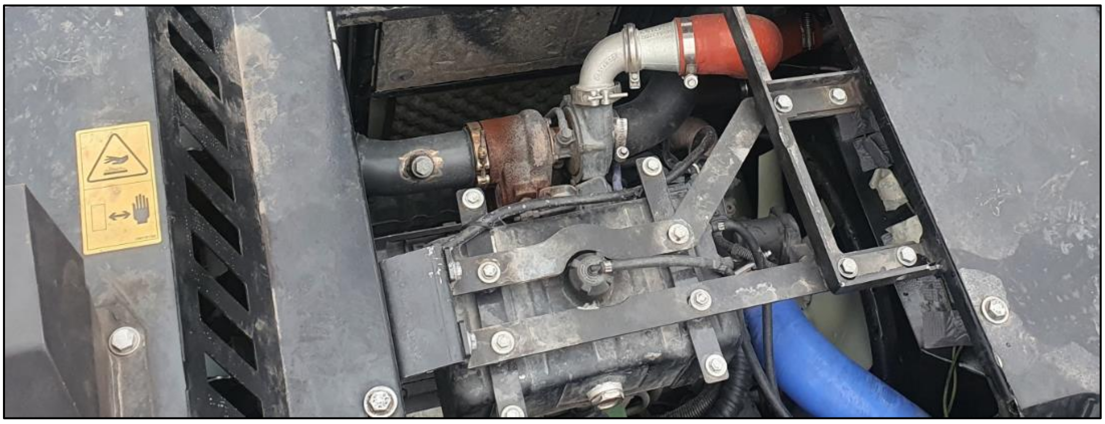

**Figure 1:** The view of the Diesel Engine

To mitigate the environmental impact of diesel engine emissions, regulatory bodies have established emission standards aimed at reducing toxic NOx gases generated during fuel combustion. These standards are categorized into different stages, including Stage 3/Stage 3A, Stage 4f, and Stage 5. A key distinction between Stage 3 and Stage 4 is the introduction of the Diesel Exhaust Fluid (DEF), commonly known as AdBlue, which helps reduce harmful emissions. Stage 5 further builds upon this by incorporating a Selective Catalytic Reduction (SCR) system alongside the DEF system. While these emission control technologies effectively lower NOx emissions, they can also introduce operational challenges, as they interact with the engine's performance and efficiency within the system’s cycle [2].

These emission standards are defined under the European Union's non-road mobile machinery (NRMM) Regulation (EU) 2016/1628, which outlines permissible emission limits for NOx, particulate matter (PM), hydrocarbons (HC), and carbon monoxide (CO) across various power categories [3].

1. Stage IIIA (Directive 97/68/EC as amended) limits NOx to approximately 6.0 g/kWh for engines in the 130–560 kW range [4].
2. Stage IV significantly tightens NOx limits to 0.4 g/kWh, mandating the use of advanced after-treatment systems like SCR.
3. Stage V, which became mandatory in 2019–2021 depending on engine category, further reduces PM and introduces Particulate Number (PN) limits, requiring Diesel Particulate Filters (DPFs) in addition to SCR and DEF systems [Directive (EU) 2016/1628].

## 1.3. HYDRAULIC SYSTEM AND THEIR COMPONENTS

Hydraulic systems generate motion by utilizing power transmitted through fluid flow, making them essential in construction machinery, particularly in excavators. These systems consist of key components such as a piston pump, a main control valve (MCV), safety valves, and spools. The efficiency and performance of a hydraulic system depend on several factors, including flow rate, operating speed, and the material and diameter of the conduits. Among these components, the piston pump serves as the core of the hydraulic system, providing the necessary pressure and flow to drive various machine functions. Proper design and maintenance of hydraulic systems are crucial for ensuring reliable and efficient operation in demanding construction environments [5].

### 1.3.1. Piston Pumps

Piston pumps, classified as positive displacement pumps, operate distinctly from centrifugal pumps by not relying on centrifugal force. Instead, they displace fluids mechanically through a reciprocating piston motion—hence their name. The piston moves back and forth within a cylinder, which is equipped with check valves at both the inlet and outlet. During the suction stroke, the piston retracts, opening the intake valve and allowing fluid to enter the cylinder. In the discharge stroke, the piston advances, closing the intake valve, opening the outlet valve, and forcing the fluid out of the pump [5]. A schematic representation of a typical piston pump is provided in Figure 2.

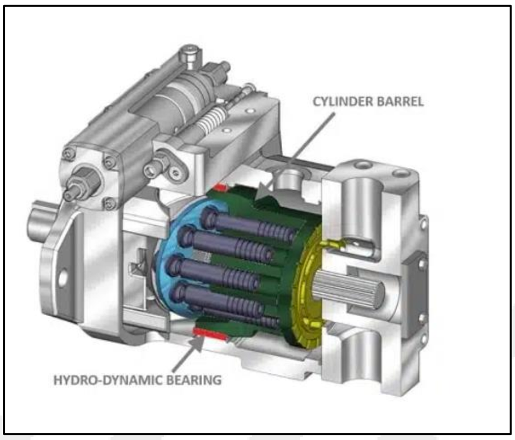


**Figure 2:** Piston Pump

### 1.3.2. Control Valves

Control valves are essential components in hydraulic systems, regulating key parameters such as flow, pressure, temperature, and fluid level. These parameters are continuously monitored by sensors, which transmit signals to the control unit responsible for adjusting the valve opening to maintain the desired setpoint. The actuation of control valves is typically carried out by electrical, hydraulic, or pneumatic actuators. To enhance precision, positioners interpret incoming electrical or pneumatic signals and fine-tune actuator movements accordingly.

Inside the control valve, spools are responsible for directing hydraulic flow in response to joystick inputs from the machine operator. These signals are relayed to the Main Control Valve (MCV) through a pilot pump, which activates the relevant spool to guide the hydraulic flow toward the corresponding attachment or actuator. In construction machinery, the pilot pressure of the MCV is typically regulated at 40 bar [6]. A schematic representation of the Main Control Valve is provided in Figure 3.

**Figure 3:** Main Control Valve

### 1.3.3.Safety Valve

Safety valves in construction machinery serve a critical function by preventing potential work-related accidents caused by hydraulic oil leaks, particularly during the operation of attachments. These valves are engineered to activate in response to abnormal pressure differentials within the hydraulic system. By doing so, they act as protective devices that help maintain system stability, protect equipment components, and ensure safe operation under varying load conditions [6]. In Figure 4, safety valve is given.

**Figure 4:** Safety Valve

### 1.3.4.Spools

Spools, positioned within the Main Control Valve (MCV), play a vital role in directing hydraulic flow in construction machinery. Their geometric configuration is specifically engineered to ensure balanced pressure distribution across the valve body, enabling precise control of fluid flow at designated pressure levels. This design not only enhances flow regulation accuracy but also contributes significantly to the overall efficiency, responsiveness, and stability of the hydraulic system [6,7]. Schematic representation of a spool is given in Figure 5.

**Figure 5:** Spool configuration

Control systems are employed to monitor, manage, and optimize the operational performance of construction machinery. Typically computer-based, these systems provide operators with real-time data on key performance parameters, such as engine load, hydraulic pressure, and fuel consumption. By facilitating automated functions and precision control, they significantly enhance operational efficiency while simultaneously reducing operator workload and the likelihood of human error [6,7].

### 1.4. IMPORTANCE OF UNDERHOOD THERMAL MANAGEMENT IN CONSTRUCTION MACHINERY

Under-hood airflow is a critical parameter that directly affects the performance, efficiency, and durability of construction machinery components. Effective airflow management plays a vital role in regulating engine temperature, preventing thermal degradation, and ensuring optimal operating conditions. In construction equipment, particularly excavators, maintaining stable under-hood temperatures is essential to mitigate the risk of overheating, reduce failures associated with thermal stress, and sustain reliable performance in demanding environments. Moreover, the efficiency of the cooling system is closely tied to the quality of airflow distribution, which impacts both the engine and hydraulic subsystems. A well-optimized under-hood airflow system not only enhances thermal performance but also contributes to lower maintenance requirements and reduced risk of unplanned downtimes [8,9].

This thesis aims to experimentally investigate the under-hood airflow dynamics of construction machinery. A series of improvement studies will be carried out to address heat accumulation in critical under-hood components of excavators. Following the implementation of these design enhancements, a comparative analysis between pre- and post-modification scenarios will be performed to assess their effectiveness in optimizing airflow patterns and minimizing thermal stress [9].

## 1.5 BACKGROUND AND RELATED WORK

### 1.5.1. Numerical Investigations on Under-Hood Airflow Modeling

With recent technological advancements, numerous Computational Fluid Dynamics (CFD) and Finite Element Analysis (FEA) studies have been carried out to model under-hood airflow and thermal behavior. Due to the high cost and time-consuming nature of experimental methods, CFD has become increasingly favored for its lower operational expenses and its ability to produce highly accurate results, as demonstrated in several studies from the literature. Below is a summary of selected numerical studies conducted in recent years.

Ljungskog and Nilsson [10] utilized CFD modeling to perform a comparative investigation of under-hood airflow in passenger vehicles, aiming to identify the most efficient simulation approach. Two methodologies—referred to as Method A and Method B—were evaluated. Method A utilized a polyhedral mesh generated in STAR-CCM+, while Method B implemented a hexahedral mesh structure. The study aimed to assess the influence of mesh type on simulation accuracy and computational efficiency. When the simulation results were compared with wind tunnel measurements, it was observed that heat rejection in the radiator was approximately 13% lower, while heat rejection in the charge air cooler was 4.5% lower in Method A and 6.0% lower in Method B. Due to uncertainties in the experimental results, further research is required to validate these methods.

Among the two approaches, Method A demonstrated higher potential for use in production due to its time efficiency and better convergence behavior. However, additional research and experiments are necessary before fully integrating these methods into industrial workflows. Compared to the methods currently used in Volvo vehicles, Method A offers an estimated 30% reduction in computational time, making it a promising alternative for optimizing under-hood airflow analysis.

Nordin [11] investigated the influence of aerodynamic drag on fuel consumption and driving performance in conventional vehicles, with particular focus on its effects on battery efficiency and driving range in electric vehicles. Recognizing the dual challenge of ensuring adequate component cooling while minimizing the aerodynamic penalties associated with it, the study explores two distinct under-hood heat exchanger configurations—series (Concept A) and parallel (Concept B).

Using the DrivAer model and simulating airflow via the Reynolds-Averaged Navier–Stokes (RANS) method with the k-ε turbulence model in STAR-CCM+ software, Nordin evaluated both configurations in terms of mass flow rate, cooling drag, and flow field characteristics. In both concepts, airflow behavior was analyzed by defining specific air inlet and outlet boundaries. The simulation results revealed a cooling drag difference of 2 units between the two configurations; however, this variation remained within the uncertainty limits of the computational method, making it inconclusive to definitively favor one configuration over the other.

Nonetheless, the parallel configuration demonstrated superior thermal exchange potential due to increased contact surface area between the coolant and ambient air, which could be particularly beneficial under high-temperature operating conditions. Moreover, the parallel setup facilitates on-demand airflow control, such as through active grille shutters, whereas in the series configuration, both heat exchangers are subjected to the same airflow characteristics, limiting targeted thermal management.

Another study

A. Dhumal et al. [12] highlighted the critical role of fin density in determining the thermal efficiency of radiator systems. The study evaluated three fin configurations—6 FPI (fins per inch), 8 FPI, and 10 FPI—and compared their thermal performance under identical operating conditions. Among these, the 10 FPI configuration yielded the lowest operating temperature and exhibited the highest thermal efficiency. The 8 FPI model demonstrated improved heat dissipation compared to the 6 FPI version, which operated at higher temperatures and provided only moderate thermal performance.

Fins with greater surface area enhance convective heat transfer by increasing contact with the surrounding air; however, this also introduces higher airflow resistance, which can negatively impact overall system efficiency. Therefore, an optimal radiator design requires a balanced trade-off between improved heat transfer and minimized flow resistance to ensure effective cooling performance.In addition to analyzing fin density, the study also examined the alignment of radiator cooling packages and its influence on under-hood thermal management in agricultural tractors. Experimental measurements, including temperature distribution and heat flux, were employed to support the thermal analysis and evaluate the effectiveness of different layout configurations.

S. A. Kadir and M. S. Yousif [13] utilized CFD simulations in ANSYS Fluent to analyze three-dimensional underhood airflow and heat transfer for automotive engine cooling applications. Fan speeds between 1000 and 3500 rpm and grille openings at 30%, 50%, and 70% were modeled. Boundary temperatures included engine surface temperatures between 150 and 250 °C and ambient temperature set at 25 °C.

Simulations showed airflow velocity increasing to 13 m/s at 3500 rpm fan speed. Heat transfer coefficient on the radiator surface ranged between 280 and 320 $W/m^2K$. A grille opening of 50% resulted in minimal pressure drop (190 Pa) and maximum cooling efficiency (18% increase). Temperature distribution across the engine surface was homogeneous with ±6 °C variation. Results correlated within 8% of experimental data.

Y. Zhang et al. [14] conducted a 3D CFD analysis to examine the impact of engine cooling fan speeds at 1200, 2400, and 3600 rpm on underhood airflow velocity and temperature distribution. Simulations were performed with and without fans and with varying fan blade angles. Engine surface temperature was set at 200 °C and ambient temperature at 27 °C.

At 3600 rpm, fan-induced airflow velocity reached 14.5 m/s, and radiator surface temperature decreased to 65 °C. Use of the fan reduced temperature peaks by 15% and lowered average underhood temperature by 8 °C. The optimal fan blade angle of 25° achieved the most uniform airflow distribution.
Pressure drop was approximately 250 Pa. This study provides guidance for optimizing fan performance for cooling efficiency and energy consumption.

M. R. Hussain and S. K. Panda [15] employed a conjugate heat transfer approach to numerically analyze the thermal-fluid behavior of an underhood cooling system.Detailed 3D CAD models of the engine block, radiator, fan, and airflow ducts were used. Thermal conductivity values were set at 45 W/m·K for the engine block and 200 W/m·K for the radiator alloy.

The simulation revealed maximum engine surface temperatures of 210 °C and radiator outlet temperatures of 60 °C. At a fan speed of 2800 rpm, airflow velocity reached 13 m/s, increasing heat transfer by 20%. Small changes in fan blade angles affected cooling performance by 5–10%. The results highlighted critical hot spots and offered insights for airflow improvement in the engine compartment.

### 1.5.2. Experimental Studies on Under-Hood Airflow

Experimental studies on simplified under-hood environments have been conducted since the 1980s to analyze critical aspects such as engine temperature distribution, pressure variation, cooling system optimization, and airflow behavior. Despite the advancements in numerical modeling, experimental investigations remain indispensable for accurately capturing complex physical phenomena and validating computational results. Therefore, experimental efforts continue to play a key role in improving under-hood thermal management strategies.

Golin and Björk [16] conducted an experimental study to assess the thermal performance of six different coolant fluids in an automotive radiator. The tested coolants included pure water, pure propylene glycol (PG), and various mixtures of propylene glycol/water (PG/water) and ethylene glycol/water (EG/water) in 30/70 and 50/50 volume ratios. The study highlighted that the chemical composition of coolant fluids significantly influences under-hood thermal behavior. Key fluid properties such as density and viscosity affect the interaction between the coolant and system components during circulation, thereby impacting heat transfer efficiency.

A PLC-controlled test setup was developed to perform the experiments. The radiator inlet temperature was maintained at a constant 90 °C in all tests, while the coolant flow rate was varied between 0.10 and 0.25 L/s, in increments of 0.05 L/s. The results showed that pure water provided the best thermal performance, followed by 50/50 EG/water, 50/50 PG/water, 30/70 EG/water, 30/70 PG/water, and lastly, pure PG. Although pure PG exhibited the lowest thermal performance, it offers practical advantages over EG, such as lower cost and reduced toxicity. Thus, the authors concluded that PG-based mixtures could serve as viable antifreeze alternatives to EG mixtures in certain applications, despite the marginal loss in heat transfer efficiency.

Ismael, T. et al. [17] emphasized the importance of radiators in engine cooling systems, noting that structural modifications can significantly affect cooling efficiency.In the study of Ismael et al [17], the effects of different fin pitches on the cooling system were examined. The radiator fin dimensions used as P = 2.5, 2.4, 2.3, 2.2, and 2.1 mm. The JB2293-1978 Wind Tunnel Test Method for Automobile and Tractor Radiators was used for cooling performance testing.

The test bench system is a continuous air suction-type wind tunnel. Based on the results obtained from the tests, it was demonstrated that increasing the fin phase in radiators enhances cooling performance and reduces costs by saving material.

Tomoyuki Tsuchihashi et al. [18] examined the operational challenges of excavators, highlighting their performance under dusty and high-demand working conditions. In parallel with these challenging conditions, the engine requires a high-performance cooling system, and noise reduction is essential to improve environmental factors.A study was conducted on mini excavators to improve airflow under the hood and consequently reduce the noise level emitted to the environment. In construction machinery, the air trapped in the engine compartment is expelled through vents. However, this is sometimes insufficient, and the trapped air negatively affects the transmission of noise from the engine compartment to the outside.To overcome these issues, a channel geometry was designed under the hood to direct the air vacuumed through the radiator fins into the engine compartment with the help of a fan. The purpose of this design is to relieve and guide the trapped air, ensuring better airflow distribution Consequently, the heat generated by the confined air within the engine compartment was minimized, resulting in enhanced engine performance and a reduction in the noise level emitted into the surrounding environment and this system is referred to as iNDr. The newly developed iNDR system in the study is given in Figure 6.

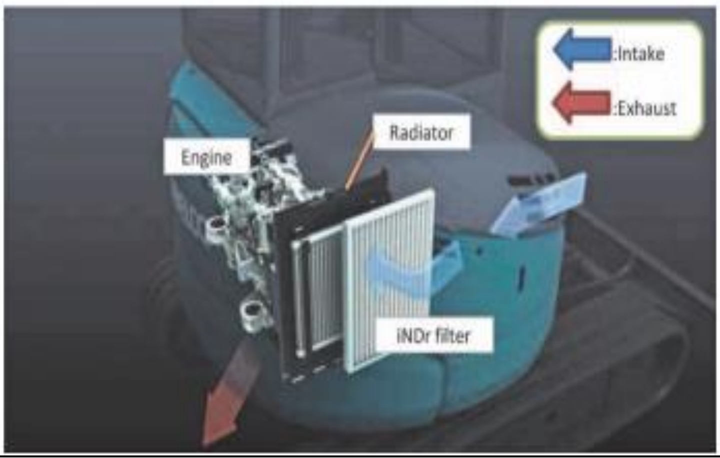


**Figure 6:** Cooling air flow of newly developed mini-excavator[18]

One of the key factors influencing passenger comfort in buses is the amount of heat transferred from the engine compartment to the passenger cabin. This issue becomes particularly significant during summer months, when elevated temperatures can severely affect interior comfort levels. Consequently, accurately assessing and improving the temperature distribution within the engine compartment—typically located beneath the passenger cabin—is essential not only for enhancing comfort but also for maintaining engine performance and reliability.

Mezarcıöz [19] experimentally investigated the thermal distribution in the engine compartment of a passenger bus under various driving conditions. To ensure spatial resolution, the engine compartment was divided into six distinct regions, and a total of fourteen thermocouples were installed to record temperature data.
The experiments were performed under three operational scenarios:

- Constant high-speed driving,
- Hill climbing, and
- Idling.

Temperature data were collected from each designated region under all three conditions. The results revealed that engine compartment temperatures increased significantly during hill climbing, attributed to the additional engine load induced by the slope. This temperature rise affected not only the main engine body but also adjacent regions housing other vital components. Interestingly, while some regions experienced peak temperatures during hill climbing, others exhibited their highest values during idle conditions, likely due to limited convective cooling in the absence of forward motion [19].

Kula [20] aimed to improve engine efficiency and reduce emissions by employing one-dimensional analysis, experimental methods, and artificial neural networks. The water-cooled turbocharger and water-cooled condenser units were positioned independently of the engine in a suitable location within the engine bay. A dual-cycle cooling system was implemented in a 1.6-liter turbocharged diesel engine to cool the heated air after turbocharging and the condenser which is shown in Figure 7. For the size optimization of the water-cooled turbocharging unit, an artificial neural network approach and optimization method were applied. When comparing experimental data with the results from the one-dimensional numerical results, a high level of consistency was observed. The findings indicate that, through the design and optimization of the dual-cycle cooling system based on one-dimensional model analysis, experimental tests, and the neural network approach, engine efficiency was improved, resulting in lower emission levels[20].

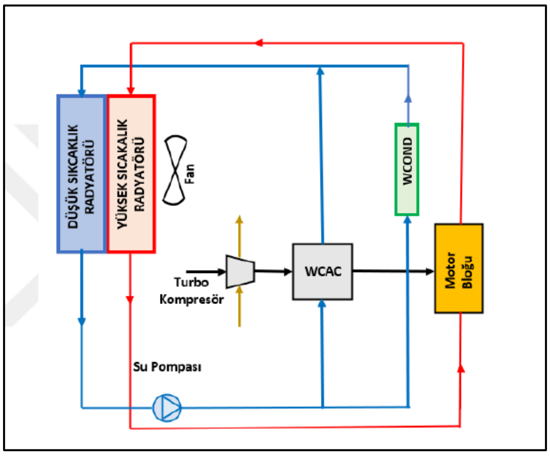


**Figure 7:** Diagrams of the Dual-Cycle Cooling System[20]

Rajput [21] experimentally investigated underhood airflow in passenger cars using a wind tunnel setup. A full-scale test rig simulating the engine compartment was used, with fan speeds varied between 1000 and 3000 rpm. Air velocity and distribution were measured with temperature and pressure sensors, while grille openings were adjusted to 20%, 40%, and 60%. The goal was to characterize underhood aerodynamics to optimize cooling efficiency.

At a fan speed of 3000 rpm, the airflow velocity in front of the engine reached 12 m/s. Grille openings between 40% and 60% provided the best balance between airflow and pressure drop (pressure loss ranged between 150 and 230 Pa). Temperature measurements showed that increasing fan speed reduced radiator outlet temperature by 15 °C. The homogeneity of airflow resulted in a thermal balance with temperature variations of ±5 °C across the engine.

J. Wang et al. [22] studied the thermal management of a heavy-duty diesel engine underhood experimentally, utilizing a wind tunnel with a constant airflow velocity of 7 m/s and fan speeds ranging from 800 to 2500 rpm. Temperature distribution was mapped using 75 thermocouples placed on the engine block, radiator, and intercooler. The study evaluated the effect of radiator types on airflow and heat transfer.

At a fan speed of 2500 rpm, the temperature above the engine decreased from 95 °C to 78 °C. Open-type radiators provided 18% higher heat transfer and an average air velocity of 9.2 m/s. Modifications to the underhood airflow channels reduced the hot zone area by 22%. Cooling efficiency was improved by 10–20% through combinations of fan speed and radiator type.

M. Baccar et al. [23] conducted experimental investigations on underhood airflow and temperature fields in high-performance vehicles using a wind tunnel at speeds between 30 and 120 km/h. Air velocity was measured with 18 anemometers, and temperature profiles were recorded using a heated engine model. Fan speeds ranged from 1000 to 4000 rpm.

Running the fan increased airflow velocity by 32% up to 14 m/s, while engine temperature dropped from 70 °C to 58 °C. Hot spots without the fan had a diameter of 12 cm, which reduced to 7 cm with the fan. Air velocity in front of the intercooler was measured at 11 m/s, and heat transfer coefficients increased by 25%. These experiments provided concrete data for aerodynamics and cooling performance.

## 1.6. ENGINE COOLING SYSTEM IN CONSTRUCTION MACHINERY

### 1.6.1. Fundamentals of Engine Cooling

#### 1.6.1.1 Functions of Engine Cooling Systems

Construction and heavy-duty machinery are designed to operate under harsh working conditions. The engine class of a machine is determined based on its tonnage. Each working condition requires different specifications. For example, excavators over 40 tons are preferred in marble quarries, while 70-ton class excavators are used in coal mines. As the machine's tonnage increases, its digging capacity, digging, and breaking forces also increase, which shortens the duration of the work. However, as the machine's tonnage increases, the required engine power also rises, leading to higher fuel consumption [23,24].

Environmental conditions play a critical role in determining the performance and reliability of engines and their components, particularly under heavy-duty operating conditions. Fluctuations in ambient temperature can significantly alter the thermal balance within the engine compartment.
High-speed engines, in particular, rely heavily on effective cooling systems to dissipate the substantial heat generated during combustion.

A fundamental requirement for engine operation is a continuous and sufficient fuel supply. Due to the high power demands of construction machinery, diesel engines are predominantly used, making diesel fuel the primary energy source. Given the relatively low flash point of diesel fuel, each combustion cycle generates considerable thermal energy within the engine block. This heat must be dissipated efficiently to maintain structural integrity and operational safety.

Conduction heat transfer is the first mechanism through which this thermal energy is distributed away from the combustion zone. The efficiency of conduction depends primarily on the material properties and geometric design of engine components. Among these, the thermal conductivity coefficient (k) of the solid material is the most critical parameter. Cast iron alloys are commonly used in diesel engine blocks due to their high resistance to wear, corrosion, and mechanical stress. Cast iron also offers acceptable thermal performance, with a melting temperature range of 1150–1300°C and a thermal conductivity varying between 20 and 70 W/m·°C, depending on the alloy composition.

However, cast iron alone is insufficient to manage the extreme temperatures produced during combustion, which can reach up to 2750°C in localized regions of the combustion chamber. Without proper thermal regulation, these high temperatures may lead to material deformation, seal failure, and ultimately engine overheating. Therefore, conduction must be supported by convection heat transfer to ensure effective thermal management.

Convection cooling occurs at the interface between the engine's solid surfaces and a moving fluid, either air or liquid coolant. Accordingly, engine cooling systems are typically categorized into two types based on the working fluid[23,24]:

- Air cooling, and
- Water (liquid) cooling.

Each approach has distinct thermal and structural design considerations, which will be further explored in the following sections.

#### 1.6.1.1.1. Air-Cooled Systems

While automobile engines are predominantly water-cooled, air-cooled systems are frequently utilized in heavy machinery due to their structural simplicity and reliability under harsh operating conditions. In air-cooled engines, cooling fins are integrated into the cylinder block and cylinder head to increase the surface area available for heat dissipation.

In naturally ventilated systems, where no fan is employed, the relative wind generated by machine movement flows over the engine surfaces—specifically the cylinder and crankcase housing—facilitating direct heat transfer from the engine to the ambient environment. In forced air-cooled systems, however, a fan (ventilator) is used to direct airflow over these components, enhancing the cooling process.

These systems do not include conventional components such as coolant fluid, radiator, water pump, expansion tank, radiator cap, coolant hoses, internal water jackets, or heater cores. Instead, the cooling mechanism comprises engine cooling fins, air deflection plates, and a cooling fan.

The axial fan draws in air and discharges it in a circumferential direction, with the air deflection plate guiding the airflow across the cylinder surfaces. Thin fins on the exterior of the cylinder and head improve convective heat transfer by increasing surface exposure to the cooling air. This mechanism is effective in environments where space, weight, or mechanical complexity constraints make liquid cooling less feasible.

Despite the prevalence of liquid cooling systems in modern engines, air-cooling remains a complementary method in heavy-duty construction machinery, which often operates under high thermal loads. In such applications, a hybrid cooling configuration is employed, combining liquid cooling with air-based intercoolers to enhance thermal performance and prevent engine overheating during sustained high-load conditions [25].

An intercooler as depicted in Figure 8, is a specialized heat exchanger used in turbocharged engines to cool the compressed intake air before it enters the combustion chamber. As air is compressed by the turbocharger, its temperature increases, reducing its density. By routing the compressed air through a radiator-like finned structure, the intercooler lowers the air temperature, thereby increasing its molecular density—more air molecules per unit volume. As a result, volumetric efficiency improves, leading to enhanced combustion and increased engine power output [26].

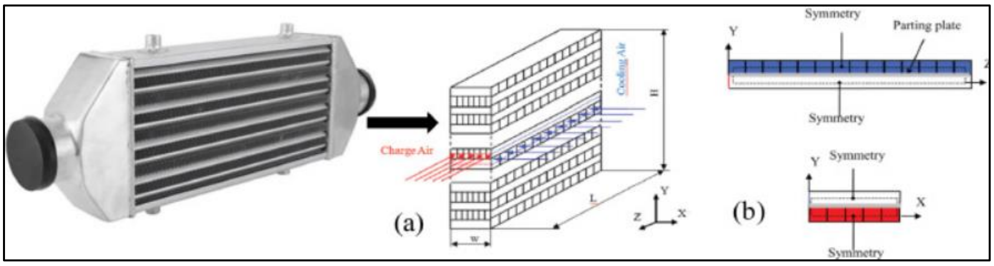


**Figure 8:** View of the Intercooler [26]

### 1.6.1.1.2.Liquid-Cooled Systems

In liquid-cooled engines, water or a water–antifreeze mixture is typically used as the cooling medium. The heat generated during engine operation is transferred to the coolant via the engine's internal water jackets, and the heated coolant is subsequently cooled in the radiator before recirculating through the system. A water pump ensures continuous circulation of the coolant throughout the engine block and cylinder head.

Upon starting a cold engine, the thermostat remains closed, preventing coolant from flowing to the radiator. This allows the engine to reach its optimal operating temperature more quickly, as the coolant initially circulates only within the engine block and cylinder head.

Once the engine reaches a predetermined temperature threshold, the thermostat opens, allowing coolant to pass through the radiator where it is cooled by airflow—either generated by the radiator fan or resulting from vehicle forward motion. In some engine designs, a portion of the coolant is routed through the intake manifold to promote fuel–air mixture vaporization, thereby improving combustion efficiency [27].

The cooling process in liquid-cooled systems is indirect: the coolant absorbs heat from engine components without direct contact and then transfers that heat to the surrounding air through the radiator fins. This closed-loop cycle continues as long as the engine is in operation, maintaining thermal stability and protecting engine components from overheating as shown in Figure 9 [27,28].

In construction machinery, engine cooling is only one aspect of the overall thermal management system. Due to the presence of high-load hydraulic systems, additional cooling components such as hydraulic oil radiators and fuel cooling radiators are also integrated into the design. These systems operate on similar principles: the fluid (hydraulic oil or fuel) passes through a radiator, where it is cooled by forced airflow generated by an engine-driven or electric cooling fan, and then continues circulating within the respective subsystem. These auxiliary cooling loops are essential for maintaining system efficiency, component longevity, and operational safety under demanding working conditions.

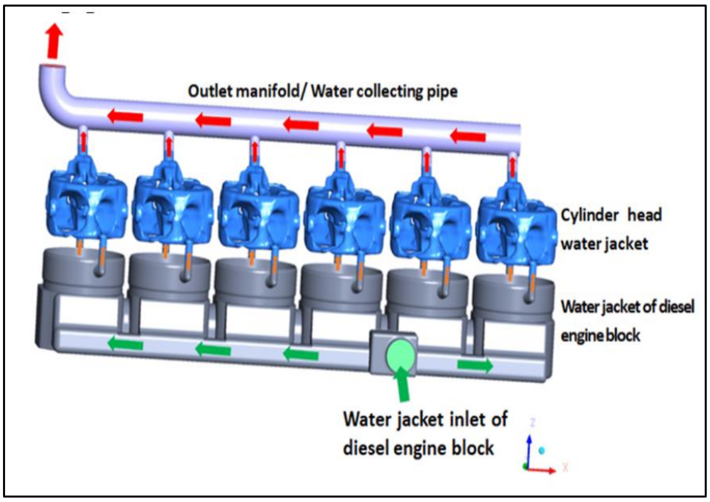


**Figure 9:** Liquid Cooling of Engine [27,28]

### 1.6.2. Methods for Coolant Circulation(Thermo-syphon vs. Forced)

Several methods are employed to circulate coolant around the engine cylinder and cylinder head, ensuring effective heat dissipation and stable engine operation. The two primary methods are as follows [29]:

#### 1.6.2.1.Thermo-Syphon Cooling

It is a system where water circulates through convection currents without the need for a pump. The water heated in the engine cylinder jackets mixes with the cooler water from the radiator within the same loop, and the cooling process occurs through heat transfer between the two.

Since there is no pump in this loop, the radiator, which cools the water, must be positioned higher than the engine to ensure effective circulation [29]. The thermo-syphon cooling system is given in Figure 10.

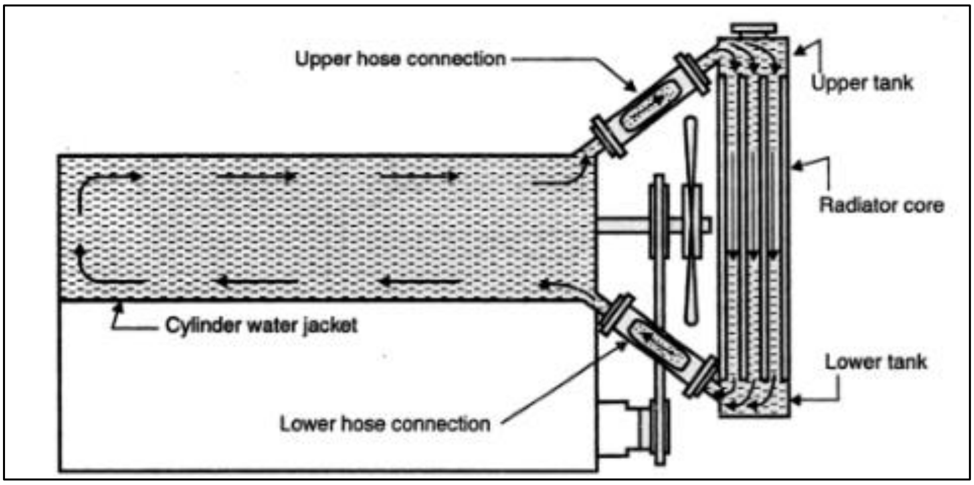


**Figure 10:** Thermo-syphon cooling system [29]

### 1.6.2.2.Forced or Pump Cooling

A force element is required to circulate the water in the engine cylinder jackets. In vehicles, the water is typically sent to the cooling system through a pump called a circulation pump, and the cycle continues in this way[29]. Thermostatically controlled cooling system is shown in Figure 11.

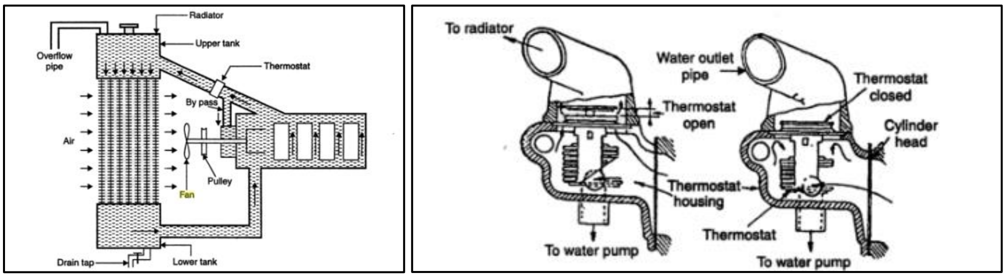


**Figure 11:** Thermostatically controlled cooling system[29]

## 1.6.3. Liquid-Cooled Engine Architecture

### 1.6.3.1. Radiators

The radiator is a fundamental component of liquid-cooled engine systems, responsible for transferring heat from the engine coolant to the surrounding air. It achieves this by maximizing the surface area exposed to airflow while maintaining a sufficient volume of coolant within its channels.

Structurally, a radiator consists of a core containing liquid-carrying tubes, an upper tank that receives the hot coolant from the engine, and a lower tank (or in some designs, side tanks) that returns the cooled liquid back to the engine block [30].

During operation, hot coolant exits the engine and enters the upper tank of the radiator. It is then distributed across the vertical tubes within the radiator core. As the coolant flows downward through these tubes, it releases heat, which is transferred first to the tube walls, then to the attached metal fins, and finally to the airflow passing over the radiator surface. This process results in the cooling of the engine coolant before it re-enters the engine.

Radiators are typically manufactured from copper, brass, or increasingly aluminum alloys. Copper and brass are preferred for their high thermal conductivity, corrosion resistance, and ease of soldering, while aluminum radiators offer lightweight construction, making them favorable for modern applications. In traditional designs, thin copper or brass fins are soldered around vertical tubes to increase the total heat exchange surface area. In aluminum radiators, resin tanks and aluminum fins are used to reduce weight while maintaining sufficient heat transfer efficiency [31].

Several functional features are incorporated into radiator design:

- The upper tank typically includes a water filler cap for adding coolant.
- Some models use water deflectors to evenly distribute hot coolant across all tubes.
- An overflow pipe allows excess pressure to be released.
- The lower tank often includes a drain valve for maintenance or coolant replacement.

In some radiator configurations, adjustable shutters are mounted in front of the core to regulate incoming airflow. These shutters may close during engine warm-up phases, reducing airflow to limit cooling and help the engine reach optimal operating temperature more quickly [31,32].

Radiators are classified based on the tube design and the finned structure used to enhance convective heat transfer. The most common core types include:

- Tubular radiators, which feature cylindrical tubes arranged in parallel.
- Flat-fin radiators, commonly used in passenger vehicles.
- Corrugated-fin radiators, the most widely adopted in heavy-duty applications, where copper or brass tubes run between the tanks and corrugated fins are soldered between them.

In aluminum radiators, the fin–tube structure is optimized for weight reduction, and the use of resin tanks further contributes to thermal efficiency and cost-effectiveness. Overall, the larger the radiator core and surface area, the more efficient the system is at dissipating heat, making radiator size and geometry critical factors in engine cooling performance.

#### 1.6.3.1.1.Tubular Radiators

These radiators are constructed from a series of round or flattened water tubes (also referred to as water pipes) that are soldered to the headers of the upper and lower tanks. While the tubes are typically oriented vertically to facilitate downward coolant flow, some radiator designs utilize a horizontal flow configuration, depending on the spatial and functional constraints of the vehicle or machinery as shown in Figure 12.

Air fins, generally made of thin copper or brass, are either flat or curved in shape and are soldered directly onto the water tubes. This soldering process not only provides structural integrity but also plays a crucial role in enhancing thermal conductivity, ensuring efficient heat transfer from the water tubes to the fins. These fins, by virtue of their large surface area, facilitate effective convective heat transfer to the surrounding air.

To further improve airflow turbulence and heat dissipation, bellows-like (corrugated) plates are installed parallel to the tubes and between the fins. These structures increase the air–surface interaction and promote better mixing of the airflow, thereby improving the radiator's overall thermal performance [31,32]. An enlarged view of the water tubes and fin pitch arrangement is shown in Figure 13 [32].

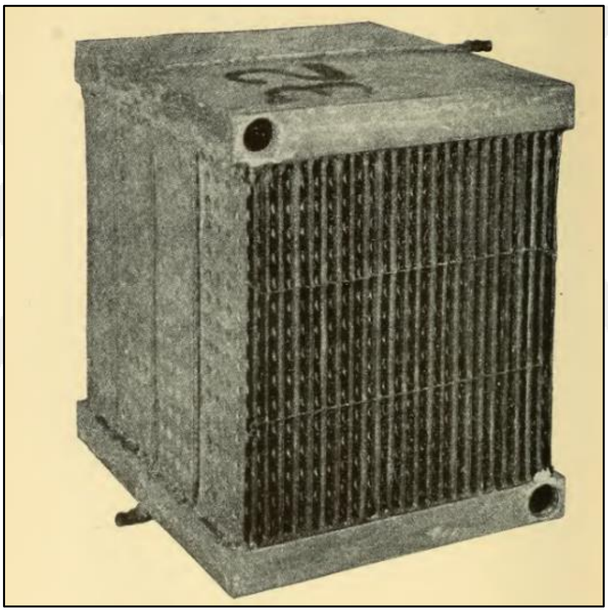

**Figure 12:** Tubular Radiator [32]

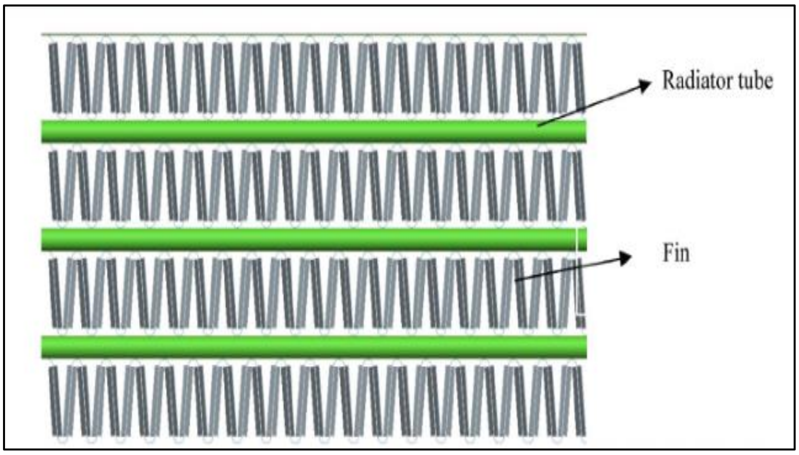


**Figure 13**: The water tubes and the fins pitch with an enlarged view. [32]

#### 1.6.3.1.2. Wing Radiators

Wing-type radiators are constructed from thin metal strips arranged and soldered together in a zigzag pattern, forming paired flat tubes that serve as coolant channels. These strips establish a continuous connection between the upper and lower radiator tanks, giving the overall structure a beehive-like appearance.

Within the radiator core, the water passages are formed by the space between these metal strips, while the same strips also define the air passages. As a result, the radiator core integrates both coolant flow paths and airflow channels within a compact configuration. The width of the water passages is typically designed to match the total width of the radiator core, ensuring uniform distribution of coolant.

During assembly, the air passages created between the zigzag-arranged strips typically form a hexagonal pattern, resulting in a honeycomb-like geometry. This design maximizes the air contact surface area, enhancing convective heat transfer while maintaining a lightweight and space-efficient structure [32].

The radiator shown in Figures 14 and 15 is a type designed with a cellular structure, used in early motor cooling systems. This type of radiator provides high heat transfer efficiency thanks to its honeycomb form, which is surrounded by numerous narrow channels through which the fluid passes

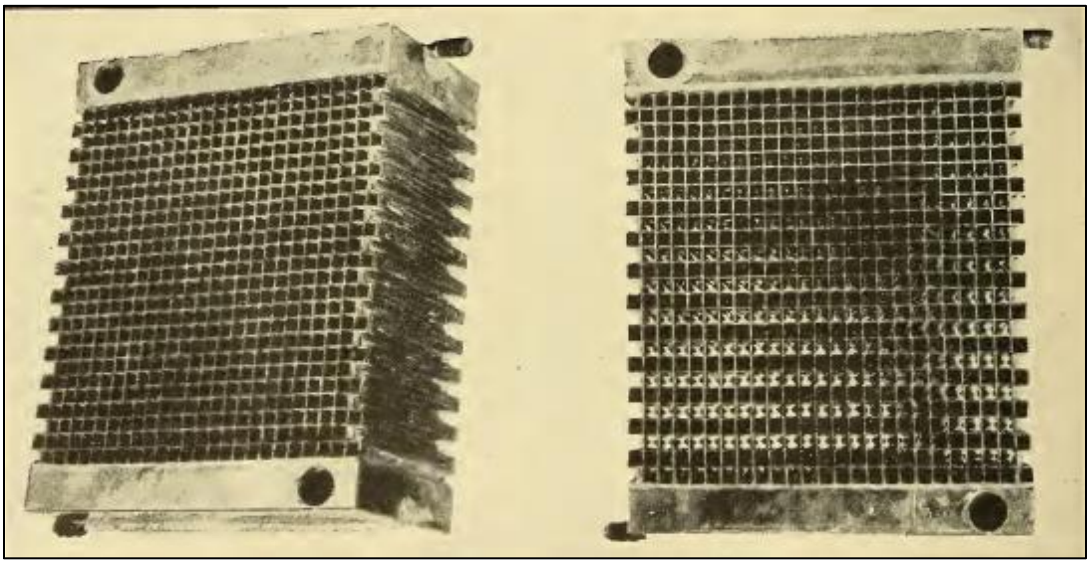

**Figure 14**: Wing Radiator[32]

**Figure 15:** Radiator that is used in excavator

## 1.7. COOLING FANS AND REVERSE FLOW SYSTEMS

### 1.7.1. Hydraulic Fan Drive Systems

In hydraulic fan drive systems, the vehicle's cooling fan is powered by a hydraulic motor, which is driven by a hydraulic pump. This pump is typically powered via the Power Take-Off (PTO) mechanism or through a belt drive. The primary function of the hydraulic fan is to dissipate the heat energy transferred to the radiator during the internal combustion cycle, thereby maintaining optimal engine cooling performance [33].

In internal combustion engines, rapidly reaching and maintaining the optimal operating temperature is critical for maximizing thermal efficiency and minimizing mechanical wear on engine components. One of the key advantages of hydraulic fan systems is their ability to operate on demand, meaning the fan is only activated when cooling is required. This not only improves fuel efficiency by reducing parasitic power losses but also contributes to more precise thermal regulation.

Hydraulic fan systems are particularly common in construction machinery, such as excavators, where variable engine load conditions require flexible cooling strategies.An example of a hydraulic fan used in an excavator is shown in Figure 16.

**Figure 16:** Hydraulic Fan that is used in excavator

Hydrostatic fan drive systems can be classified into four groups. Depending on the need, hydrostatic fan systems can be operated hydromechanically or electrohydraulically. These two systems are further classified as variable displacement pump systems and fixed displacement pump systems as shown in Figure 17 [33].

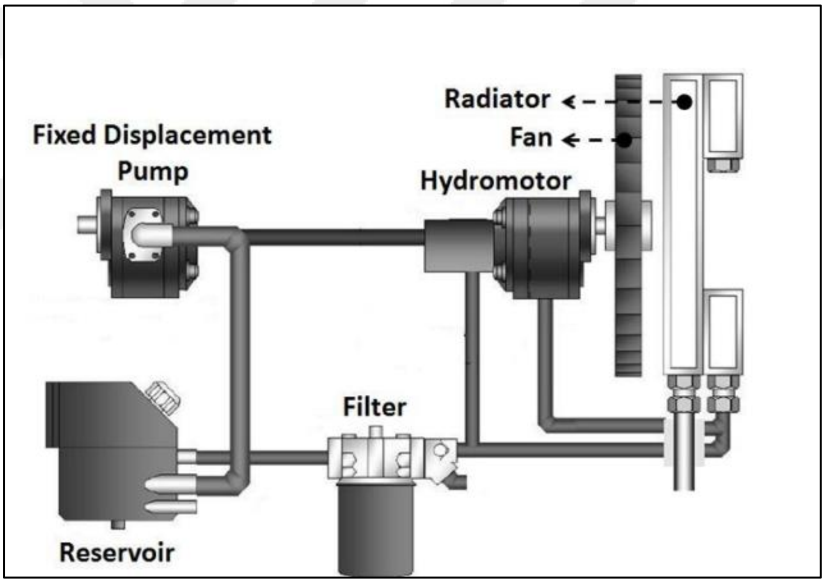


**Figure 17**: Fixed Displacement Pump and Motor[33]

### 1.7.1.1 Hydromechanical Control in Hydraulic Fan Drive Systems

Hydromechanical control is commonly employed in relatively simple cooling systems, where monitoring is limited to one or two fluid temperatures (such as coolant or hydraulic oil). This control strategy is often sufficient for systems with stable operating conditions and moderate thermal loads. In contrast, electrohydraulic control offers distinct advantages, including faster response times and improved control precision. Through the integration of microcontrollers and multiple temperature sensors (for both gas and liquid), more complex and adaptive control architectures can be achieved [33].

#### 1.7.1.1.1.External Gear Pump and Motor with Hydromechanical Control

In a hydrostatic fan drive system featuring a fixed displacement gear pump and a priority valve, the system continuously supplies the required pressure and flow to the fan motor based on the engine's thermal load. The priority valve functions to ensure that adequate hydraulic flow is always available to the fan circuit, and the system is regulated by a thermal pressure relief valve.

This valve adjusts pressure in direct response to cooling demand, which is influenced by the airflow requirement needed to dissipate heat from the diesel engine. Excess flow from the priority valve may be diverted to other hydraulic subsystems or returned to the hydraulic reservoir. The priority valve can either be integrated into the pump's rear cover or mounted separately within the hydraulic circuit.

The thermal pressure relief valve used in this configuration is a direct-acting, seat-type poppet valve. Its nominal cracking pressure varies proportionally with temperature, allowing it to dynamically modulate the system in accordance with thermal conditions [34].

#### 1.7.1.1.2.Axial Piston Pump and Motor with Hydromechanical Control

In systems using a variable displacement axial piston pump with remote pressure control, the pump's operating pressure is regulated by a thermal pressure relief valve based on the cooling fluid temperature (water or oil). This configuration allows the pump flow rate to be adjusted without requiring throttling, enabling the fan to operate at the necessary speed with maximum energy efficiency.

As temperature rises, the thermal relief valve modulates pressure through a remote control port on the pump's control mechanism, ensuring that the cooling demand is precisely met. This dynamic adjustment allows for balanced heat dissipation, avoiding both overcooling and overheating under variable load conditions [34].

The system may incorporate fixed displacement piston motors, operating according to the swash plate or inclined axis principle. These motors can be of either standard or embedded type. To prevent cavitation, an anti-cavitation check valve is typically installed between the inlet and outlet ports of the motor. This valve may be located in the hydraulic line or integrated directly into the motor’s port plate [34,35].

#### 1.7.1.2 Electrohydraulic Control in Hydraulic Fan Drive Systems

##### 1.7.1.2.1.Internal Gear Pump and Motor with Electrohydraulic Control

If the fixed displacement internal gear pump produces more oil than necessary to drive the fan motor at the required pressure and speed, the excess oil is diverted back to the tank via the electro-proportional pressure relief valve (also called a bypass valve) mounted on the motor. The fan speed and capacity are regulated by this proportional pressure relief valve, which can be integrated into the motor or installed separately in the hydraulic line [34,35].

The pilot-operated proportional pressure relief valve has a descending characteristic curve, meaning that in the event of a control system failure, the fan will operate at maximum power as a safety measure. If the electrical current to the valve is cut off, the valve reaches its maximum setting, closing the bypass and directing all oil from the pump to the fan motor [34,35].

The current sent to the proportional valve in the fan system is controlled by the digital electronic control unit based on temperature readings obtained from sensors in the system.

##### 1.7.1.2.2.Axial Piston Pump and Motor with Electrohydraulic Control

The ED electronic pressure regulator is designed for fan drive systems that use an A10..-type variable displacement axial piston pump operating on the swash plate principle. This system allows for the creation of a cost-effective, compact, and flexible fan drive solution. System pressure is controlled by the current sent to the proportional pressure relief valve mounted on the pump. The variable displacement pump maintains a constant system pressure within the adjustment range, regardless of the oil flow rate supplied to the system. The electrical current sent to the proportional valve on the pump is regulated by the digital electronic control unit, based on temperature information received from the system’s sensors. As the diesel engine speed changes, the pump automatically adjusts itself to supply the necessary oil flow without throttling losses, ensuring that the required fan speed is maintained.Fixed displacement axial piston motors operating on the inclined axis or swash plate principle (either standard or embedded types) can be used. An anti-cavitation check valve between the motor's inlet and outlet ports can be integrated into the hydraulic line or directly into the motor's port plate [34,35].

This system is as shown in figure 18 mainly used in machinery requiring fan power above 10 to 15 kW, such as cranes, excavators, loaders, heavy-duty transport vehicles, and locomotives.

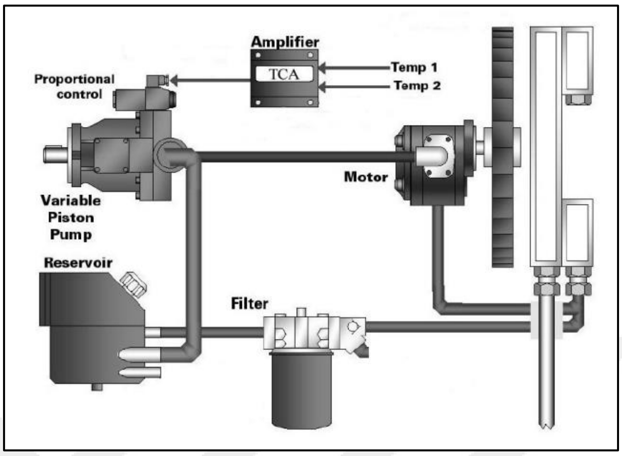


**Figure 18**: Variable Displacement Pump and Motor[34,35]

### 1.7.2.Reversible Fan

Machines operating under heavy load conditions are frequently exposed to harsh environmental factors, particularly dusty working environments, which can significantly impair the performance of their cooling systems. Dust accumulation in air filters, radiators, and across heat exchange surfaces can reduce heat transfer efficiency and, if left unaddressed, may lead to engine overheating. To mitigate this problem and maintain the effectiveness of the cooling system, reversible fan technology has been developed as a low-cost, effective solution for periodic self-cleaning of the radiator. The primary function of the reversible fan is twofold: it provides airflow for radiator cooling in one direction, and periodically reverses airflow to dislodge and expel accumulated dust from the radiator surface. This dual-direction fan mechanism not only enhances cooling efficiency but also reduces the need for manual maintenance and cleaning interventions.The system architecture includes a fixed displacement hydraulic pump, a fixed displacement fan motor, and a directional control valve integrated with a dedicated hydraulic distributor. To avoid damage during sudden direction changes at high fan speeds, a variable displacement pump is placed upstream of the directional valve, allowing the system to gradually reduce fan speed before reversal.

This design eliminates the need for an additional speed adjustment valve and prevents power loss due to oil being discharged through a pressure relief valve. However, one limitation of this setup is that the maximum operating pressure of the directional control valve restricts overall system performance when compared to conventional closed-loop hydraulic fan systems.

Despite this drawback, the compactness of the reversible fan design provides space-saving advantages, making it particularly suitable for construction machinery with limited engine bay space [35,36].The working principle of the reversible fan system is illustrated in Figure 19.

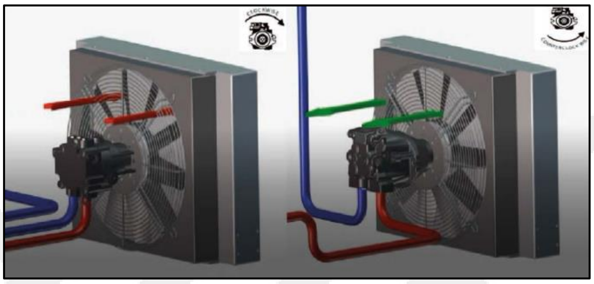

**Figure 19**: Working Principle of Reversible Fan [35,36]

## 1.8.THERMOSTAT

The main purpose of the engine cooling system is to cool the engine and prevent deformities that may arise due to overheating. The cooling fluid used in the engines circulates through the engine jackets, cooling the engine block. However, constantly keeping the engine temperature low can also cause negative effects. A good example of this is when the engine is started in cold weather, as it needs to warm up to a certain temperature to function efficiently. If there is a continuous flow of coolant, it will prevent the engine from warming up, which can damage the engine. Therefore, the flow to the radiator must be limited. This is done by the thermostat. The thermostat is essentially a temperature regulator since it opens and closes according to the need and provides assistance in cooling the system. As the coolant circulates through the engine jackets, the heated fluid, due to heat transfer between the engine block and the coolant, exits the engine. If the fluid is not at the set temperature, the thermostat opens to allow the fluid to flow to the radiators to cool down. After cooling, the fluid returns to the system to cool the now-heated engine [36,37].The working principle of thermostat for two Engine conditions as Show in Figure 20.

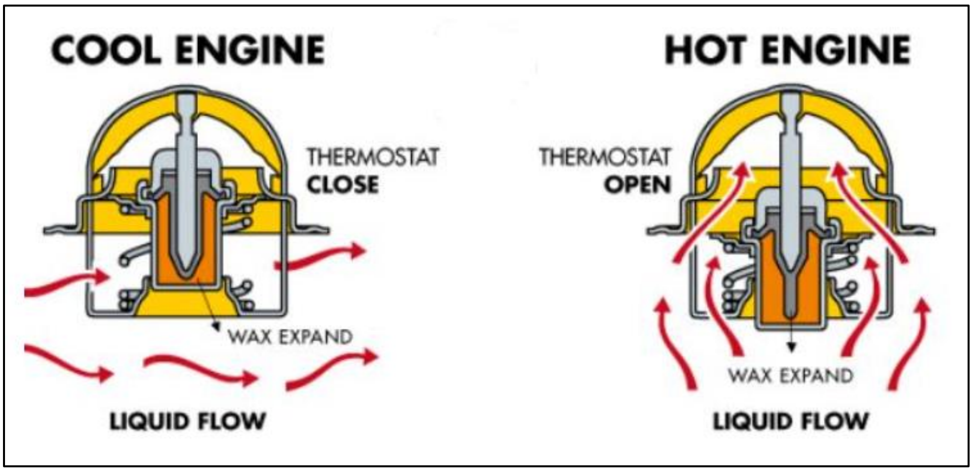


**Figure 20:** Working principle of Thermostat

## 1.9.PURPOSE AND SCOPE OF THE STUDY

The primary objective of this thesis is to optimize under-hood airflow in excavators by enhancing ventilation design. This is achieved by implementing air intake and exhaust vents on both the intake side (where the air filter and radiator are located) and the exhaust side (where exhaust and hydraulic pump components are positioned). These modifications aim to improve cooling effectiveness by ensuring balanced airflow across thermally critical engine zones.

To evaluate performance:

- Temperature measurements will be taken on the engine and surrounding components.
- Optimal heat transfer conditions will be identified through comparison.
- External noise levels resulting from the modified vents will be assessed in accordance with the ISO 6395 standard for construction machinery noise measurement [38].

The study will include four different vent configurations, and for each:

- Thermal performance and
- Sound pressure levels will be measured.

The goal is to determine the most efficient configuration, balancing effective cooling performance with acceptable noise emissions.

# CHAPTER II
# EXPERIMENTAL METHODS

## 2.1. EXPERIMENTAL SETUP FOR UNDERHOOD AIRFLOW EVALUATION

Construction machinery operates under harsh environmental conditions and demands high engine performance to ensure continuous and efficient operation. During field use, engine performance is influenced not only by external environmental factors such as dust, temperature, and terrain, but also by the design and spatial arrangement of components under the hood.

This thesis focuses on the experimental evaluation of under-hood airflow in construction machinery—specifically excavators—and assesses the effectiveness of ventilation-based improvements. A comparison is made between the baseline configuration and modified versions in terms of thermal and acoustic performance.

Construction equipment typically utilizes a combination of air-cooled and liquid-cooled systems for engine and component temperature management. To support airflow within this system, air intake and exhaust vents are strategically placed on the top surface of the hood and on the side panels. These vents play a vital role in:

- Enhancing heat dissipation under the hood,
- Reducing the risk of engine overheating,
- Improving engine efficiency, and
- Ultimately contributing to lower fuel consumption.

However, while these openings improve cooling performance, they may also lead to increased noise emissions, particularly in high-performance engines. To address this issue, acoustic insulation foams are applied beneath the hood. While these foams are effective at absorbing sound and thermal radiation, they may also impede heat transfer, potentially trapping heat in the engine compartment.

Given these conflicting effects, it is crucial to optimize vent placement and verify the system’s performance through systematic measurements of both thermal and acoustic parameters. The following core experimental evaluations were conducted to analyze the effectiveness of the modifications:

- Intercooler Pressure Difference Measurement
- Exhaust Back Pressure Measurement
- Measurement of Air Intake Pressure
- Measurement of Underhood Cooling Performance
- Measurement of External Noise of the Excavator

Each of these measurements is discussed in detail in the subsequent sections.

To ensure accurate and meaningful data collection, specific measurement points were identified and instrumented throughout the system. The critical zones selected for data acquisition include the following:

- Measurement Points in the Intercooler Pressure Difference Measurement
- Measurement Points in the Exhaust Back Pressure Measurement
- Measurement Points in the Air Intake Pressure Measurement
- Measurement Points in the External Noise Measurement
- Overheated (Cooling Performance) Measurement Points
- Heat Damage Measurement Points

These measurement locations represent the most significant points in the system where performance losses, thermal accumulation, or noise emissions are most likely to occur. Detailed illustrations and descriptions of each point are provided in the corresponding subsections.You can see the flowchart summarizing the experiment in Figure 21.

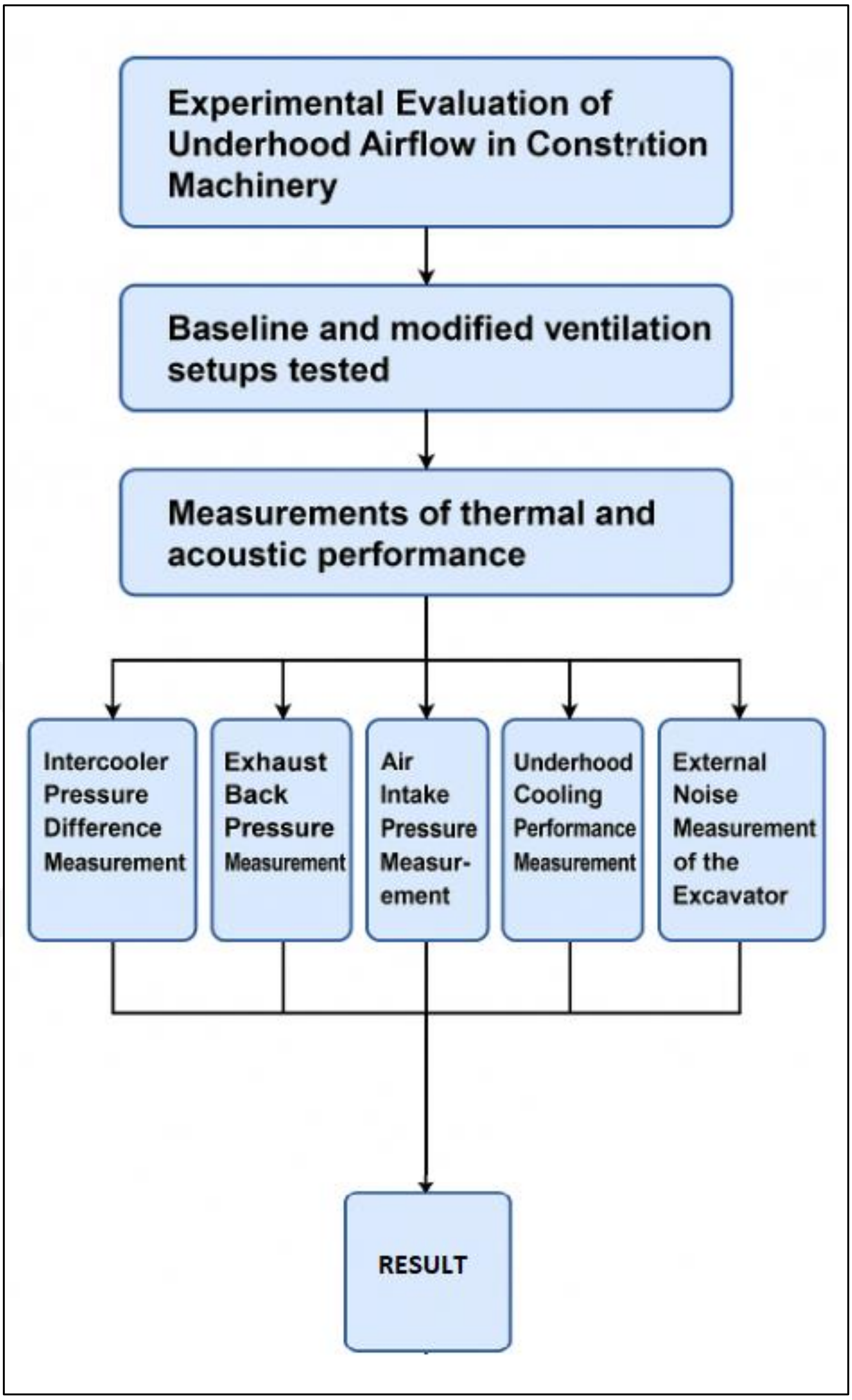


**Figure 21:** Flowchart

*Objective and Scope of the Test*

Experimental evaluation of airflow in the engine compartment (underhood) of construction machinery, focusing on improving cooling and acoustic performance. Pressure measurements are taken across the intercooler, exhaust system, and air filter, alongside engine cooling capacity and external noise levels.

*Pre-Test Preparations*

- Cooling system checks: Radiator fluid level, antifreeze concentration (50%), and air bleeding (purging) are performed.
- Hydraulic oil level control and viscosity verification at operating temperature (>50°C).
- Thermocouple calibration and proper placement to avoid direct contact with hot components.
- Calibration of data acquisition devices (Hexa, SCADAS XS) and manometers is completed.

*Engine Load Setting and Application*

- Engine load is increased stepwise to 70%, 75%, and 80% via the machine's control panel using the P-Q test screen and stabilized at each level.
- Pump current and hydraulic arm relief mode are adjusted accordingly.

*Pressure Measurements*

- Intercooler Pressure Difference: Measured with manometers at the intercooler inlet and outlet to verify pressure drop remains within manufacturer limits.
- Exhaust Back Pressure: Measured digitally between turbocharger and muffler; high back pressure indicates flow resistance that should be minimized.
- Air Intake Pressure: Measured before the air filter to assess filter resistance; pressure values should stay below defined thresholds.

*Underhood Cooling Performance Measurement*

- Tests conducted at high ambient temperatures.
- Engine operated at full load and maximum RPM (HP mode), with the duty cycle: 45 minutes active + 10 minutes idle + 45 minutes active operation.
- Thermocouples continuously record temperatures of engine components and airflow.
- Ambient and radiator inlet air temperatures are compared and corrected.
- Cooling fan runs at constant flow rate; effects of air density (temperature, pressure, humidity) are considered.

*External Noise Measurement*

- Sound pressure levels measured according to ISO 6395 standard, using dB(A) units.
- Three calibrated microphones positioned around the machine capture noise during operational cycles (digging, dumping, turning).

- Each cycle repeated three times; the difference between consecutive noise measurements should be less than 1 dB(A).
- Data logged via SCADAS XS system in real time.

*Data Collection and Analysis*

- All pressure, temperature, and noise data are digitally recorded.
- Interpolation is used to estimate parameters at 100% engine load.
- Measured values are compared against manufacturer-specified limits.
- Relationships between cooling performance, acoustic data, and pressure parameters are analyzed.
- Effects of design modifications (e.g., ventilation hole placement, sound insulation materials) are reported.

### 2.1.1. Intercooler Pressure Difference Measurement

Connection points are prepared on the intercooler inlet and outlet pipes at locations specified by the engine manufacturer for accurate pressure measurement using a manometer. One end of the manometer is connected to the inlet-side port, while the other end is connected to the outlet-side port. The engine is gradually loaded to designated levels—typically 70%, 75%, and 80% of full load—and at each load level, a 10-minute test is conducted while recording the pressure values.

Following the data collection, interpolation techniques are used to estimate the pressure drop at 100% engine load, which is then compared to the maximum allowable limit defined by the engine manufacturer. This limit may vary depending on the specific engine model and application.

Engine loading is performed by accessing the P-Q test screen on the digital control display. During this process, the machine's arm attachment is kept in relief condition, and the pump current is gradually increased until the desired engine load percentage (70%, 75%, or 80%) is reached and stabilized. Under these test conditions, the differential pressure across the intercooler is monitored using the manometer.
The measured pressure drop must remain below the manufacturer's threshold to ensure proper system performance and to avoid performance degradation due to intercooler flow resistance.

To obtain reliable and precise differential pressure readings, the Manometer, shown in Figure 22, isused. . The manometer  is a highly accurate and user-friendly differential pressure manometer, ideal for both industrial and laboratory settings. It allows users to select from 11 different pressure units, enabling flexible data interpretation. The device offers a measurement range of 0 to 344.7 mbar, with an accuracy of ±0.2% FS and a resolution of 0.1 mbar, making it suitable for precise intercooler pressure evaluations. Its straightforward interface and robust performance make it a dependable tool for field measurements in construction machinery applications.

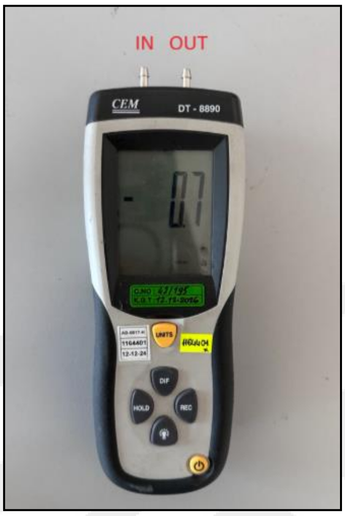


**Figure 22:** Manometer

### 2.1.2. Exhaust Back Pressure Measurement

The aim of this test is to determine whether the back pressure created by the exhaust system remains within the allowable limit specified by the engine manufacturer. For this purpose, a pressure measurement point is prepared at the location specified by the manufacturer, between the turbocharger and the exhaust muffler. One end of the digital manometer is connected to this point, while the other end is left open to atmospheric pressure. The pressure reading is recorded while the engine operates under manufacturer-specified conditions. Measurements are taken in HP mode at 70%, 75%, and 80% engine load, with each test lasting 10 minutes. Using the collected data, interpolation is applied to estimate the back pressure at 100% engine load, which is then compared to the manufacturer’s threshold value.

Engine load adjustments are made via the P-Q test screen on the machine interface. During the test, the machine arm is held in relief position, and the pump current is gradually increased until the engine load is stabilized at 70%, 75%, and 80% (Figure 23). Additionally, it is verified that the hydraulic oil temperature exceeds 50°C, ensuring appropriate viscosity conditions for consistent results.

The engine loads applied during the three main experimental tests—including intercooler, exhaust, and intake pressure measurements—are illustrated in Figure 22. As shown, these loads were configured using the machine’s control system via the P-Q test interface, with load levels gradually set to 70%, 75%, and 80% while the hydraulic system remained in arm relief mode.

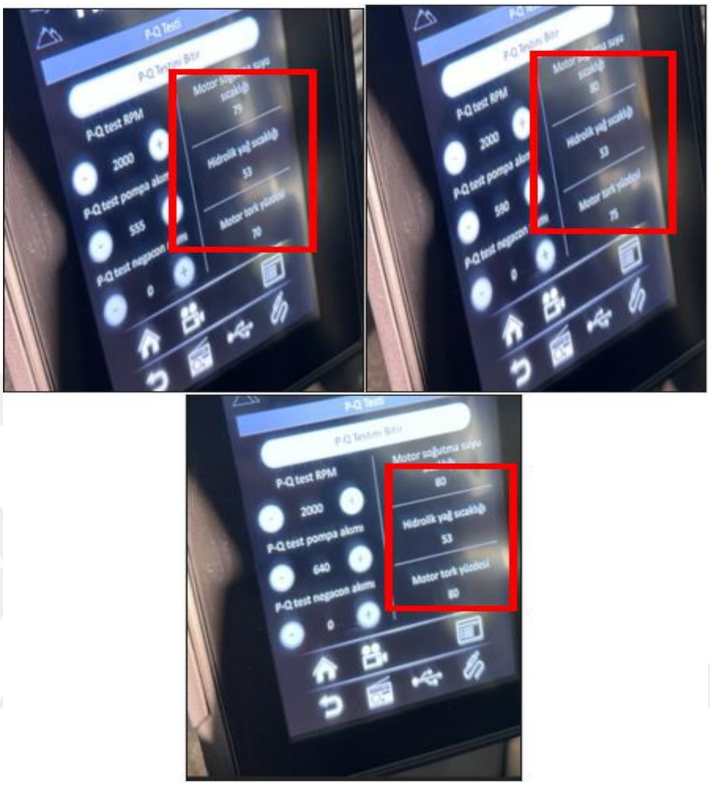


**Figure 23:** P-Q Test Screens(Engine Load %70/75/80)

### 2.1.3. Air Intake Pressure Measurement

The aim is to measure the resistance of the engine air filter and the airflow supplied to the engine and to examine whether these values remain below the limit values specified by the engine manufacturer. The excavator is operated until it reaches normal working conditions. One end of the digital manometer is placed as close as possible to the air filter.The other end of the manometer remains open to the atmosphere. The pressure value on the manometer is read while the engine is running at maximum RPM under load (in relief condition).The measured value must be lower than the permitted value. Based on the tests conducted at specified load levels, interpolation is applied to determine the pressure at 100% load in the machine's working condition. This value is then added to the engine mapping list and checked for complianceas given in Figure 24.

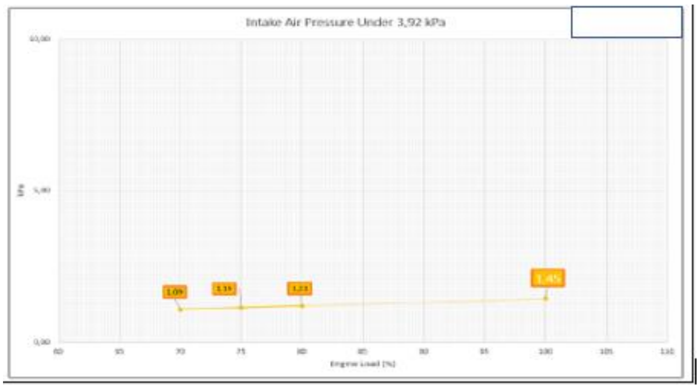


**Figure 24:** Combustion Air Graph(Sample)

### 2.1.4. Underhood Cooling Performance Measurement

In hot weather conditions, the engine components of construction machinery are at risk of thermal overload due to elevated ambient temperatures. To mitigate this risk and assess the effectiveness of the cooling system, performance tests must be conducted under the most demanding operating conditions.

Prior to testing, several pre-operational checks must be performed to ensure the accuracy and consistency of the results:

- The hydraulic oil level should be verified at the attachment position specified in the machine's user manual (Figure 25). The oil level must be above the red line.
- The radiator must be completely filled with coolant, and all air pockets within the system must be purged to ensure proper circulation.
- The coolant mixture should contain 50% antifreeze to ensure thermal stability and prevent boiling at elevated temperatures.
- The fuel tank must be sufficiently filled to allow for uninterrupted testing.
- The hydraulic pump flow settings should be checked and adjusted to manufacturer-specified values.
- The functionality and accuracy of both the engine control unit (ECU) software and the display panel must be confirmed.
- The thermostats in the cooling system should be set to the open position to allow maximum coolant flow.
- The hot water line to the cabin heating system should be closed, preventing coolant from circulating through the heating circuit. This step ensures that the coolant remains concentrated within the engine cooling loop, enabling the

system to reach higher operating temperatures, which are critical for assessing worst-case thermal performance.

These preparatory steps establish a controlled and consistent testing environment to accurately evaluate underhood airflow and cooling performance under thermal stress conditions.

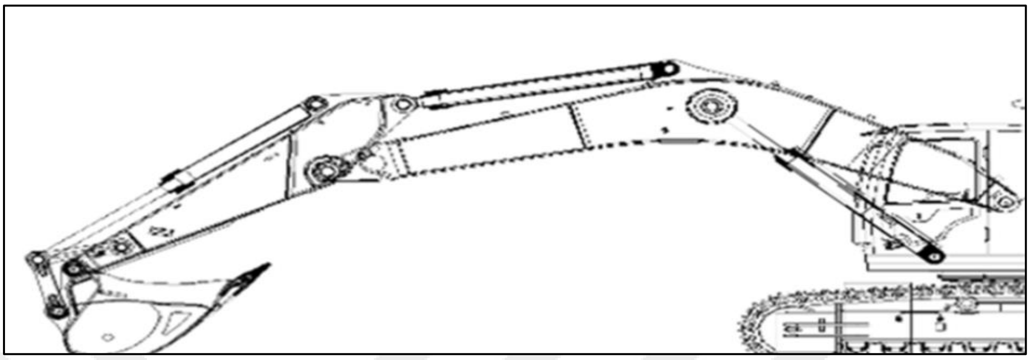

**Figure 25:** Attachment Position for hydraulic oil check

Prior to the test, the accuracy and functionality of all thermocouples to be connected to the machine must be verified. The data logging device should be configured to record at a frequency of one sample per second. After connection, thermocouples must be securely fixed to prevent contact with hot surfaces that could cause damage or lead to erroneous readings. When measuring air temperature at a specific location, thermocouples should be positioned so that they are not in contact with nearby heated components, ensuring that they record the true air temperature only.

The engine load and other operational parameters should be collected via the CAN-bus system, using the Hexa device. At both the beginning and end of the test, ambient air temperature should be recorded using a digital thermometer, positioned in the shade, approximately 10–15 meters away from the machine to avoid thermal interference. This value should then be compared to the temperature measured in front of the radiator. If a significant difference is observed, the ambient temperature will be assumed to remain constant throughout the test, and the shaded digital thermometer reading will be used for all calculations.

Before testing, ensure that all engine lower plates and hood panels are properly installed, as missing components may influence airflow. Additionally, the battery level of the data acquisition system must be checked and confirmed to be sufficient for the full duration of the test.

If available, the air conditioning system should be activated during the test, set to the lowest temperature and maximum fan speed, to replicate realistic working conditions. Thermocouples must be connected to the data logger, and it must be verified that data recording is active throughout the test. Under no circumstances should the battery be removed during recording, as this can cause irreversible data loss**.**

The tests should be conducted in HP mode at maximum engine speed (RPM)**.** Each test run consists of 45 minutes of active operation, followed by a 10-minute idle period at approximately 900 RPM, during which the machine is kept running. After the idle period, the excavation cycle is repeated for another 45 minutes to validate and cross-check the recorded data.

The data logger should be mounted securely on the machine in a location protected from hydraulic oil, water, dust, or other potentially damaging substances. Throughout the test, continuous excavation should be performed as consistently as possible. The operation should involve repetitive digging and dumping at a depth or height equivalent to approximately three bucket levels (Figure 26), avoiding deep trenching or atypical load cycles.

**Figure 26:** Excavating Position

The cooling capacity of a radiator is directly related to the mass flow rate of air passing through it, typically expressed in [kg/s]. While the cooling fan operates as a volumetric device—delivering a constant volume of air under all conditions—the mass of air in this volume varies depending on air density.

Air density decreases under the following conditions:

- Increasing ambient temperature,
- Decreasing atmospheric pressure (e.g., at higher altitudes),
- Increasing humidity.

As a result, even though the fan blows the same volume of air, the effective cooling may be reduced in hot, humid, or high-altitude conditions due to lower air mass and consequently diminished heat transfer capability.

To ensure accurate evaluation of the cooling system under demanding conditions, the machine should be operated at maximum working intensity during the excavation phase. The average engine load should be maintained in the range of 77% to 80% throughout the test.

Upon completion of the test, the measured thermal data should be compiled into a summary table, structured similarly to Figure 27, to allow for clear analysis and comparison of key performance parameters.

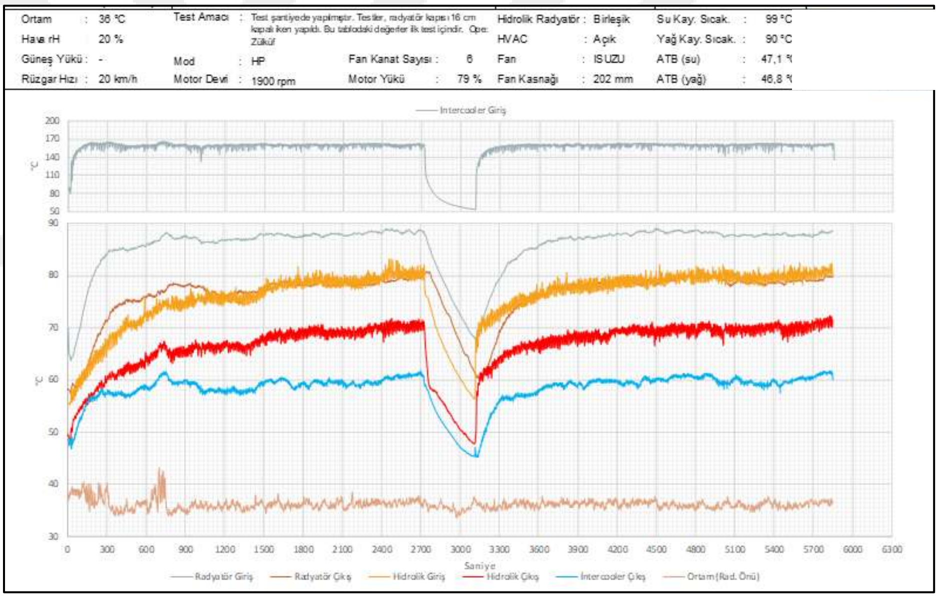


**Figure 27:** Summary figure of thermal performance data during excavation.

Following the completion of the excavation tests and the compilation of the performance data, a detailed evaluation of the thermal behavior of the cooling system is conducted. To quantitatively assess how close the system operates to critical thermal thresholds, the Air to Boil (ATB) calculation method is applied. This parameter provides a clear indication of the thermal margin remaining before the coolant or hydraulic oil reaches its maximum allowable temperature.

To evaluate the thermal safety margin of the cooling system, the Air to Boil (ATB) value is calculated using the following approach

- First, the test data graphs are reviewed to identify the interval during which the machine reaches thermal equilibrium. Within this steady-state range, the average temperature values for both coolant and hydraulic oil are determined.
- Based on these averages, the ATB is calculated separately for the coolant and the hydraulic oil using the relevant formulas provided below.
- The maximum allowable temperature values used in the ATB calculation are defined as follows:
- Coolant:99°C for Tier 3A machine, 95°C for Tier 3B and Tier 4 Final machines
- Hydraulic Oil: • 90°C for all machine types

The ATB value represents the temperature margin between the measured fluid temperature and its allowable limit, serving as a key indicator of whether the cooling system operates within safe thermal boundaries.

$$ATB = TBP - (TCI - TAI) \tag{2.1}$$

where,

**TBP**: Boiling point of the coolant depending on temperature and altitude (°C),

**TCI**: Coolant radiator inlet temperature (°C) and

**TAI**: Ambient temperature (°C) value.

**Example calculation for the table above:**

- **ATB(water)** = 99 – (88.2 – 36.3) = 47.1°C
- **ATB(oil)** = 90 – (79.5 – 36.3) = 46.8°C

**Note**: The ATB values indicate the maximum ambient temperature at which the machine can operate smoothly. This value is at least 46°C for the test machine. The intercooler outlet air temperature, shifted to a 25°C ambient temperature, should be determined to be below the following values:

$$T_{intercooler,out}^{25°C} < \begin{cases} 50°C, & Tier3A \\ 45°C, Tier3B\ and\ Tier\ 4\ Final \end{cases} \tag{2.2}$$

When reviewing the results, it is essential to specify the average engine load corresponding to the period in which the temperature values are averaged. This ensures that the calculated ATB values are accurately contextualized in relation to the engine's operational intensity, providing a more reliable basis for performance evaluation.To support precise temperature data acquisition throughout the test, the Graphtec data logger was utilized (Figure 28). This portable, high-capacity logging device is wellsuited for industrial testing environments due to its compatibility with a wide range of sensors and its modular, expandable input structure, accommodating up to 20 channels**.** The GL840 offers a fast sampling rate of up to 1 ms, enabling accurate tracking of rapid thermal changes. It supports various sensor types including thermocouples, voltage, current, and resistance sensors, and allows for data communication via USB or wireless connectivity. Equipped with a user-friendly LCD screen interface, the device is commonly employed in temperature monitoring**,** vehicle engine testing**,** industrial system diagnostics, and environmental data collection. In this study, it played a key role in recording thermal data with high resolution and reliability.


**Figure 28:** Graphtech Measurement Device

K-type thermocouples are widely used temperature sensors that can operate over a broad temperature range. They are made of Nickel-Chromium (Ni-Cr) and Nickel-Aluminum (Ni-Al) alloys. The operating range is from -200°C to +1350°C, offering high accuracy and fast response times. They are also resistant to oxidation and can directly contact metal surfaces for temperature measurement. K-type thermocouples are commonly used in a wide range of applications, including measuring the temperature of engine components, monitoring temperature in electrical panels, temperature control in metallurgy and glass industries, and temperature monitoring in HVAC systems.It’s shown in Figure 29(a).

J-type thermocouples, on the other hand, provide higher accuracy, especially at lower temperatures. They are made from Fe-CuNi (Iron-Copper-Nickel) materials. The operating range is from -40°C to +750°C, and they offer fast response times.

However, they are more sensitive to oxidation and are specially designed for immersion use. J-type thermocouples are widely used for temperature measurements in liquid and gas environments, in the chemical and food industries, in steam boilers and industrial processes, and for fuel and oil analysis.It’s shown in Figure 29(b).

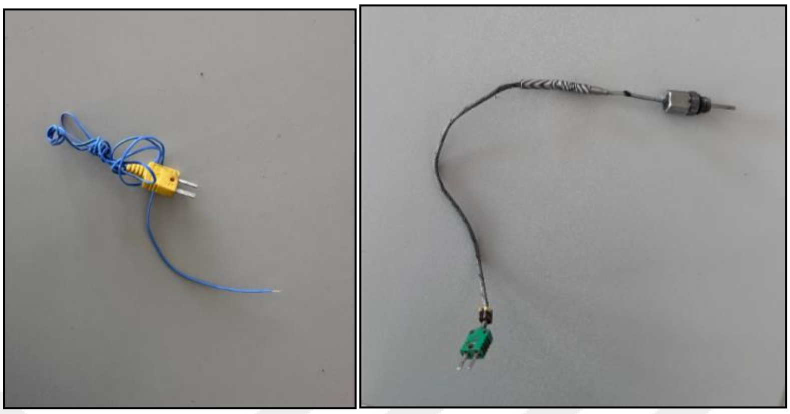

**Figure 29**: (a) K-type thermocouple (b) J-type thermocouple

HEXA is a testing device used to analyze the load condition of construction machinery and motorized equipment, playing a crucial role in engine performance evaluations. It offers real-time engine load monitoring, torque and power measurement capabilities, and is compatible with industrial data loggers. Equipped with high-accuracy sensors, HEXA is widely used for construction machinery motor load analysis, engine efficiency testing, overload detection, preventive maintenance, and engine performance evaluation in the construction and mining sectors.It’s shown in Figure 30.


**Figure 30:** Hexa-Engine Load Measurement Device

### 2.1.5 External Noise of the Excavator Measurement

Excavators emit noise during operation due to their engine and mechanical components. To prevent adverse effects on both the operator and individuals in the surrounding area, this noise must comply with specific standards. The conditions defined in the ISO 6395 standard must be met to ensure environmental and occupational health[38].

ISO 6395 provides standardized guidelines for measuring noise levels emitted by motor vehicles and machinery. It outlines specific test methods and measurement conditions, particularly for mobile equipment such as construction and agricultural machines. The goal of the standard is to minimize safety, health, and environmental risks caused by noise emissions by offering a consistent testing framework under defined operating conditions.

Technicians conducting the test must hold a valid excavator operation certificate. Measurements must be taken in an open area, with the machine positioned on a hard surface such as asphalt or concrete. The test environment must remain acoustically consistent; thus, the positions of reflective surfaces such as nearby structures or materials must not be altered.

Measurements must not be conducted during precipitation (rain, snow, etc.). If snowfall has recently stopped, the area within the measurement radius must be cleared before testing. Testing should also be avoided when:

- Air temperature is below –10°C or above +35°C,
- The test surface is covered with snow,
- Wind speed exceeds 8 m/s.

If the wind speed is above 1 m/s, a microphone windscreen must be used to reduce interference. During the test, environmental conditions such as temperature, humidity, and wind speed must be recorded. Additionally, the machine must be equipped with a bucket, and climatic parameters (e.g., humidity, temperature, pressure) must be within the acceptable range specified by the measurement device manufacturer.


**Figure 31:** Measurement Area

To begin the test, the machine is brought to a stationary position, and ambient noise is recorded from all microphones for approximately 15 seconds.The test are as shown in Figure 31.The resulting ambient noise level must be at least 10 dB(A) lower than the machine's operational noise measured during the test. In machines equipped with a hydraulic fan, which operates independently of the engine, the fan speed must be fixed at 70% of its maximum value throughout the test procedure.

According to ISO 6395, the noise emission test for excavators consists exclusively of the digging cycle. During this test [38]:

- Three microphones are positioned at designated measurement points, with the microphone tips oriented toward the center of the machine.
- After the initial measurements are completed from these three points, the machine is rotated 180°, and measurements are repeated from the opposite set of points.
- For each configuration, the machine must remain positioned at the center of the measurement circle (Figure 30), and the engine should be running at maximum RPM.

The test cycle involves the following sequence:

- The machine performs a digging simulation at its current position.
- It then rotates 90° to simulate the dumping operation.
- It finally returns to the original position to complete one cycle.

This sequence is performed three times at maximum engine speed. However, the hydraulic system pressure must remain below the relief pressure limit, ensuring that the system operates without triggering pressure relief valves.

Measurements begin with the initiation of the first digging cycle and conclude after the completion of the third cycle. All noise level readings are recorded for each microphone.

To ensure data consistency and repeatability, the test for each set of measurement points is only considered valid if three consecutive readings are obtained for each microphone with a variation of less than 1 dB(A) between them.To ensure accurate and standard-compliant data collection during the ISO 6395 noise measurements described above, the following device was used[38]:

The Siemens SCADAS XS is a compact data acquisition system designed for measuring noise emissions from industrial machines and equipment. The device interfaces with microphones and various sensors to collect data on environmental noise, vibration, temperature, and pressure with high precision, and transmits this data to a computer or external processing systems.

SCADAS XS streamlines the data collection and analysis process, particularly in tests requiring compliance with standards such as ISO 6395. The acquired data is processed using user-friendly software**,** which enables efficient analysis and reporting of the test results.

Thanks to its rugged and compact design, the SCADAS XS operates effectively in field environments and integrates smoothly with various sensor and microphone types**,** ensuring both data accuracy and test reliability**.**The device used in the experiment is shown in Figure 32.


**Figure 32:** Siemens Scadas XS

The SCADAS XS system works in coordination with high-precision microphones to ensure reliable noise measurements. These microphones, used in noise tests, are designed to operate with high accuracy in capturing both environmental noise and machine-generated emissions. They are positioned at specific distances and angles relative to the machine under test, with the microphone heads oriented toward the sound source or the center of the machine. To ensure measurement reliability, each microphone is calibrated prior to testing.During the test, the microphones record sound pressure levels in dBA, and the data is transmitted to the SCADAS XS unit for logging and subsequent analysis. To prevent interference from environmental factors such as wind, appropriate microphone covers (windscreens) are used when necessary.Proper placement, orientation, and calibration of the microphones are essential for obtaining accurate and repeatable measurement results. The microphones used in this study are shown in Figure 33**.**

**Figure 33:** Microphone

To ensure the validity and reliability of the noise measurements, each microphone must undergo a calibration process prior to testing. A calibration level of 94 dBA is commonly used as a reference standard in noise measurement applications.The calibration vehicle is shown in figure 34.

During this process, a sound calibrator is attached to the microphone to verify that the instrument reads the reference value accurately. The calibration confirms that the microphone's sensitivity is aligned with the expected standard and that the device will produce accurate and consistent measurements during testing.

By verifying that the measured sound level matches the 94 dBA reference, the calibration process ensures the integrity of all recorded data. Proper calibration is therefore essential for maintaining measurement accuracy**,** compliance with standards**,** and the overall validity of the test results.

**Figure 34:** Sound calibrator for microphone sensitivity at 94 dBA reference.

## 2.2. MEASUREMENT POINTS IN THE EXPERIMENT

The selection of measurement points within the scope of this study was based on areas where maximum thermal or acoustic effects are observed during machine operation. These critical points were determined in collaboration with, and verified by, the engine supplier, ensuring alignment with manufacturer specifications and performance-critical zones. Detailed descriptions of the identified measurement points for each specific test are provided in the following sub-sections.The flowchart related measurement points are shown in figure 35.

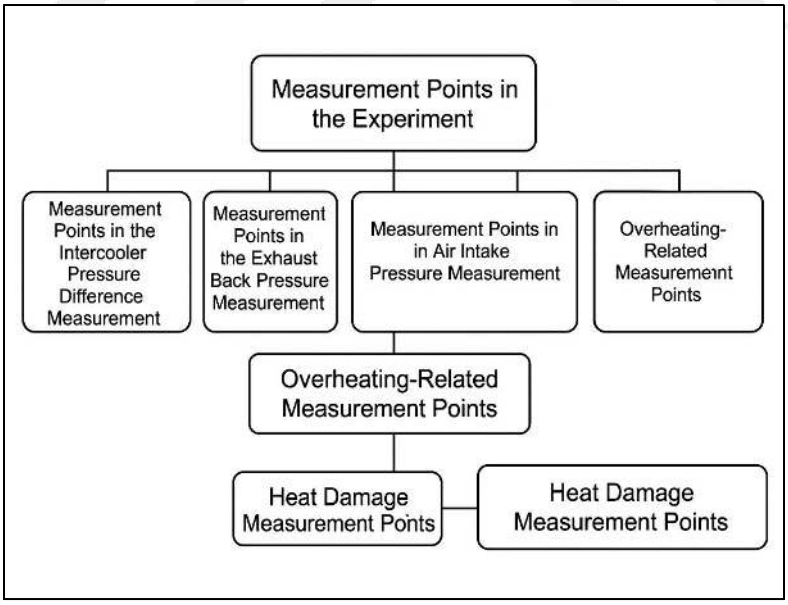


**Figure 35:** Flowchart of the Measurement Points

### 2.2.1.Measurement Points in the Intercooler Pressure Difference Measurement

The measurement points shown in Figure 36, labeled as "Intercooler In" and "Intercooler Out," are selected to monitor the pressure across the intercooler system.

The intercooler cools compressed air before it enters the engine, improving both efficiency and power in turbocharged or supercharged systems. Temperature and pressure readings at these points indicate the intercooler's performance. Deviations may suggest issues such as blockage, leakage, or damage. Regular monitoring of these points helps ensure optimal engine performance and prevent potential failures.

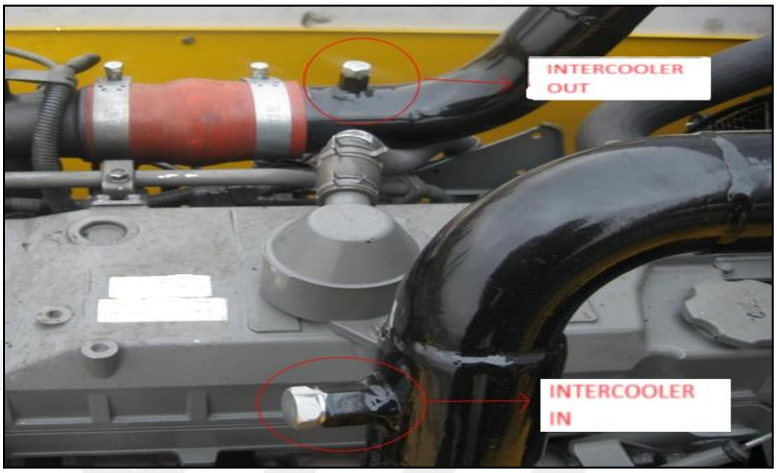


**Figure 36**: Intercooler Pressure Drop Measurement Points

### 2.2.2.Measurement Points in the Exhaust Back Pressure Measurement

The Exhaust Back Pressure Measurement Point, shown in Figure 37, is used to measure the resistance encountered by exhaust gases as they exit the combustion chamber. This back pressure can significantly impact engine performance and efficiency. Regular monitoring is essential to maintain optimal engine operation and to detect potential issues early.


**Figure 37:** Exhaust Back Pressure Measurement Point

### 2.2.3.Measurement Points in the Air Intake Pressure Measurement

In construction machines, fresh air from the outside passes through a pre-filter and then a secondary air filter before reaching the intake manifold. As the air pressure changes across these filters, the most accurate measurement should be taken as close as possible to the intake manifold. This measurement point is shown in Figure 38.

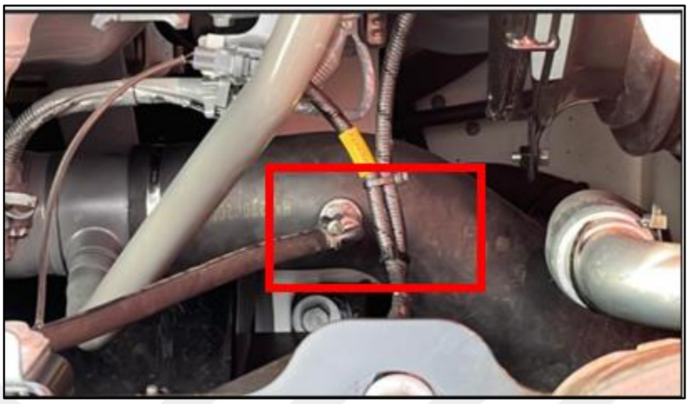

**Figure 38:** Measurement Point of Air Intake Pressure

### 2.2.4. Measurement Points in the External Noise Measurement

For excavators with a boom length (L) less than 4 meters, the 6 measurement points shown in Figure 39 (10 m radius) are used. For boom lengths between 4 and 8 meters, the measurement points shown in Figure 40 (16 m radius) apply. All dimensions are given in millimeters.

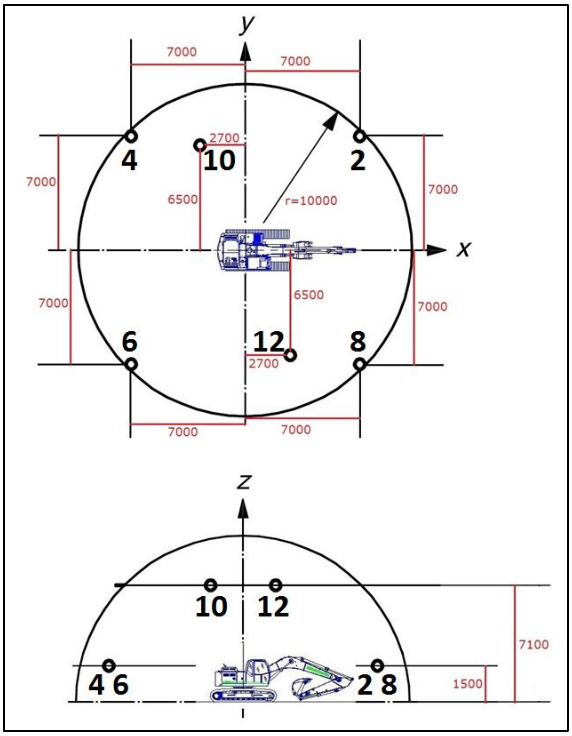


**Figure 39**: Measurement Points for 10m radius

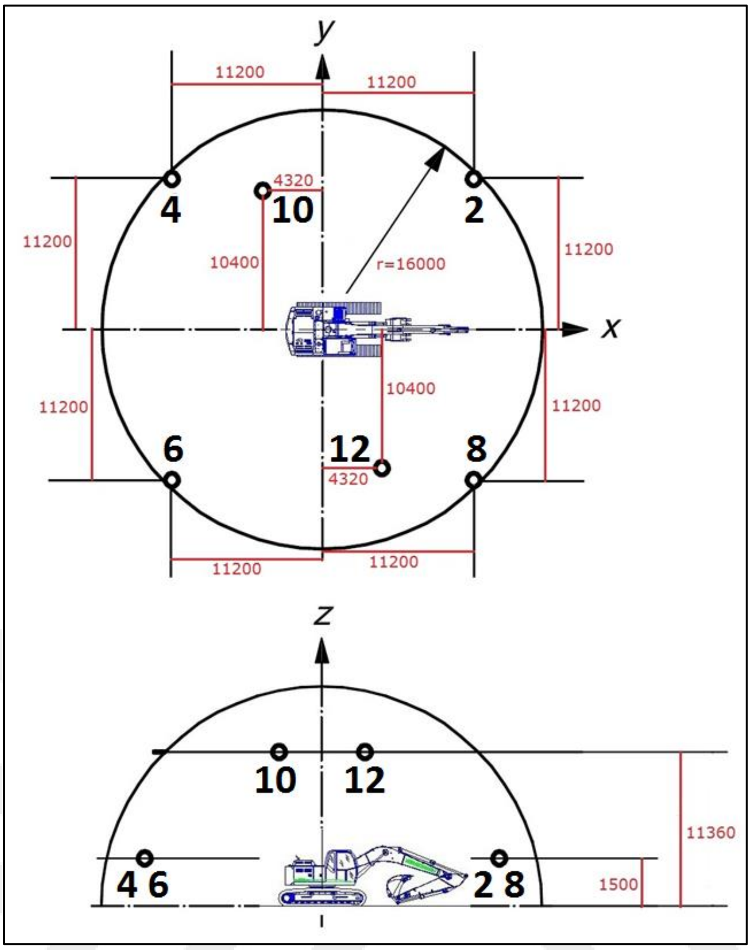


**Figure 40:** Measurement Points for 16m Radius

We can address the temperature measurement points under the hood in two main categories:

### 2.2.5. Overheating-Related Measurement Points

J-type thermocouples are used to take measurements from key points in the cooling system, covering both air and liquid cooling components. These points include the inlet and outlet of the water radiator ,hydraulic oil cooler, intercooler and the ambient temperature. Ambient temperature, measured in front of the radiator as shown in Figure 41, plays a critical role in evaluating cooling performance, as it directly influences heat transfer within the engine compartment. According to engine supplier specifications, ambient temperature readings are offset to 42°C and 46°C (if the actual temperature is below these values), where 42°C represents a reference for regions far from the equator, and 46°C reflects optimal climatic conditions.

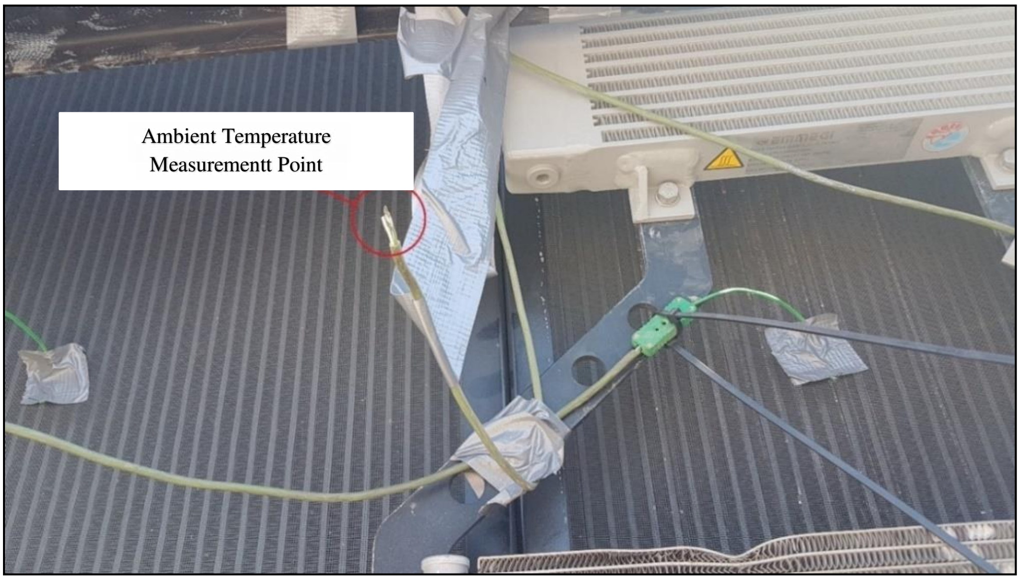


**Figure 41:** Ambient Temperature Measurement Point

The liquid cooling system, based on water circulation, is the primary component of the engine cooling system. Water flows through the engine block, is cooled via the radiator and fan, and then recirculated to maintain optimal engine temperature. In this study, temperature measurements were taken at the inlet and outlet of the cooling water radiator to evaluate the impact of air intake and exhaust pathways on the engine compartment. These measurement points are shown in Figure 42.

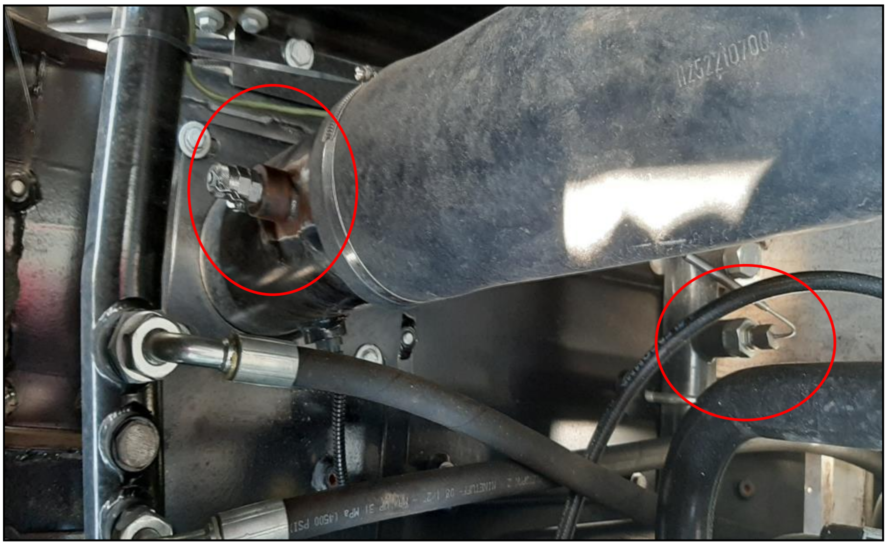

**Figure 42:** Water Cooling Radiator Inlet-Outlet

The intercooler cools the air within the system to prevent damage to vehicle components and maintain engine performance. In turbocharged engines, energy from exhaust gases powers a turbine, which compresses the air, allowing more oxygen to mix with the fuel for combustion. The intercooler cools the compressed air, sending cooler, denser air into the engine cylinders to produce more energy during combustion. This results in higher power and torque. In the study, temperature values were taken from the inlet and outlet of the intercooler to examine the effect of air intake and exhaust pathways on the engine room.It’s shown in Figure 43.

**Figure 43:** Intercooler Inlet-Outlet Points

In excavators, attachments are powered by hydraulic force, and the power transmitted by the pump is delivered to the attachments through the MCV. In this context, the hydraulic oil, which heats up during operation, needs to be cooled. The radiator and fan play a role in this cooling cycle. In the study, temperature values were taken from the inlet and outlet of the hydraulic oil radiator to examine the effect of air intake and exhaust pathways on the engine room.It’s shown in Figure 44.

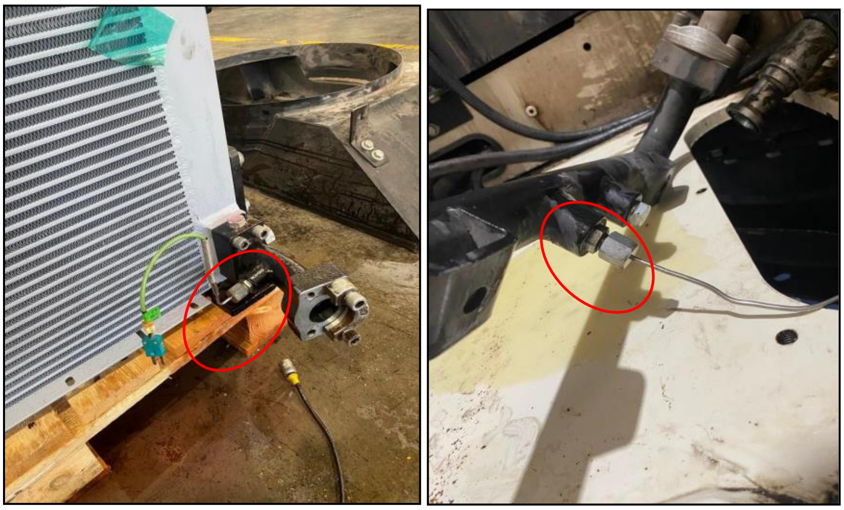

**Figure 44**: Hydraulic Radiator Inlet-Outlet Points

### 2.2.6. Heat Damage Measurement Points

To assess the thermal impact on components located under the hood, measurements are taken using K-type thermocouples at the locations shown in Figure 45. These components include the rubber hose, fan belt, alternator, ECM, starter, and engine harness connection. Each point is surface-exposed to engine room temperatures and exhibits unique thermal behavior due to material properties. Since prolonged exposure to high temperatures can degrade performance, these measurements aim to evaluate thermal effects and airflow conditions beneath the engine. The measurement points were identified and validated by the engine supplier.

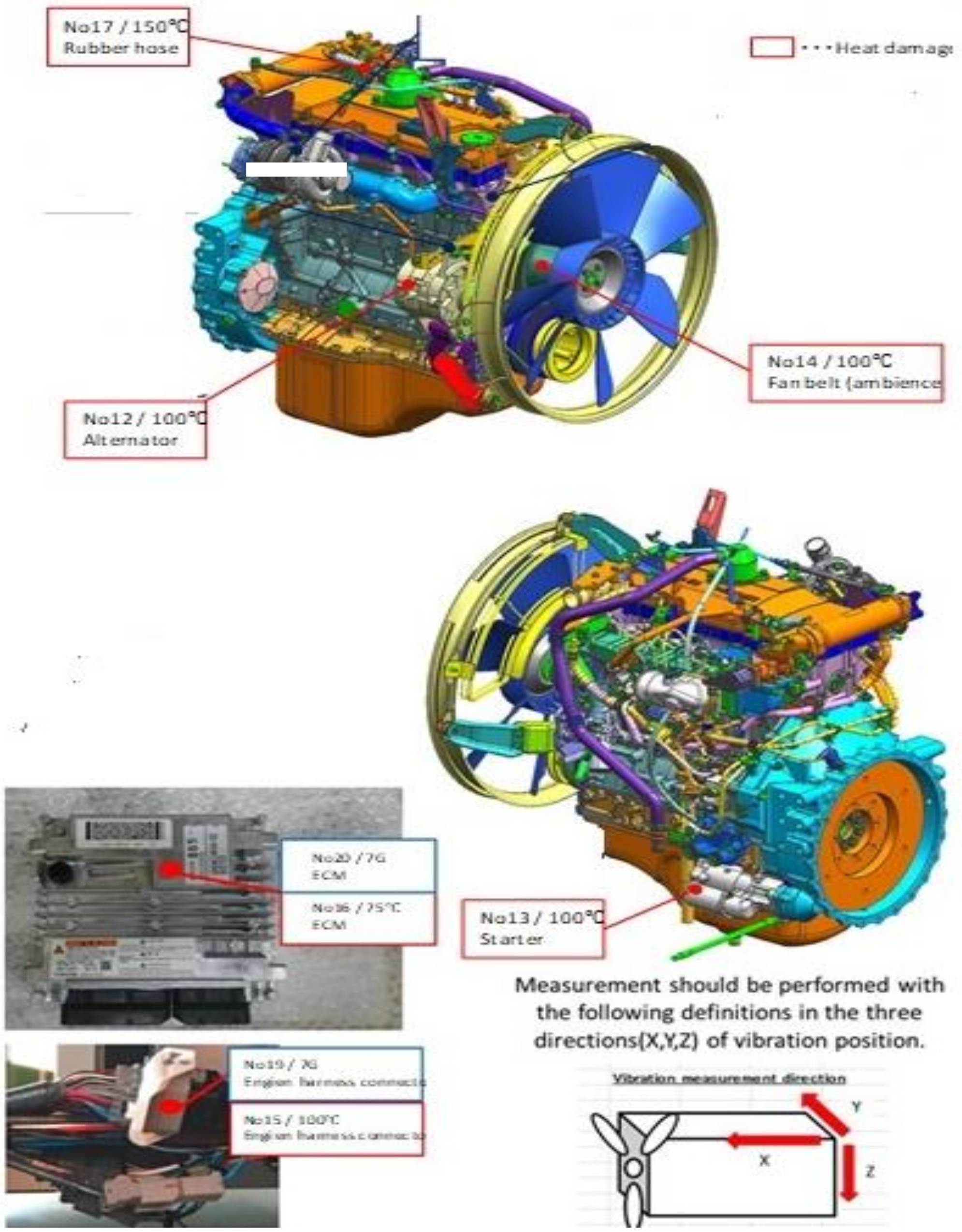


**Figure 45:** Heat Damage Measurement Points

### 2.2.7. Effect of Fan Speed on Cooling Performance

Engine cooling fans are essential for maintaining the engine within its optimal temperature range, thereby ensuring efficiency and extending engine life. Their primary role is to enhance airflow over the radiator, facilitating heat dissipation from the coolant that has absorbed engine heat. While natural convection and vehicle motion contribute to cooling, they may be insufficient under certain climate or operational conditions. In such cases, the cooling fan becomes critical, especially when the vehicle is stationary or moving slowly.

The fan directs air through the radiator fins, improving heat transfer from the coolant to the surrounding air. As the engine runs, coolant absorbs the generated heat and circulates to the radiator, where the fan-driven airflow helps reduce its temperature. This continuous cycle is vital to prevent overheating and to maintain stable engine performance.

In construction machinery such as excavators, operating conditions are typically stationary, resulting in limited heat dissipation through natural convection. In this context, the cooling fan becomes especially critical. Excavator engines and components tend to generate more heat due to demanding work conditions, requiring higher fan speeds—typically between 1800 rpm and 2200 rpm—to maintain effective cooling. The higher the fan speed, the greater the cooling efficiency. However, in some high-tonnage excavators, standard fan capacity may be insufficient, necessitating the use of hydraulic-driven fans to boost airflow and cooling performance.

In addition to speed, the fan's blade structure and pitch are key factors influencing cooling efficiency. To effectively direct airflow, the fan blades must rotate at an optimal angle. Depending on the machine type, the fan pitch in excavators generally ranges between 30° and 45°.

## 2.3.EXPERIMENTAL OBJECTIVES,CHALLENGES,IMPROVEMENTS

To enhance heat dissipation under the hood of excavators in the construction machinery class, various studies have been conducted. In demanding operating conditions, if the heat generated by the engine and components accumulates in the engine compartment, cooling elements must operate at high performance. This increases fuel consumption, accelerates wear on components, and raises operational costs. In some cases especially under extreme climate conditions—this high demand can exceed the capacity of the cooling system, leading to insufficient cooling. The most critical consequence of this is engine overheating due to inadequate heat dissipation or limited airflow from the outside.

Since the engine also powers the hydraulic system in excavators, overheating can impair its function and damage associated components, resulting in costly repairs and downtime. To address this, air vents were added around the radiator section of the hood, and several configurations were tested to identify the most effective solution. These vents improve airflow by drawing in outside air, reducing the heat trapped under the hood and improving overall cooling efficiency.

# CHAPTER III
# ANALYTICAL MODELING

In this section, the numerical methods used for evaluating thermal and acoustic performance were presented. Pressure and temperature measurements were conducted using sensor-based approaches, and thermocouple outputs were analyzed through empirical models. The ATB method was applied to assess the cooling system's thermal margin, while the A-weighted sound power level provided a standardized evaluation of acoustic performance.

## 3.1. PRESSURE MEASUREMENT METHODOLOGY

In the pressure measurements, the approach was based on two methods: the pressure difference between two distinct points and the pressure difference between a single point and atmospheric pressure. The general gas law, expressed as[39]

$$P \cdot V = n \cdot R \cdot T_P \tag{3.1}$$

was used to relate pressure, volume, and temperature in the system.

## 3.2 TEMPERATURE MEASUREMENT WİTH THERMOCOUPLES

In the cooling performance test, temperatures were measured using thermocouples. These devices operate based on the principle that two dissimilar metals joined at one end will generate a voltage difference when subjected to a temperature gradient. The expansion and contraction of the metals at the thermocouple tip are dependent on heat, and due to the temperature difference between the measurement (junction) end and the reference (cold or tail) end, a voltage is generated. This voltage is proportional to the temperature difference, making the thermocouple function as a temperature-to-voltage transducer.

## 3.3 TEMPERATURE–VOLTAGE RELATIONSHIP OF THERMOCOUPLES

The temperature–voltage relationship of a thermocouple is typically nonlinear and can be approximated by empirical equations or represented using standard calibration tables, such as[40]:

$$V=a_0+a_1T+a_2T+a_3T+\ldots+a_nT^n \qquad (3.2)$$

where: V is the output voltage (in millivolts), T is the temperature (in °C or K), $a_0$,$a_1$ ,…,$a_n$ are calibration coefficients specific to the thermocouple type (e.g., Type K, Type J, etc.).

An alternative representation based on Seebeck effect is given by[41]:

$$Emf = \int_{T1}^{T2} S_{12}\, dT \qquad (3.3)$$

Where,

Emf is the electromotive force or voltage produced at the tail end,$T_1$and $T_2$ are the temperatures of the reference and measuring ends, respectively,$S_{12}=S_1-S_2$ is the net Seebeck coefficient, determined by the materials used in the thermoelements.

## 3.4. CALCULATION OF A-WEIGHTED SOUND POWER LEVEL

### 3.4.1. A-Weighted Sound Power Level

The A-weighted sound power level**,** denoted as $L_{WA}$ (in decibels), represents the total acoustic energy emitted by the machinery and is calculated according to the following equation[42]:

$$L_{WA} = L_{pA,T} + 10\log_{10}(\frac{S}{S_0}) + K_{1A} + K_{2A} \qquad (3.4)$$

Where:

- $L_{pA,T}$ is the energy-average of the time-averaged A-weighted sound pressure levels measured over a defined surface surrounding the machine (in decibels, referenced to 20 μPa),
- $K_{1A}$ is the background noise correction factor (in decibels), applied to account for ambient noise during measurements,
- $K_{2A}$ is the environmental correction factor (in decibels), accounting for sound reflections and environmental influences on measurements
- S is the area of the hemispherical measurement surface (in square meters),
- The term $10\log_{10}(S/S_0)$ is used to normalize the measured sound power to the reference surface area.

### 3.4.2. Energy Averaging of Pressure Levels

The energy average $L_{pA,T}$ is calculated from multiple microphone readings taken at specific positions on the hemispherical surface[42]:

$$L_{PA,T} = 10\log_{10}(\frac{1}{N}\sum_{i=1}^{N} 10^{\frac{L_{pA,i}}{10}} \quad (3.5)$$

Where,$L_{pA,i}$ time-averaged A-weighted sound pressure level measured at microphone position iii (in decibels, reference: 20 μPa), and N is the total number of microphone positions, typically N=6N = 6N=6 for a hemispherical setup.

<u>*Surface Area and Correction Values*</u>

The measurement surface S is determined based on the radius rrr of the hemisphere surrounding the noise source[42]:

$$S=2\pi r^2 \quad (3.6)$$

The corresponding correction 10log10($S/S_0$) common measurement radii is:

- 20.0 dB for a radius of 4 m
- 28.0 dB for a radius of 10 m
- 32.1 dB for a radius of 16 m

These values reflect the logarithmic scaling of the measurement surface relative to the 1 m² reference and are necessary for consistent comparison of sound power levels across different setups.

## 3.5. EVALUATION OF THERMAL SAFETY MARGIN VIA ATB METHOD

The Air to Boil (ATB) method is used to determine whether the cooling system operates within a safe thermal range.

### 3.5.1. Methodology

1. **Equilibrium Identification**: Test data is reviewed to determine when the machine reaches steady-state temperature.
2. **Average Temperature Extraction**: Coolant and hydraulic oil average temperatures are calculated within this range.
3. **ATB Calculation**[43]

$$ATB=TBP-(T_{c1}-T_{a1}) \quad (3.7)$$

Where:

- TBP:Boiling point of coolant (function of altitude and pressure)

- $T_{CI}$: Coolant radiator inlet temperature
- $T_{AI}$: Ambient temperature

### 3.5.2. Temperature Limits

- Coolant max temperature: 99°C (Tier 3A),95°C (Tier 3B and Tier 4 Final)
- Hydraulic oil max temperature:90°C for all tiers

### 3.5.3. Intercooler Constraint

The intercooler outlet air temperature, adjusted to a 25°C ambient baseline, must remain below:

- **< 50°C** for Tier 3A
- **< 45°C** for Tier 3B and Tier 4 Final

## 3.6. UNCERTAINITY

In engineering measurements, quantifying the uncertainty associated with experimental data is essential to ensure the validity and reliability of the results. The following formulas are used in accordance with the Guide to the Expression of Uncertainty in Measurement (GUM) and are applicable to both temperature and acoustic measurements conducted in this study.

### 3.6.1. Combined Standard Uncertainty

This expression calculates the combined standard uncertainty ucu_cuc by taking the root-sum-square of all relevant individual uncertainty components uiu_iui. These components may arise from both Type A evaluations (based on statistical analysis of repeated observations) and Type B evaluations (based on instrument specifications, calibration data, or expert judgment).

$$\mathrm{U_c} = \sqrt{\mathrm{U_1^2} + \mathrm{U_2^2} + \cdots + \mathrm{U_n^2}} \tag{3.8}$$

### 3.6.2. Expanded Uncertainty

Expanded uncertainty U is obtained by multiplying the combined standard uncertainty $U_c$ with the coverage factor k, typically set as k=2 to represent a 95% confidence level under a normal distribution.

$$\mathrm{U} = \mathrm{k}.\mathrm{U_c} \tag{3.9}$$

### 3.6.3. Uncertainity Experimental Methodology

In this study, temperature and noise measurements were performed using calibrated sensors and data acquisition systems. Measurement uncertainties were evaluated using the Root Sum of Squares (RSS) method in accordance with the Guide to the Expression of Uncertainty in Measurement (GUM) and associated calibration certificates. The combined standard uncertainties are calculated using individual components and then expanded with a coverage factor of k = 2 to obtain the expanded uncertainties, which correspond to approximately 95% confidence level.

#### 3.6.3.1.Temperature Measurement Uncertainty

The sources of uncertainty encountered in the temperature measurement system are summarized in Table 1. Factors such as thermocouple accuracy, data acquisition device tolerance, and surface contact quality directly affect the overall measurement reliability.

**Table 1**: K-Type Thermocouples (Surface Measurement)

| Source | Uncertainty (± °C) | Description |
|---|---|---|
| Thermocouple Accuracy | ±2.2 | According to ANSI Standard |
| GL840 Device | ±0.6 | Manufacturer specification |
| Surface Contact Quality | ±1.0 | Estimated thermal resistance mounting |

$$U_K = \sqrt{(2.2)^2 + (0.6)^2 + (1.0)^2} = \sqrt{6.40} \sim \pm 2.53°C \qquad (3.10)$$

The sources of uncertainty in the temperature measurement system are summarized in Table 2. As shown, thermocouple accuracy (±2.2 °C), the GL840 data acquisition device (±0.5 °C), and immersion contact quality (±0.7 °C) each contribute to the overall measurement reliability.

**Table 2:** J-Type Thermocouples (Immersion Measurement)

| Source | Uncertainty(± °C) | Description |
|---|---|---|
| Thermocouple Accuracy | ±2.2 | According to ANSI Standard |
| GL840 Device | ±0.5 | Manufacturer specification |
| Immersion Contact Quality | ±0.7 | Estimated due tostable fluid contact |

$$\mathrm{U}_J = \sqrt{(2.2)^2 + (0.6)^2 + (0.7)^2} = \sqrt{5.89} \sim \pm\, 2.43°\mathrm{C} \quad (3.11)$$

### 3.6.3.2.Noise Measurement Uncertainty

Noise measurements were performed using PCB microphones (model 377B02 with preamplifier 378B02). The sensors were calibrated, an ISO/IEC 17025-accredited lab (AB-0089-K). According to the certificate:

Uncertainty in the 31.5–5000 Hz range is ±0.29 dB

Uncertainty in the 5000–10000 Hz range is ±0.49 dB

In this study, measurements were mostly evaluated within the 31.5–5000 Hz range, hence the dominant uncertainty is taken as ±0.29 dB.In Table 3, Uncertainty is shown.

**Table 3:** Uncertainty of Noise Measurement

| Source | Uncertainty(± °C) | Description |
|---|---|---|
| Microphone Calibration(Type B) | ±0,29 | As per  certificate for 31.5-5000Hz |
| Environmental Effects (wind/reflection) | ±0.6 | Estimated due to open measurement environment |
| Mounting &Positioning Variability | ±0.4 | Estimated variability due to sensor location |

$$\mathrm{U}_{Noise} = \sqrt{(0.29)^2 + (0.6)^2 + (0.4)^2} = \sqrt{0.6041} \sim \pm\, 0.78\ \mathrm{dB} \quad (3.12)$$

Table 4 presents the equipment used and the corresponding expanded uncertainty values for different types of measurements. For surface temperature measurements, a K-Type thermocouple paired with the GL840 device yielded an expanded uncertainty of ±2.53 °C. In fluid temperature measurements, a J-Type thermocouple with the same data acquisition device resulted in an uncertainty of ±2.43 °C. For noise level measurements within the 31.5 Hz to 5 kHz frequency range, the PCB377B02 microphone (with calibration certificate) was used, and the expanded uncertainty was calculated as ±0.78 dB.

**Table 4:** Summary Table:Measurement Uncertainty

| **Measurement Type** | **Equipment Used** | **Expanded Uncertainty** |
|---|---|---|
| Surface Temperature | K-Type Thermocouple+ GL840 | ±2.53°C |
| Fluid Temperature | J-Type Thermocouple+ GL840 | ±2.43°C |
| Noise Level(31.5-5kHz) | PCB377B02 Microphone +Cal.Cert. | ±0.78dB |

# CHAPTER IV
# RESULTS

Tests were conducted by opening various vents on the radiator hood to improve the under-hood airflow. The vents numbered P1, P2, and P3, as shown in Figure 46, were examined under three different configurations and compared with the machine's standard condition through experimental studies. Since these modifications directly affect the cooling system, measurements such as intercooler inlet and outlet pressure difference, exhaust back pressure, and air intake pressure—specified in the engine sign-off criteria—were also taken to ensure that the improvements did not negatively impact these parameters. Additionally, to monitor and control possible temperature increases or decreases in the cooling systems, temperature measurements were taken at the inlet and outlet points of the water radiator, hydraulic radiator, and intercooler radiator.

**The P1 vent (Figure 46(a))** was opened on the right side of the excavator's hood. Behind this vent lies the exhaust system, from which air is discharged via natural convection. This vent was placed near the exhaust outlet to prevent the hot air wave generated during operation from becoming trapped under the hood around the SCR system and to allow heat transfer through natural convection, thus avoiding exhaust system failures in the machine.

**Behind the P2 grille (Figure 46(a))** are located the hydraulic pumps along with fuel and oil filters. Axial piston pumps, particularly under high-performance conditions, are exposed to high heat levels, which can negatively affect their operational efficiency. The vent opened in this region aids heat transfer through natural convection. In addition to thermal concerns, the noise generated by the pumps during operation significantly influences the machine's overall acoustic environment. Fully closing this vent could reduce noise propagation to some extent; however, this would restrict heat dissipation, resulting in increased temperatures under the hood. This thermal buildup may negatively affect the performance and durability of the hydraulic system. On the other hand, keeping this area fully open improves thermal ventilation by allowing some heat to escape efficiently through natural convection. However, it also increases the risk of excessive noise emission, potentially pushing the machine's acoustic profile beyond regulatory limits, contributing to environmental noise pollution, and ultimately posing health risks to the operator or individuals in the surrounding area. To find the optimal balance between thermal management and acoustic performance, a series of tests were conducted under both open and closed grille configurations. These tests aimed to evaluate the impact of each configuration on pump temperature and noise emission levels, in an effort to determine a solution that satisfies both performance and legal requirements.

**Behind the P3 grille (Figure 46(b))** is an air intake chamber that supplies airflow to the engine compartment. This chamber contains key components of the cooling system, including the air filter and radiators. During operation, external air is drawn in with the help of fans, providing forced convection for heat transfer and directly influencing the performance and efficiency of the cooling system. In the open grille configuration, more external air is allowed to enter the chamber, increasing airflow over the radiator surfaces and enhancing the cooling efficiency. This additional cooling capacity becomes especially critical under high load conditions or in high ambient temperature environments.

However, this design also introduces some acoustic drawbacks. A more open grille allows internal noise sources—such as fans, motors, or turbulent airflow—to propagate more easily to the exterior. This can lead to higher external noise levels, potentially exceeding regulatory limits and negatively affecting the perceived comfort of the vehicle. Therefore, tests were conducted with the P3 grille in both fully open and partially closed configurations to assess the balance between improved cooling performance and potential noise increases.

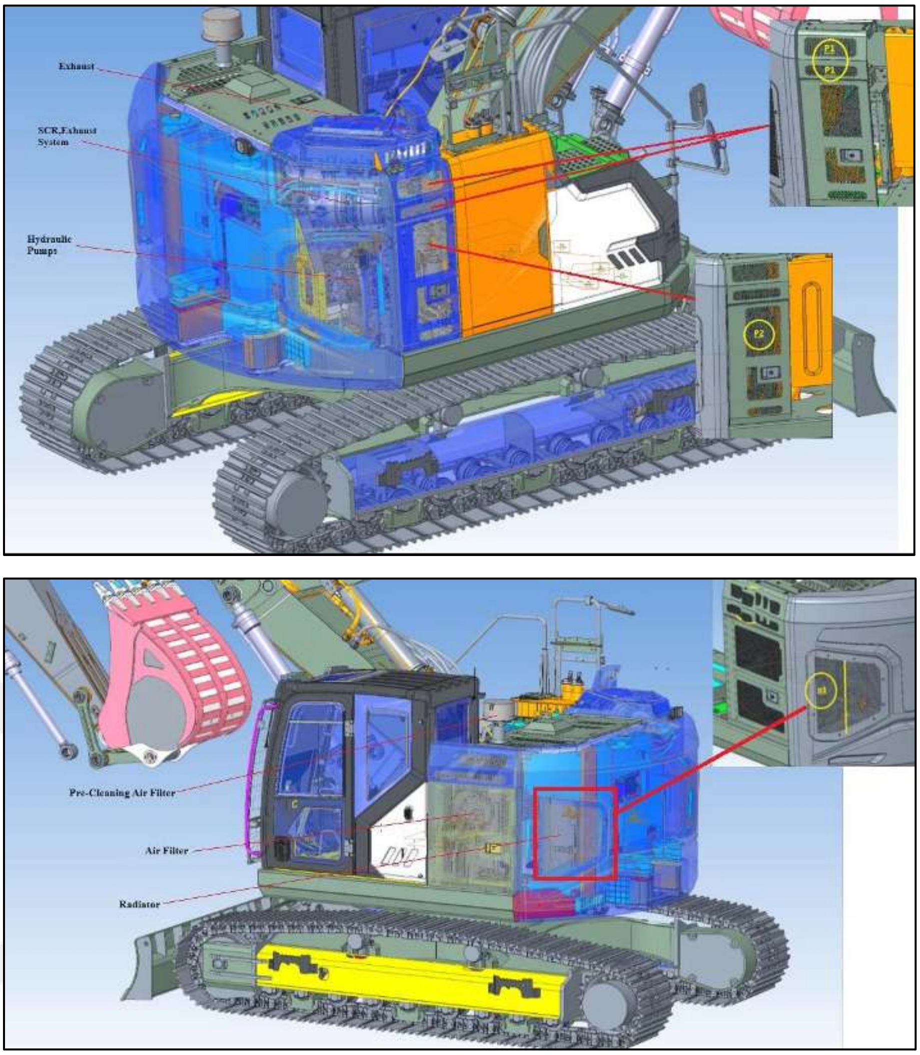


**Figure 46:** Improvements made on the Machine Hood (a) P1,P2 (b) P3

The airflow behavior of the P1, P2, and P3 vents on the machine is illustrated in Figure 47. Air is drawn into the engine compartment through the P3 vent via forced convection, driven by the suction power of the cooling fan, providing additional cooling support to the radiator located in the P3 region. The incoming air circulates within the engine bay and contributes to the cooling of the exhaust system located behind the P1 and P2 vents through natural convection before being discharged to the outside.

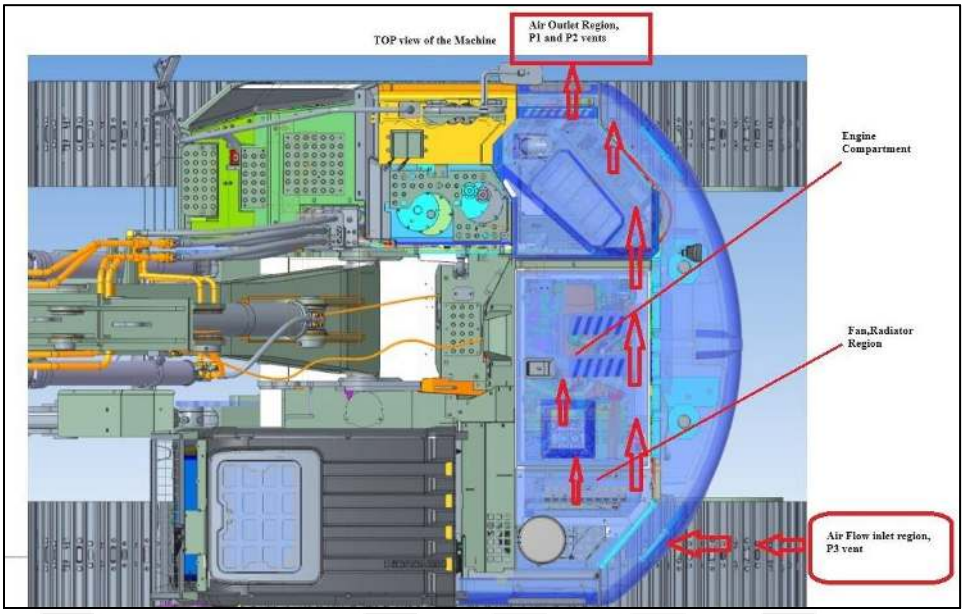


**Figure 47:** Under-Hood Airflow and Thermal Interaction of the Vents

To better understand the combined thermal and acoustic effects of the hood ventilation design, a comparative summary of each vent and grille configuration is provided in Table 5 This table outlines the impact of both open and closed configurations for the P1, P2, and P3 ventilation components. It highlights the thermal performance benefits in terms of heat dissipation and airflow, as well as the acoustic implications related to noise propagation. The goal is to identify a balanced design approach that satisfies cooling efficiency requirements without exceeding permissible sound emission levels under varying operating conditions.

**Table 5:** Summary of Thermal and Acoustic Impacts of Hood Vents and Grilles

| Vent/Grille | Location / Function | Open Conf. Thermal Impact | Open Conf. Acoustic Impact | Closed Conf. Thermal Impact | Closed Conf. Acoustic Impact |
|---|---|---|---|---|---|
| **P1 Vent** | Right side of hood; adjacent to exhaust | Promotes natural convection; reduces heat accumulation near exhaust | Minimal impact (air exit point) | Potential heat entrapment under hood | No significant change |

**Table 5 Cont.**

| Vent/Grille | Location / Function | Open Conf. Thermal Impact | Open Conf. Acoustic Impact | Closed Conf. Thermal Impact | Closed Conf. Acoustic Impact |
|---|---|---|---|---|---|
| **P2 Grilles** | Near hydraulic pumps | Promotes natural convection; maintains pump temperature within safe range | Increases noise from hydraulic pumps | Risk of overheating during heavy-duty use | Reduces external noise emissions |
| **P3 Grilles** | Air intake for engine compartment | Forced convection; increases cooling system efficiency | Allows fan/motor noise to propagate outward | Reduced airflow; risk of thermal inefficiency in hot climates | Helps suppress noise from internal components |

Based on the vent configuration logic described above, four different test scenarios were designed to evaluate the combined thermal and acoustic impacts of various vent positions. Each scenario represents a practical combination of open, partially open, or closed states for the P1, P2, and P3 ventilation elements, allowing for comparative analysis under controlled conditions. Among these configurations, **Case 2 represents the baseline condition of the machine**. The other configurations were compared against Case 1. The configurations are listed below:

- **Case 1:** P1, P2, and P3 grilles fully open
- **Case 2:** P1 and P2 grilles fully closed; P3 grille half open(**baseline condition of the machine**)
- **Case 3:** P2 grille fully open; P3 grille half open; P1 grille fully closed
- **Case 4:** P1 and P2 grilles fully closed; P3 grille half closed

These scenarios were selected to explore the trade-offs between cooling efficiency and noise control, and to guide design decisions that comply with both thermal performance targets and acoustic regulations.

## 4.1. RESULTS OF INTERCOOLER PRESSURE DIFFERENCE MEASUREMENT

In construction machinery, the intercooler cooling system must operate within a specific pressure range defined by the engine supplier to ensure effective heat exchange and maintain engine efficiency. According to the engine specifications provided in Table 6, the allowable intercooler pressure difference should remain within the range of 7 ± 2 kPa. This pressure differential is measured during engine operation at load levels of 70%, 75%, and 80%, which represent standard working conditions as defined by the engine supplier. Since direct measurement at 100% engine load is not always feasible or recommended under test conditions, the corresponding pressure difference at full load is determined through interpolation based on the available data points.

**Table 6:** Engine Specifications

| **Engine Specifications** | |
|---|---|
| **Model** | 4HK1X |
| **Application** | Hydraulic Excavator |
| **Engine Type** | 4cycle,Water cooled,overheated camshaft,certical in-line,direct injection type,with turbocharger |
| **No. Of cylinders- bore x stroke** | 4-115.0 mmx125.0mm |
| **Total piston displacement** | 5.193 lt |
| **Compression Ratio** | 17.5:1 |
| **Rated Output** | 120±3kW/2000min^-1 |
| **Maximum Torque** | 657±33 Nm / 1500 min^-1 |
| **Idle Speed** | 800±10 min^-1 |
| **Max. Speed no load** | 2000±10min^-1 |
| **Air Intake Pressure Loss** | less than 2.45 kPa |
| **Exhaust Back Pressure Loss** | 26.5±2 kPa |
| **Pressure loss by ıntercooler system** | 7±2kPa |
| **Type of Fuel** | Diesel Fuel only |
| **Rotating Direction** | Clockwise viewed from fan side |
| **Lubricating system** | Full forced pressure feed type,oil cooled type |
| **Oil Cooling System** | Integrated water cooled,4 core |
| **Cooling Device Cooling system** | Pressurized water forced circulation type |
| **Cooling fan** | 650mm,7blades,sucker type,plastic |
| **Driving system of Fan** | Belt driven from crankshaft, pulley ratio : 0.95 |
| **Water Pump** | Impeller type , belt driven from crankshaft pulley |
| **Termostat Regulating system** | Wax-pellet type |
| **Water temperature indicating device** | Coolant temp sensor&Overheat warning switch(operating temp. 105± 2 deg C) |

**Table 6 Cont.**

| Engine Specifications | |
|---|---|
| **Intake Air Temperature** | 141 degC |
| **Outlet air temperature** | less than 50 deg C |
| **Intake air pressure** | 120kPa |
| **Intake air flow** | 10.3 kg/min |

To conduct the test, the required engine load levels were set with the machine's display interface by accessing the P-Q test section and incrementally increasing the pump current until stabilization was achieved. Prior to testing, the hydraulic oil was preheated to 50°C, as this is the minimum temperature at which the oil attains optimal viscosity and flow characteristics, ensuring stable chemical and mechanical behavior during operation.For each specified engine load level, data was collected over a 10-minute period. This duration was selected to allow the intercooler cooling system to reach its standard thermal operating cycle, thereby ensuring the reliability and repeatability of the recorded measurements.

The Figure 48 illustrates the relationship between engine load (%) and the intercooler pressure drop ΔP (kPa) for four grille configurations tested under controlled conditions. The pressure drop is a critical performance metric, as it reflects the resistance to airflow through the intercooler system.

General trend shows that The pressure drop ΔP increases steadily with rising engine load across all cases, which is expected due to increased airflow and heat rejection demands at higher loads. The measured pressure values for all four cases remain within the specified target range of 7 ± 2 kPa, indicating compliance with the engine supplier's design constraints. When the cases compared with each other it is obvios that, Case 1 (fully open configuration) shows a slightly lower pressure drop compared to the others at 70–90% load. This suggests improved airflow and less resistance due to the open grille configuration. Case 4 (P3 half closed, P1 and P2 fully closed) exhibits a slightly higher pressure drop, especially as engine load approaches 100%. This is consistent with the reduced airflow caused by more restricted grille openings. But also it is seen that, The differences among cases are minimal, with all four lines converging closely, especially at higher engine loads. This indicates that the intercooler system is robust enough to maintain consistent performance despite moderate variations in grille configuration.

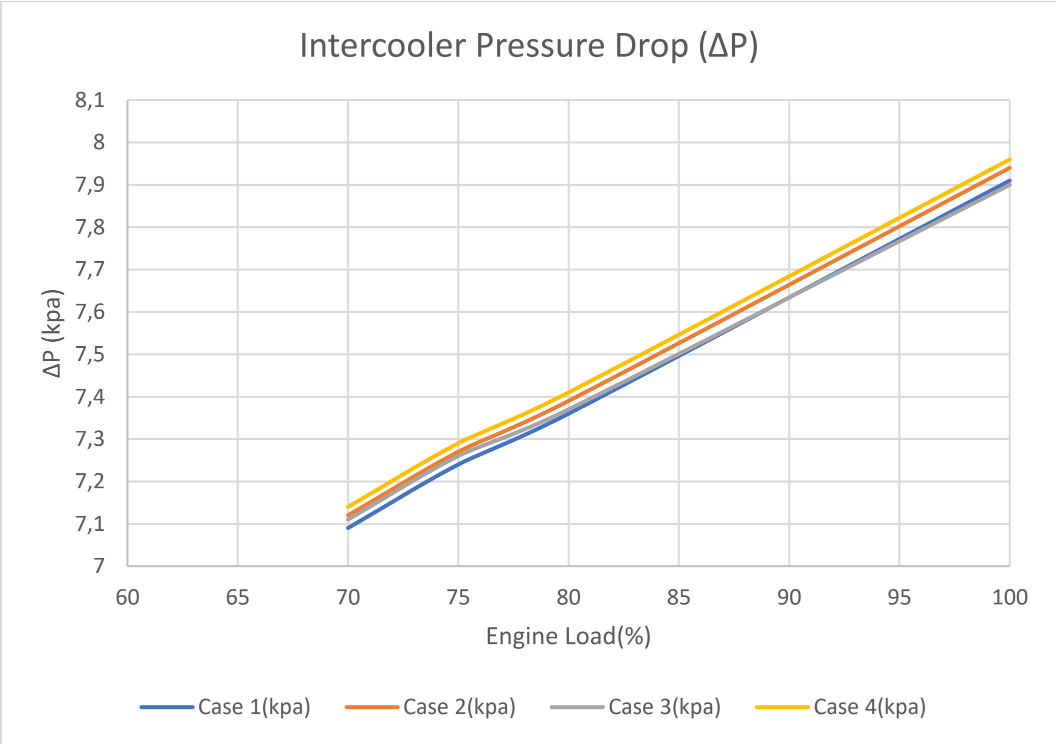


**Figure 48**: Intercooler Pressure Loss (ΔP)

Table 7 indicateas that indicates that while the specific grille configurations have a small influence on airflow resistance, the intercooler system effectively maintains pressure drop ΔP at acceptable levels across the full spectrum of engine loads tested. Case 1 appears to provide a marginal improvement in airflow, but all the configurations examined are suitable for the specified operating conditions. To identify the ideal design that balances airflow efficiency and noise control, additional acoustic and thermal evaluations are required.

**Table 7:** Intercooler Pressure Loss (ΔP)

| | **Engine Load(%)** | **Case 1(kpa)** | **Case 2(kpa)** | **Case 3(kpa)** | **Case 4(kpa)** |
|---|---|---|---|---|---|
| **Intercooler Pressure Drop (ΔP)** | **70** | 7,09 | 7,12 | 7,11 | 7,14 |
| | **75** | 7,24 | 7,27 | 7,26 | 7,29 |
| | **80** | 7,36 | 7,39 | 7,37 | 7,41 |
| | **100** | 7,91 | 7,94 | 7,9 | 7,96 |

## 4.2. RESULTS OF EXHAUST BACK PRESSURE MEASUREMENT

In construction machinery, the emission of nitrogen oxides (NOx) produced during engine operation is regulated according to engine emission standards, and additional aftertreatment systems are employed to minimize the release of these harmful gases. The final stage of this process is the exhaust system, where combustion gases are discharged into the environment. However, if the exhaust back pressure becomes excessive, it can negatively impact engine performance and efficiency. For this reason, engine manufacturers specify an upper limit for allowable exhaust back pressure to maintain optimal operation.

According to the engine specifications provided in Table 6, the acceptable range for exhaust back pressure ΔP is 26.5 ± 2 kPa. This value is directly measured at engine load levels of 70%, 75%, and 80%, which are representative of standard operating conditions as defined by the engine supplier. The corresponding value at 100% engine load is estimated using interpolation, as testing under full load may not be feasible or advisable during routine validation.

To conduct the tests, the required engine load levels were configured using the machine's onboard display, specifically by entering the P-Q test section and gradually increasing the pump current until the desired load stabilized. Prior to data collection, the hydraulic oil was preheated to 50°C, which is the minimum temperature required to achieve effective viscosity and flow properties, ensuring that the oil's chemical and mechanical behavior is consistent during testing.

At each load level, data was recorded for 10 minutes, providing sufficient time for the exhaust system to reach a steady-state operating cycle, and ensuring the validity and repeatability of the measured back pressure ΔP values.It’s shown in Figure 49.

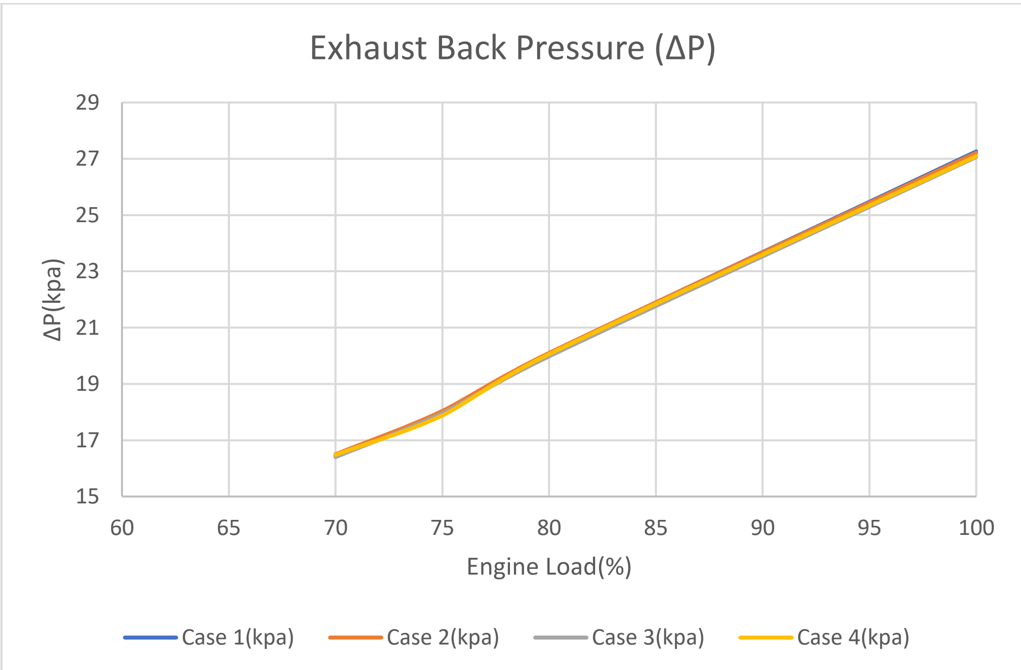


**Figure 49:** Exhaust Back Pressure Loss (ΔP)

The Table 8 presents the measured exhaust back pressure ΔP values (kPa) at four different engine load levels: 70%, 75%, 80%, and 100%, under four different grille configurations (Case 1 to Case 4). These configurations correspond to varying degrees of hood ventilation openness, particularly around the exhaust area (P1 vent and others). Anticipated, exhaust back pressure ΔP goes up as the engine load increases. This is because higher loads produce more combustion gases and increase exhaust flow. Importantly, all measured back pressure values, even at 100% engine load, stayed within the manufacturer's specified limit of 26.5 ± 2 kPa (meaning they were between 24.5 and 28.5 kPa).These results confirm that the exhaust system isn't too restrictive under any of the tested grille configurations.

**Table 8:** Exhaust Back Pressure Loss (ΔP)

| | **Engine Load(%)** | **Case 1(kpa)** | **Case 2(kpa)** | **Case 3(kpa)** | **Case 4(kpa)** |
|---|---|---|---|---|---|
| **Exhaust Back Pressure Loss(ΔP)** | **70** | 16,45 | 16,5 | 16,4 | 16,48 |
| | **75** | 18,01 | 18,04 | 17,96 | 17,88 |
| | **80** | 20,08 | 20,1 | 19,98 | 20,06 |
| | **100** | 27,26 | 27,21 | 27,06 | 27,09 |

The objective of the exhaust back pressure ΔP measurements is to ensure compliance with the allowable pressure range specified by the engine supplier, which is critical for maintaining optimal engine performance and component reliability. Both excessively high and unusually low back pressure levels can lead to undesirable consequences, including engine performance degradation, thermal stress in the engine compartment, and disruption of under-hood airflow dynamics.

As presented in Table 8, the measured exhaust back pressure ΔP values exhibit high consistency across all four grille configurations. The observed deviations between cases are minimal and within measurement uncertainty, indicating that the design modifications implemented to enhance under-hood ventilation do not adversely influence the exhaust system's pressure characteristics. These results confirm that the proposed airflow optimization strategies are thermally and mechanically compatible with the engine’s exhaust requirements.

## 4.3. RESULTS OF AIR INTAKE PRESSURE MEASUREMENT

Table 9 and Figure 50, details the air intake pressure loss ΔP (in kPa) measured across four engine loads (70%, 75%, 80%, and 100%) and four grille configurations (Case 1-4). The engine supplier's maximum allowed pressure loss ΔP is 2.45 kPa. Across all configurations and load levels, the measured values remained below this limit. Even at 100% engine load, where pressure loss ΔP is expected to be highest, no reading went above 2.35 kPa, confirming the air intake system's safe and efficient operation. As anticipated, air intake pressure loss consistently rose with increasing engine load across all setups, driven by greater air mass flow. This increase, roughly 0.4–0.45 kPa from 70% to 100% load, points to a linear and predictable system response.

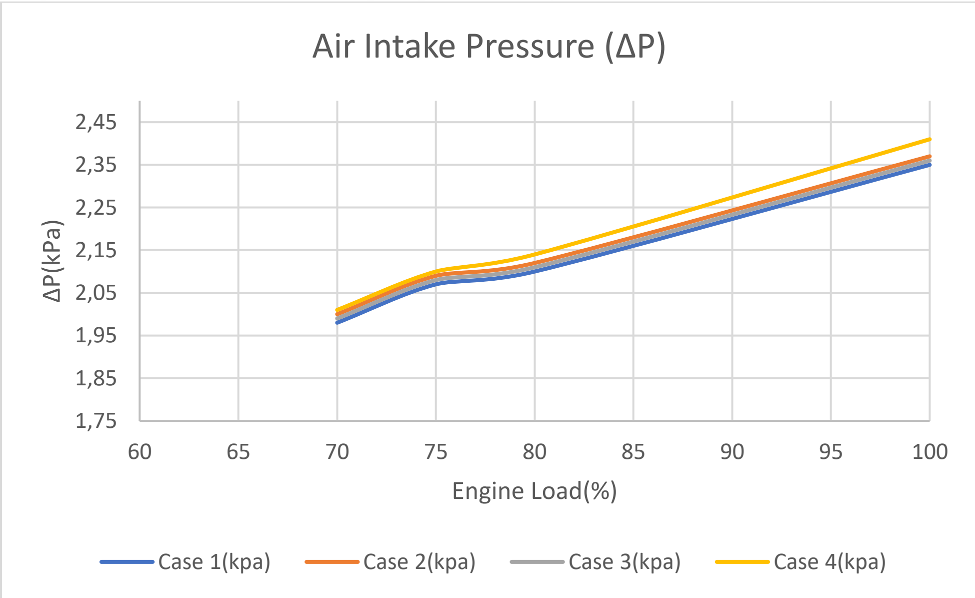


**Figure 50:** Air Intake Pressure Loss (ΔP)

**Table 9:** Air Intake Pressure Loss (ΔP)

| | **Engine Load(%)** | **Case 1(kpa)** | **Case 2(kpa)** | **Case 3(kpa)** | **Case 4(kpa)** |
|---|---|---|---|---|---|
| **Air Intake Pressure Loss (ΔP)** | **70** | 1,98 | 2 | 1,99 | 2,01 |
| | **75** | 2,07 | 2,09 | 2,08 | 2,1 |
| | **80** | 2,1 | 2,12 | 2,11 | 2,14 |
| | **100** | 2,35 | 2,37 | 2,36 | 2,41 |

### 4.4. Results of Underhood Cooling Performance Measurement

The cooling performance test is designed to evaluate the thermal behavior of machine components that are exposed to significant heat during regular operation. Excessive heat accumulation can lead to material deformation, accelerated wear, or thermal fatigue in critical areas. To monitor and mitigate such risks, temperature measurements are taken using thermocouples positioned on components with the highest exposure to thermal loads.

The test sequence consists of three phases:

1. 45 minutes of maximum-capacity digging, simulating high-load operational conditions.
2. 10 minutes of idling at low engine speed, allowing limited cooling under reduced thermal load.
3. A second round of 45 minutes of maximum-capacity digging, to evaluate sustained thermal stress effects.

Throughout the test, engine load is continuously monitored to verify that the machine is operating at or near full capacity.

During the active digging phases, the engine load is expected to average approximately 77–78%, which aligns with typical field performance conditions.

- During the first and third phases, the engine operates under high load conditions, simulating full-capacity digging. The load fluctuates between 75% and 85%**,** with an average value of approximately 77.5%**,** consistent across all cases.
- The intermediate phase represents low-speed idling, where the engine load drops significantly to around 10–20%**.**
- The near-overlapping curves for all four cases confirm that the same operational conditions were consistently applied, ensuring valid performance comparisons between configurations.

Engine Load Intervals and Descriptions are given in Table 10 summarizes the time intervals, durations, and engine load levels associated with each test phase. The table clearly outlines the structure of the test procedure, providing context for how thermal stress is applied and managed throughout the cycle.

This structured load profile ensures that the cooling system is evaluated under realistic and repeatable operational conditions, and that any thermal responses recorded later in the test (e.g., from temperature sensors or thermocouples) are directly attributable to controlled engine behavior

**Table 10:** Engine Load Profile During Cooling Performance Test

| Test Phase | Time Interval (s) | Duration (min) | Engine Load (%) | Description |
|---|---|---|---|---|
| Phase 1 – Digging | 0 – 2700 | 45 | 75 – 85 (avg:~77.5%) | Maximum capacity digging under full thermal load |
| Phase 2 – Idling | 2700 – 3300 | 10 | 10 – 20 | Low-speed idle for thermal relaxation |
| Phase 3 – Digging | 3300 – 6000 | 45 | 75 – 85 (avg:77.5%) | Second digging cycle to observe thermal accumulation |

In the cooling performance test, it is critical to monitor the thermal behavior of both the liquid-based and air-based cooling systems integrated into the machine. As an initial step, temperature measurements were taken at the inlet and outlet ports of the engine coolant radiator, hydraulic oil radiator, and intercooler to capture the maximum peak temperatures generated during operation. These peak values were then compared against the temperature limits defined by the engine supplier, as outlined in Table 11, to verify compliance with safe operating thresholds.

A majority of the components located under the hood are directly influenced by internal airflow conditions. Therefore, the design improvements introduced in the system were specifically aimed at enhancing air circulation by creating effective flow paths for trapped or compressed hot air, thereby reducing thermal stagnation zones.
Several components under the hood are susceptible to thermal deformation due to prolonged exposure to elevated temperatures. To mitigate this risk and ensure mechanical integrity, it is necessary to maintain local temperatures within the allowable limits specified in Table 11. These limits serve as critical design criteria for evaluating the effectiveness of the airflow management strategies implemented during the test campaign.

**Table 11:** Temperature Limit Values

| | | |
|---|---|---|
| **Fuel Inlet** | 80 | °C |
| **Fan Pulley** | 80 | °C |
| **Air Intake** | 80 | °C |
| **Radiator Water Outlet** | 95 | °C |
| **Hydraulic Oil Inlet** | 90 | °C |
| **Intercooler Outlet** | 50 | °C |
| **Alternator** | 100 | °C |
| **Rubber Hose** | 150 | °C |
| **Engine Harness Connector** | 100 | °C |
| **ECM** | 75 | °C |
| **Starter** | 100 | °C |

In engine cooling performance tests, ambient temperature is a significant factor as it directly affects the cooling process. Therefore, the measured ambient temperature is normalized (shifted) to 46°C. Likewise, other measured parameters are also adjusted to reflect this reference temperature.

The reason for this adjustment is that even if the machine operates at maximum efficiency during the test, if the ambient temperature is low, the resulting heat transfer will also be proportionally lower. Taking global climate conditions into account, a maximum temperature of 46°C has been defined as the reference value for regions with average working conditions. All measured values are adjusted accordingly.

Example: Let's denote the average of the measured value as X, and the average ambient temperature as Y. To shift to 46°C, the following formula is applied: $Y + (46 - X)$.

As an exception, intercooler cooling temperatures are normalized to 25°C, using the formula: $Y + (25 - X)$.

### 4.5. COMPARISON OF THE CASES

In this section, the four grille configurations (Case 2 is the baseline configuration of the machine.) tested during the cooling performance assessment are compared based on key parameters such as intercooler pressure drop, exhaust back pressure, air intake restriction, and under-hood thermal behavior. Additionally, indirect implications for acoustic performance are discussed.

This comparison is based on graphical analyses and measurements performed throughout the test sequence. Each configuration represents a different trade-off between airflow optimization and noise control, and this comparison aims to guide decision-making for design optimization depending on application needs. In Table 12, comparsion of all cases is depicted.

**Table 12:** Comparative Assessment of Test Configurations

| Criteria | Case 1 | Case 2 (baseline configuration) | Case 3 | Case 4 |
|---|---|---|---|---|
| **Intercooler Pressure Drop(ΔP)** | 7,91kpa; interval limit 7±2 kpa | 7,94kpa; interval limit 7±2 kpa | 7,9kpa; interval limit 7±2 kpa | 7,96kpa; interval limit 7±2 kpa |
| **Exhaust Back Pressure(ΔP)** | 27,26kpa; interval limit 26,5±2 kpa | 27,21kpa; interval limit 26,5±2 kpa | 27,06kpa; interval limit 26,5±2 kpa | 27,09kpa; interval limit 26,5±2 kpa |
| **Air Intake Pressure Loss(ΔP)** | ~2,35 kPa; under the limit 2.45 kpa | ~2,37 kPa; under the limit 2.45 kpa | ~2,36 kPa; under the limit 2.45 kpa | ~2,41 kPa; under the limit 2.45 kpa |
| **Engine Load Profile** | Identical load behavior in all cases | Average load ~77%, same as others | Consistent with Case 1 | Same pattern |
| **Under-Hood Thermal Exposure** | Highest exposure but validated | Moderate airflow, moderate risk | Balanced | Highest risk of local overheating |

Case 1 provides the best cooling and airflow, though it might lead to increased noise. Case 3 strikes a good balance between efficient airflow and noise reduction. Case 4, while the most restrictive for ventilation, is ideal for noise-sensitive environments, assuming any thermal risks can be managed.

All cases will be analyzed in comparison with Case 2, which is the baseline configuration of the machine.

## 4.6 COMPONENT-LEVEL TEMPERATURE DISTRIBUTION

### 4.6.1.Case 1 Configuration

The temperature parameters presented in Figure 51 correspond exclusively to Case 1. This configuration was selected to provide a comprehensive overview of all monitored components and to illustrate the overall structure and resolution of the temperature-time graph in a single figure. Displaying all parameters simultaneously allows for a full assessment of the thermal behavior of under-hood components under a high-airflow scenario.

It is important to note that some components did not exhibit any significant temperature variation across different grille configurations. Therefore, to avoid redundancy and improve clarity, only the parameters that demonstrated notable temperature changes as a result of the grille modifications will be shown in the subsequent figures for other cases.

As shown in Figure 51, the cooling performance test followed a structured cycle comprising three operational phases:

- 45 minutes of active digging under high load,
- 10 minutes of low-speed idling,
- and a second 45-minute digging phase.

This cycle was applied uniformly across all configurations to ensure consistency and comparability in thermal performance evaluation.

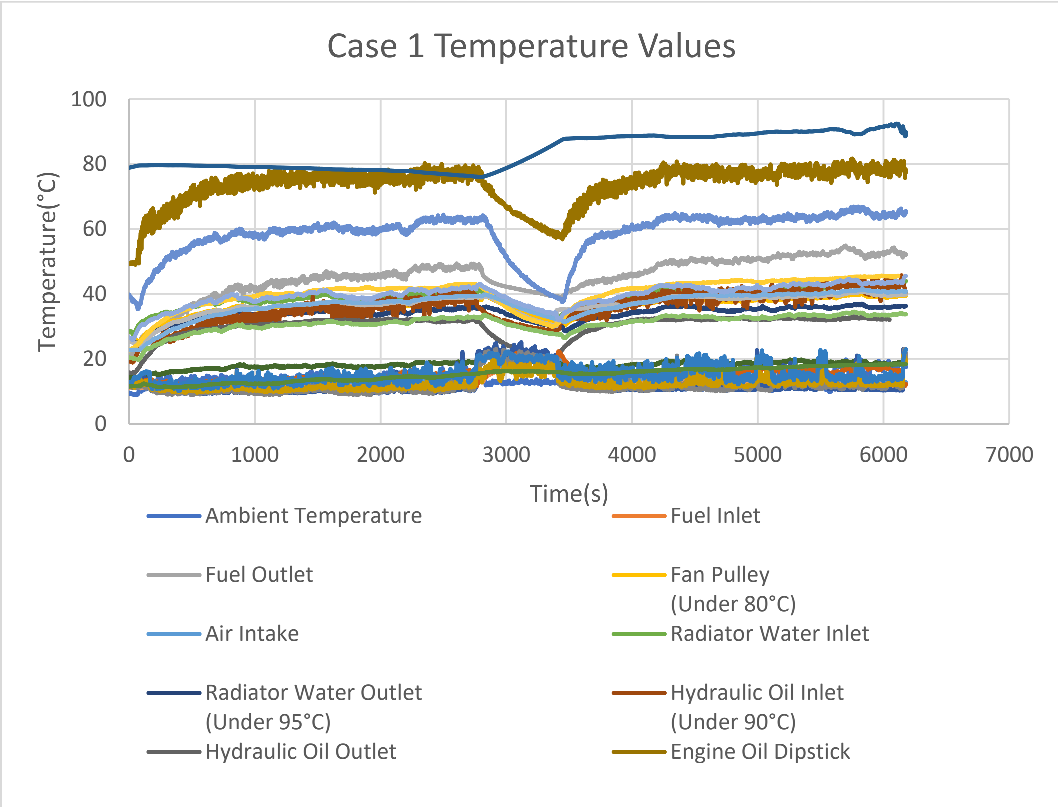


**Figure 51:** Case 1 Temperature Values

As shown in Table 13 and Table 14, all recorded temperature values remain within the maximum allowable limits defined by the engine supplier, as detailed in Table 10. The primary goal of this analysis was to assess the impact of grille configurations on under-hood airflow and thermal distribution. In this context, Case 1 demonstrated the most favorable thermal performance, with multiple components exhibiting lower peak temperatures compared to other configurations.This result is consistent with the expected effect of improved ventilation provided by the fully open grille layout in Case 1.However, it is important to note that in construction machinery, design modifications intended to improve thermal performance can also lead to increased external noise emissions, due to reduced acoustic insulation. Therefore, although Case 1 stands out thermally, it may not be the optimal configuration when noise regulations or operator comfort are taken into account. For this reason, it is recommended that acoustic measurements be conducted in parallel to temperature testing, in order to determine the most suitable configuration that achieves an effective balance between thermal management and acoustic performance.

**Table 13:** Temperature change points 1

| (Unit °C) | Ambient Temperature (Shifted 46°C) | Engine Oil Dipstick | 1.Rubber Hose | 2.Rubber Hose | 3.Rubber Hose | Engine Harness Connector |
|---|---|---|---|---|---|---|
| **Case 1** | 46 | 108,43 | 69,96 | 74,97 | 70,67 | 63,99 |
| **Case 2** | 46 | 115,05 | 75,70 | 74,96 | 76,32 | 70,61 |
| **Case 3** | 46 | 136,27 | 77,14 | 78,96 | 79,49 | 72,05 |
| **Case 4** | 46 | 117,03 | 74,41 | 73,16 | 74,63 | 73,93 |

**Table 14:** Temperature change points 2

| (Unit °C) | Radiator Right-Bottom | Radiator Right-Top | Radiator Left-Top | Radiator Left-Bottom | ECM | Starter |
|---|---|---|---|---|---|---|
| **Case 1** | 47,33 | 42,81 | 43,95 | 46,85 | 48,31 | 73,34 |
| **Case 2** | 53,81 | 45,68 | 47,06 | 57,57 | 49,99 | 79,80 |
| **Case 3** | 56,61 | 48,14 | 51,03 | 60,40 | 51,43 | 82,45 |
| **Case 4** | 53,26 | 44,57 | 48,61 | 55,86 | 56,77 | 80,68 |

#### 4.6.1.1.ECM Temperature Change

Figure 52(a) presents a comparative temperature profile of the Electronic Control Module (ECM) during the cooling performance test under the Case 1 configuration, compared to the baseline machine condition, Case 2. The ECM is mounted on the lower right side of the engine compartment—a location that is relatively protected but still subject to thermal radiation and convective currents from nearby components.

This area is situated relatively close to the P2 grille, behind which the hydraulic pumps are located. Under limited airflow conditions, thermal energy radiated from the pumps can accumulate around the ECM, potentially causing undesirable temperature rises. However, in Case 1, where all grilles are fully open, enhanced natural convection allows hot air to be expelled more effectively. This improves under-hood air circulation and helps stabilize ECM temperatures throughout the test cycle.

The graph confirms that ECM temperature remains consistently low, increasing only gradually and staying well below critical thresholds. In contrast, ambient temperature exhibits greater variability due to external fluctuations and engine cycling. The forced convection airflow entering from the P3 grille, although indirectly, also contributes to thermal management around the ECM.All Cases comparison as Figure 52 (b).

Maintaining a stable thermal environment for the ECM is crucial, as excessive heat exposure can negatively affect the performance, stability, and lifespan of electronic control systems. Therefore, the Case 1 data demonstrate that open vent configurations not only provide improved airflow for mechanical components but also offer better thermal protection for sensitive electronics. Compared to the baseline Case 2, an approximate 4% improvement in temperature reduction was achieved.

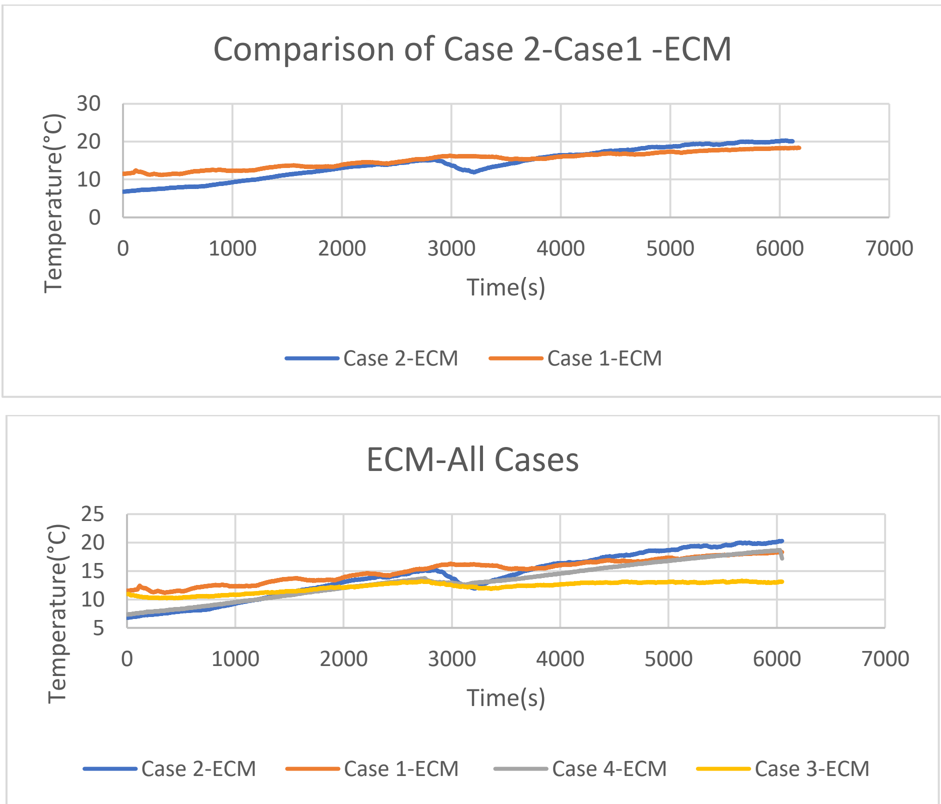


**Figure 52:** (a)Case 1 ECM temperature changes (b) All Cases Comparison

#### 4.6.1.2.Starter Temperature Change

Figure 53(a) presents a comparative analysis of the starter motor temperature variation over time under Case 1 configuration, where all ventilation grilles are fully open, and the baseline machine condition, Case 2. The starter motor is located at the lower front section of the engine compartment, in close proximity to the P1 vent, which is positioned near the exhaust system outlet.

When the P1 vent is open, as in Case 1, hot gases and thermal energy generated by the exhaust system are effectively expelled from the engine compartment through natural convection. This prevents heat buildup in the lower engine area and helps maintain a more stable thermal environment around the starter motor.

As shown in the graph, the starter motor temperature exhibits a gradual increase and stabilizes at approximately 40–45 °C, which remains well within safe operational limits. The absence of sudden spikes or thermal peaks indicates effective heat dissipation in this region throughout the testing period. In contrast, scenarios where the P1 vent is closed may restrict airflow, potentially causing localized heat accumulation. This can result in thermal stress on the starter motor's windings, insulation, and magnetic materials, ultimately compromising the component's long-term reliability.All cases comparison as Figure 53(b)

The results obtained in Case 1 clearly demonstrate the positive impact of improved under-hood ventilation on the thermal management of electrically sensitive components such as the starter motor. The thermal performance in Case 1 shows an approximate 8% improvement compared to Case 2.

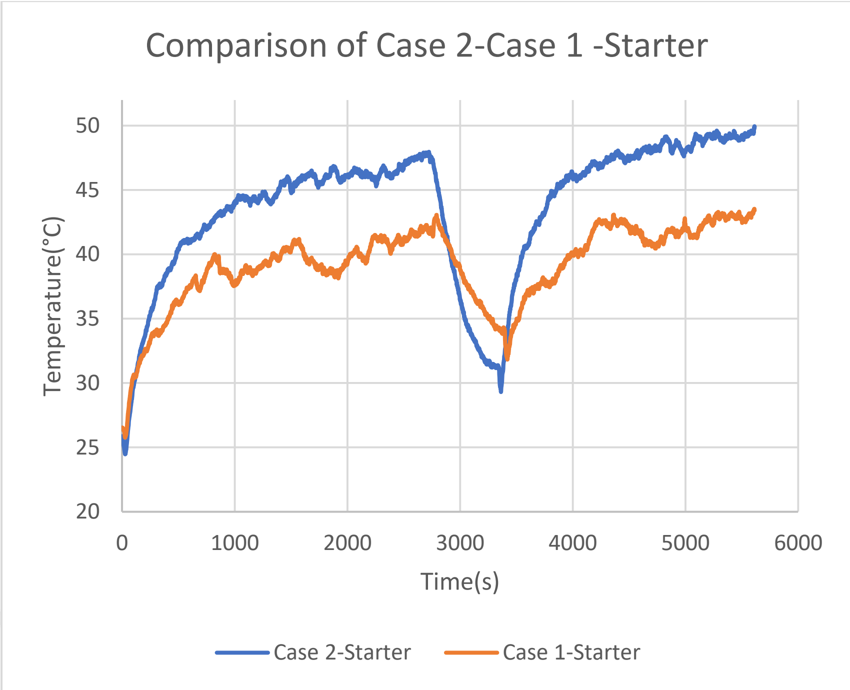


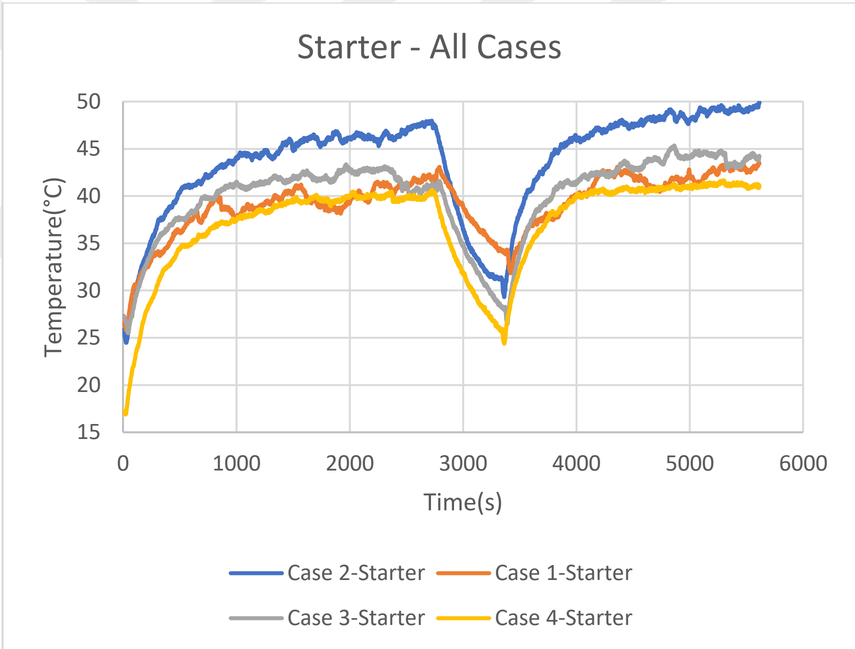


**Figure 53:** (a) Case 1 Starter temperature changes (b) All Cases Comparison

#### 4.6.1.3.Rubber Hoses temperature changes

Figure 54 illustrates the temperature variations of three different rubber hoses located within the engine compartment under Case 1 conditions. These hoses are primarily positioned in the upper region of the engine bay, an area directly affected by rising heat plumes from components such as the exhaust system.

Rubber components are particularly susceptible to thermal aging effects when exposed to prolonged high temperatures, which can result in hardening, embrittlement, cracking, or seal failure. The data from Case 1 indicate that the open-vent configuration effectively reduces thermal stress on these hoses, keeping their temperatures well below the critical threshold of 150°C, as indicated in the chart.

Maintaining hose temperatures within this safe range contributes significantly to preserving long-term sealing integrity, enhancing operational safety, and minimizing maintenance requirements. This is especially important in construction machinery, where systems often operate under continuous high-load conditions. Compared to Case 2, Case 1 achieved approximately an 8.5% improvement in thermal performance.

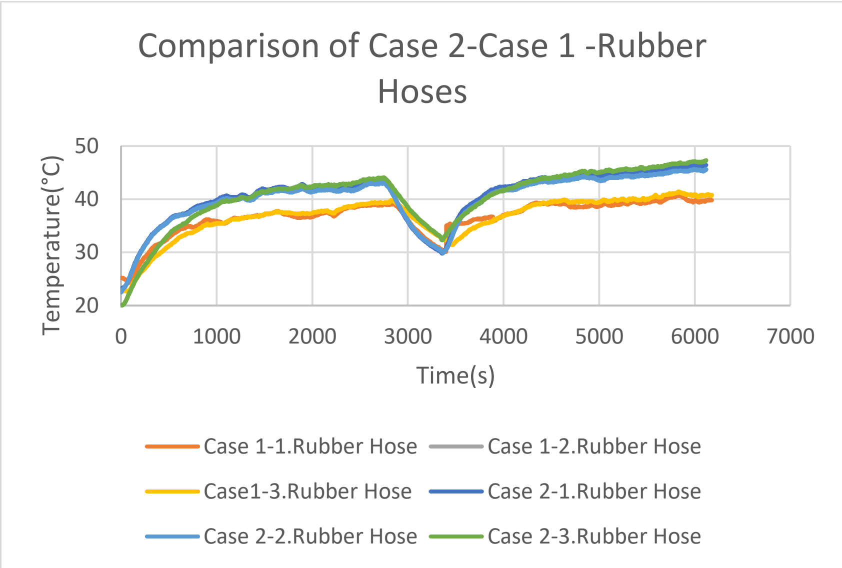


**Figure 54:** Case 1 Rubber hoses temperature changes

#### 4.6.1.4.Engine Oil Dipstick Temperature Changes

Figure 55 illustrates the temperature variations recorded at the engine oil dipstick location under Case 1 configuration. Although the dipstick itself is not a heat-generating component, its close proximity to the exhaust system and the lower region of the engine compartment makes it susceptible to ambient heat accumulation, especially under limited airflow conditions.

The P1 vent plays a critical role in managing thermal conditions in this area. When the P1 grille is open, hot air generated by the exhaust system is expelled through natural convection, thereby reducing localized heat buildup around the dipstick. This creates a more stable thermal environment, which is essential for preserving properties such as oil viscosity and ensuring accurate oil level measurements during operation.

Conversely, in scenarios where the P1 vent is closed and airflow is restricted, residual heat may accumulate in this region, potentially causing elevated temperatures around the dipstick. This can negatively affect measurement accuracy and accelerate oil oxidation or degradation, particularly during extended high-load operation.All cases comparisons are shown in Figure 55(b).

The data presented in Figure 55(a) confirm that under the optimized airflow conditions of Case 1, the dipstick temperature remains within a safe and stable range. This supports both engine health and maintenance accuracy. Compared to Case 2, Case 1 achieved approximately a 6.5% improvement in thermal performance.

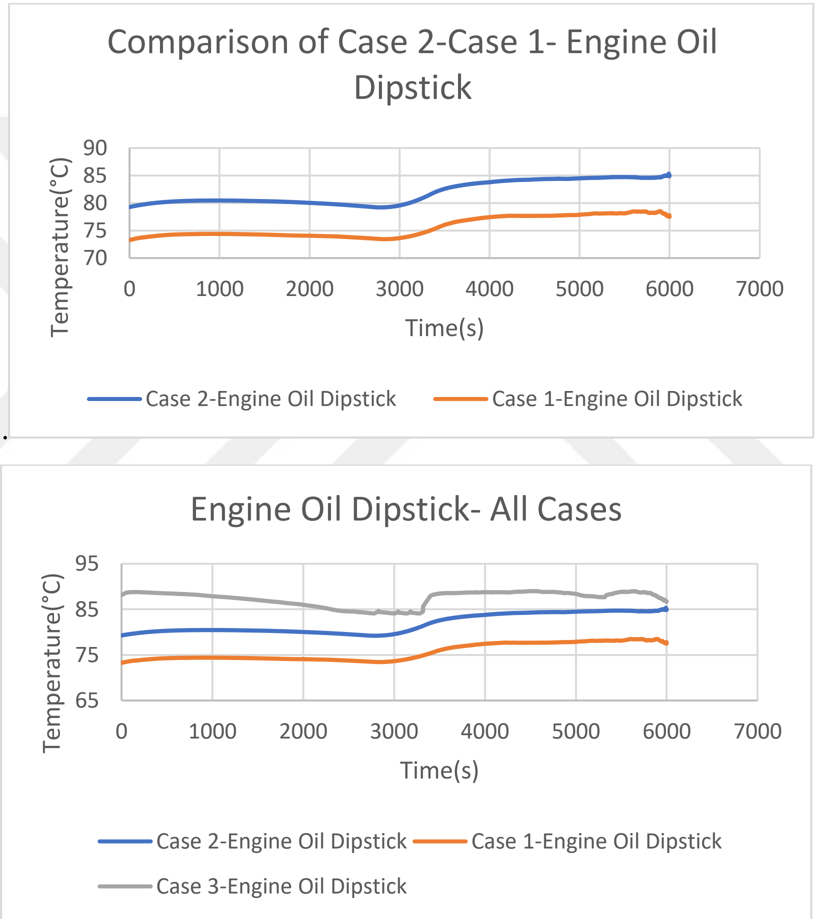


**Figure 55**: (a) Case 1 Engine oil dipstick temperature changes(b) All Cases

### 4.6.1.5.Engine Harness Connector Temperature Changes

Figure 56 illustrates the temperature variation observed at the engine harness connector location under Case 1 test conditions. This connector is positioned adjacent to the ECM and lies within the thermal influence zone of the hydraulic pump, particularly due to its close proximity to the P2 vent.

Under standard operating conditions, the hydraulic pump region emits a significant amount of heat, and if adequate ventilation is not provided, this heat can accumulate around nearby electronic and electrical components. When the P2 vent is open, natural convection is enhanced, allowing heat to be dissipated more effectively from the pump zone. As a result, the ambient temperature surrounding the connector remains within acceptable limits, thereby preserving the mechanical and electrical integrity of the harness.

In scenarios where the P2 vent is closed, prolonged exposure to elevated temperatures in this area can cause plastic insulation to deform, connector pins to lose clamping force, or electrical resistance to increase. These conditions may lead to signal loss or erratic system behavior. Therefore, maintaining a stable temperature in this area is essential for ensuring long-term operational reliability and electrical continuity.All Cases comparisons are shown in Figure 56(b).

As shown in Figure 56(a), the temperature profile under Case 1 remained stable and well below critical thresholds. This confirms that improved airflow provided by the P2 vent effectively protects sensitive electrical connectors from thermal degradation. Compared to Case 2, Case 1 achieved an approximate 11% improvement in thermal performance.

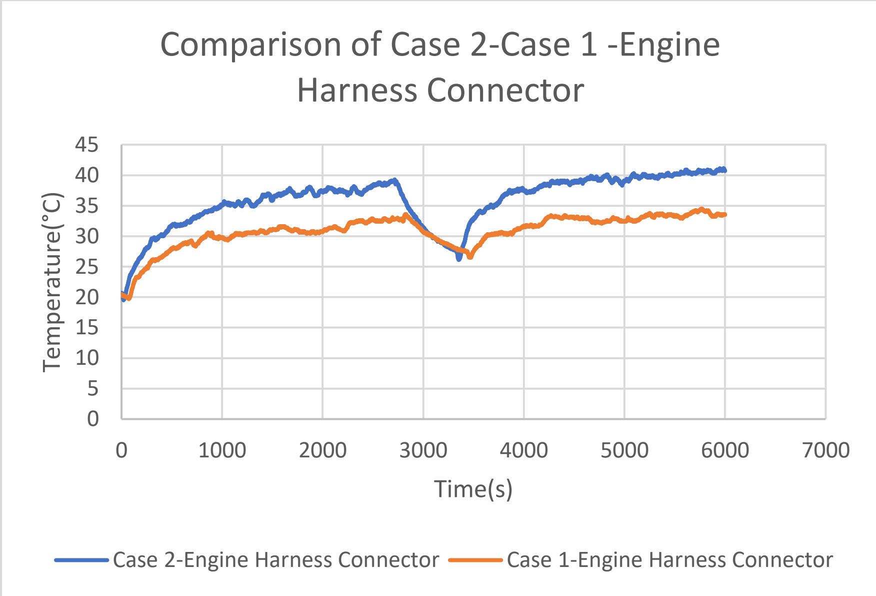


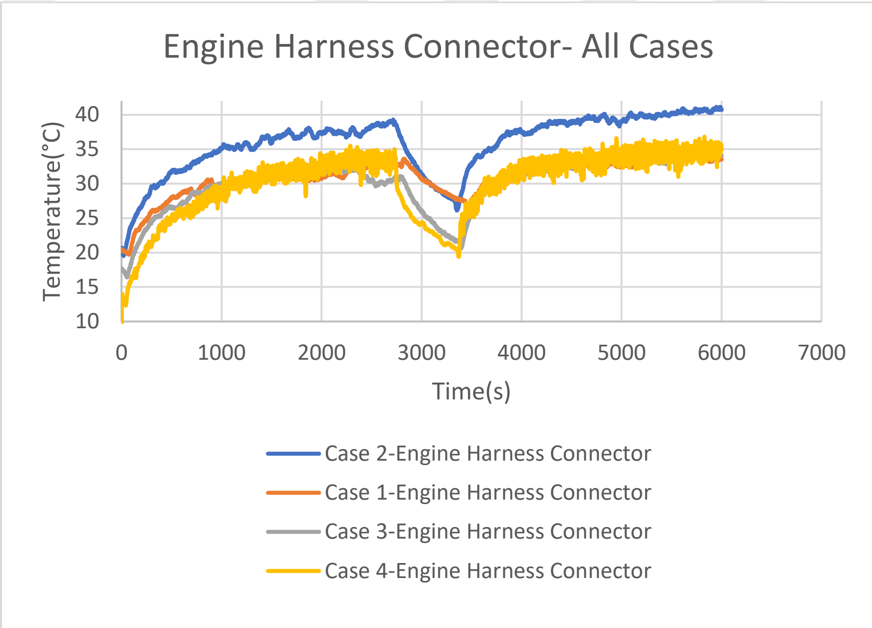


**Figure 56**: (a)Case 1 Engine harness connector temperature changes (b)All Cases Comparison

### 4.6.1.6.Radiator Regions Temperature Changes

Figure 57 illustrates the temperature variation observed in the radiator regions during the cooling performance test under Case 1 conditions. These regions are located within the air intake chamber directly behind the P3 grille, and their thermal behavior is largely dependent on the availability of forced convection airflow through this grille. When the P3 grille is open, uninterrupted ambient air intake is ensured, allowing effective forced convection heat transfer from the radiator surfaces to the surrounding air. This leads to improved cooling performance, especially under high engine load conditions or elevated ambient temperatures. The enhanced airflow also reduces the load on the cooling fans, enabling the system to maintain thermal equilibrium more effectively and lowering the risk of component overheating.

Conversely, when the P3 grille is closed, the volume of incoming air is significantly reduced. In this case, the cooling fans must operate under higher loads to compensate for the decreased airflow; this not only reduces overall cooling efficiency but can also cause engine temperatures to rise and increase thermal stress on components near the radiator.

As shown in Figure 57, the open P3 vent configuration in Case 1 supports the maintenance of stable and controlled temperature levels in the radiator region, confirming the effectiveness of the under-hood ventilation improvements in preserving the cooling system's performance. Compared to Case 2, Case 1 achieved an 8.5% thermal improvement.

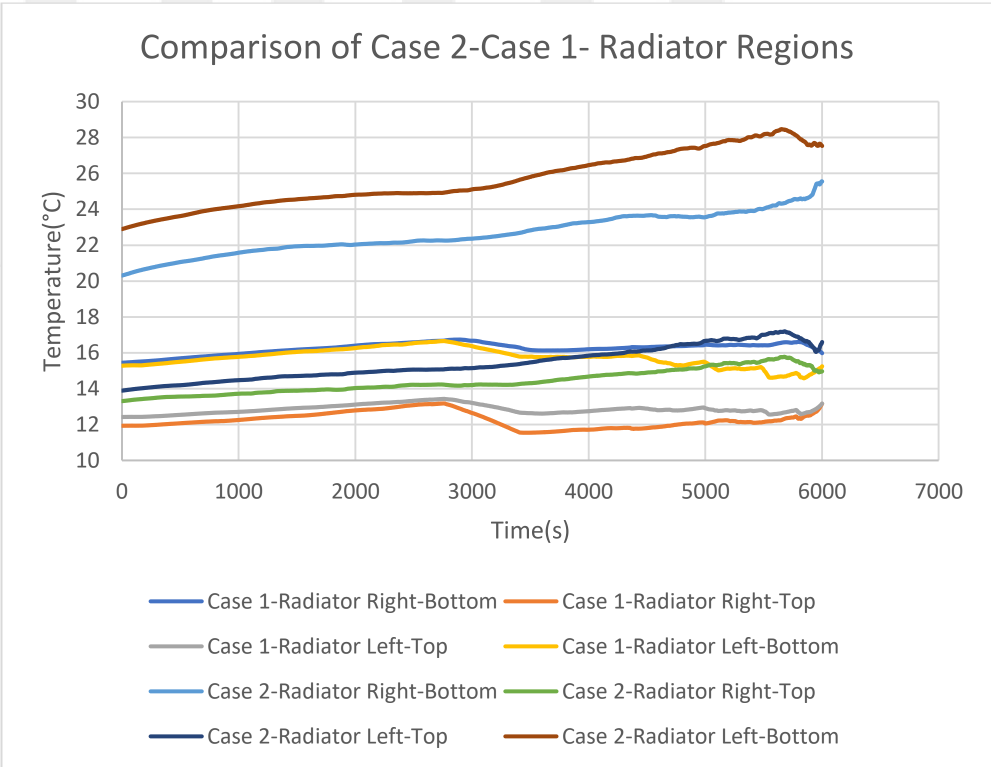


**Figure 57**: Case 1 Radiator Regions temperature changes

### 4.6.2.Case 3 Configuration

Temperature variations were examined under the configuration where the P2 vent was fully open, the P3 vent was half-closed, and the P1 vent was fully closed. Within this study, the components exhibiting the most significant temperature changes were analyzed in detail.

Since detailed information regarding the effects of the vents on the components is provided in Case 1, these details will not be repeated separately. Instead, only a comparison will be made, and the improvement rates will be indicated.

### 4.6.2.1.ECM Temperature Change

According to the thermal comparison of the ECM in Case 2 and Case 3 shown in Figure 58, Case 3 demonstrated a ~3% thermal improvement compared to Case 2.

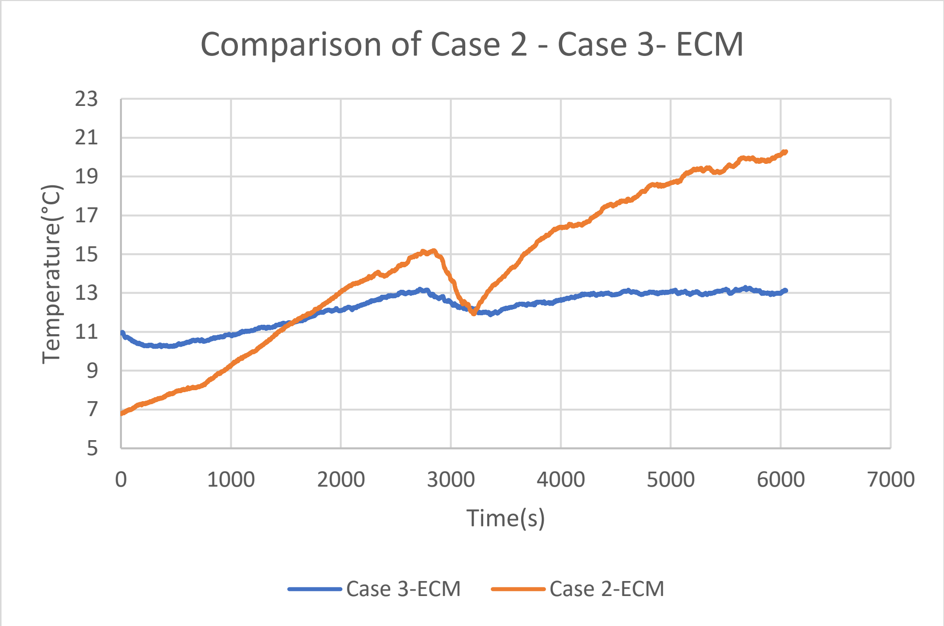


**Figure 58**: Case 3 ECM temperature changes

### 4.6.2.2.Starter Temperature Change

According to the thermal comparison of the Starter in Case 2 and Case 3 shown in Figure 59, Case 3 demonstrated a ~3 % thermal improvement compared to Case 2.

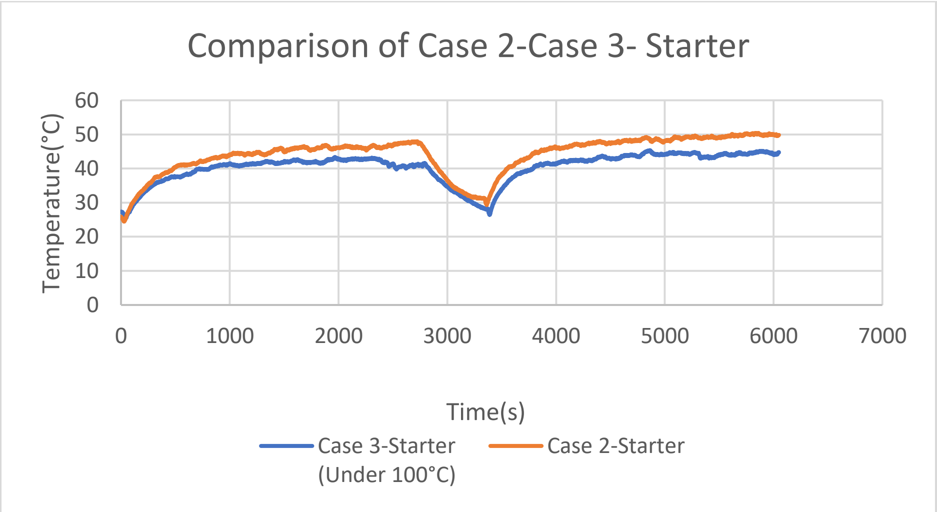


**Figure 59:** Case 3 Starter temperature changes

#### 4.6.2.3.Rubber Hoses Temperature Change

According to the thermal comparison of the Rubber Hoses in Case 2 and Case 3 shown in Figure 60, Case 3 demonstrated a ~4 % thermal improvement compared to Case 2.

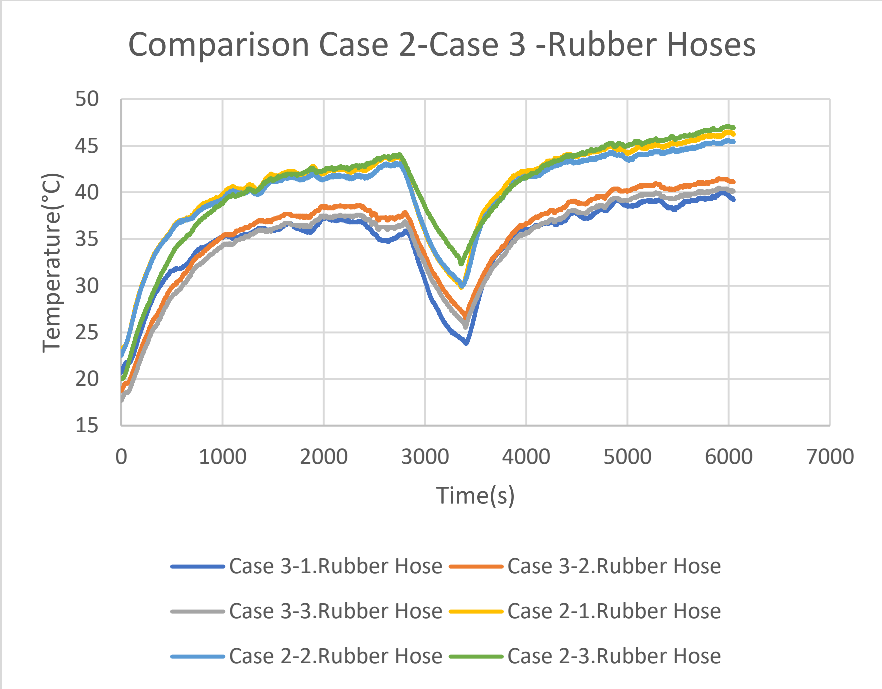


**Figure 60**: Case 3 Rubber Hoses temperature changes

#### 4.6.2.4.Engine Oil Dipstick Temperature Change

According to the thermal comparison of the Engine Oil Dipstick in Case 2 and Case 3 shown in Figure 61, Case 3 demonstrated a ~18 % thermal improvement compared to Case 2.

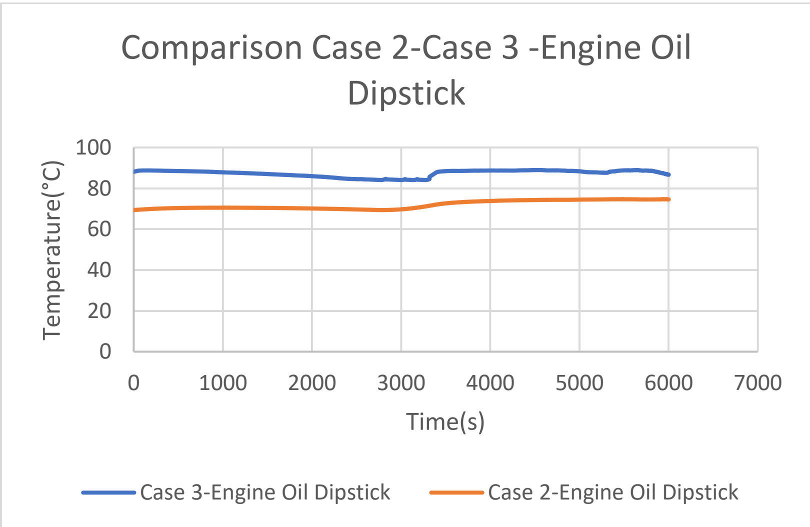


**Figure 61:** Case 3 Engine Oil Dipstick temperature changes

#### 4.6.2.5.Engine Harness Connector Temperature Change

According to the thermal comparison of the Engine Harness Connector in Case 2 and Case 3 shown in Figure 62, Case 3 demonstrated a ~2 % thermal improvement compared to Case 2.

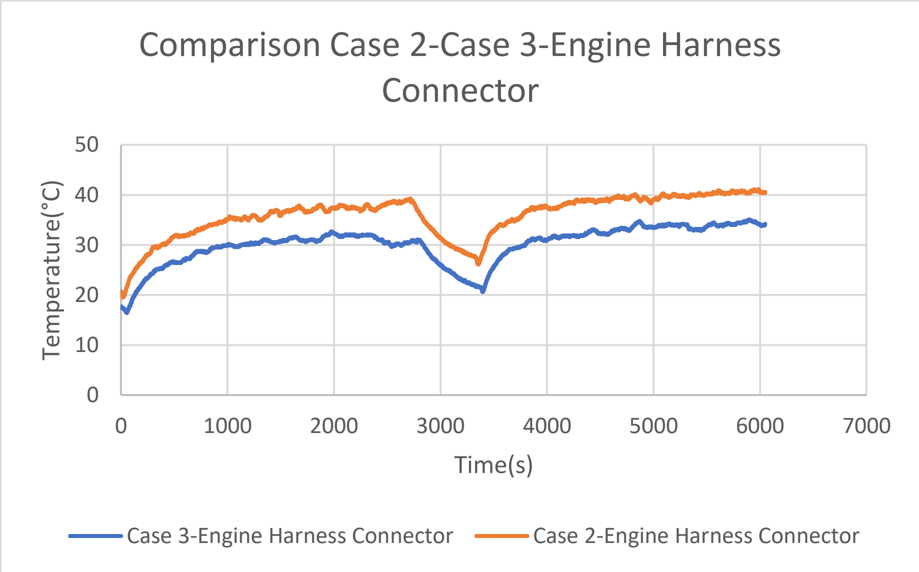


**Figure 62:** Case 3 Engine Harness Connector temperature changes

#### 4.6.2.6.Radiator Temperature Change

According to the thermal comparison of the Radiator in Case 2 and Case 3 shown in Figure 63, Case 3 demonstrated a ~7 % thermal improvement compared to Case 2.

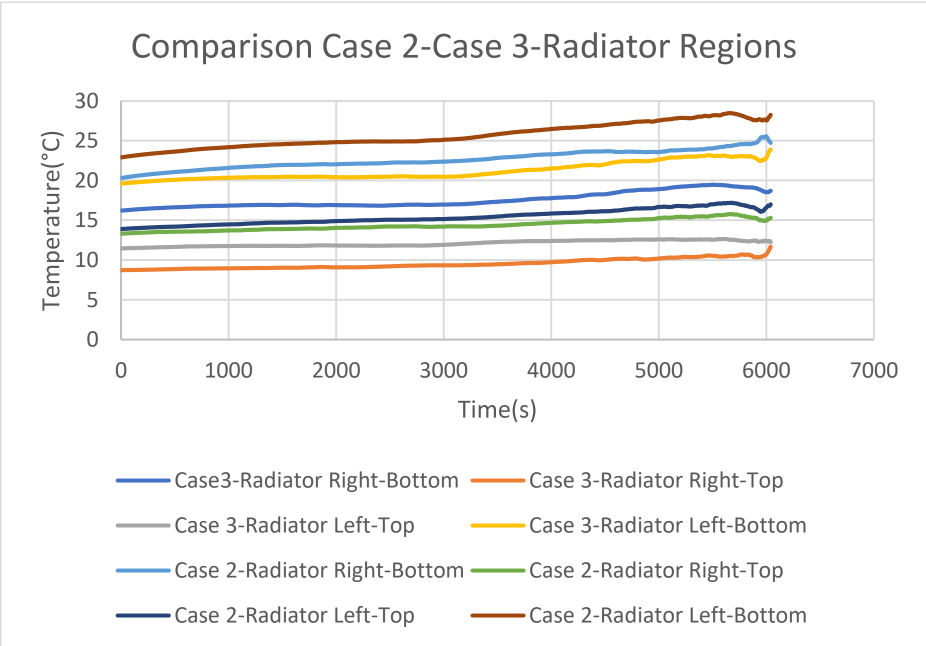


**Figure 63**: Case 3 Radiator temperature changes

#### 4.6.3.Case 4 Configuration

Temperature variations were examined under the configuration where P1 and P2 vents were fully closed and the P3 vent was half-closed. Within this study, the components exhibiting the most significant temperature changes were analyzed in detail.

##### 4.6.3.1.ECM Temperature Changes

According to the thermal comparison of the ECM in Case 2 and Case 4 shown in Figure 64, Case 4 demonstrated a ~13 % thermal improvement compared to Case 2.

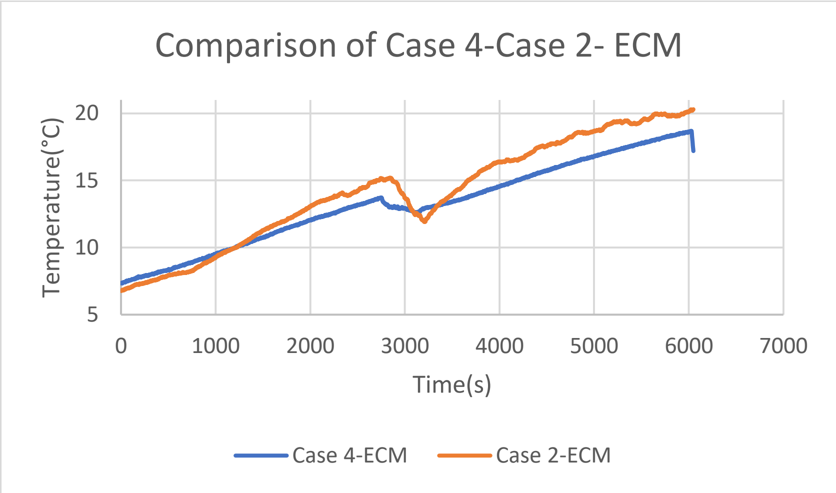


**Figure 64:** Case 4 ECM temperature changes

##### 4.6.3.2.Starter Temperature Changes

According to the thermal comparison of the Starter in Case 2 and Case 4 shown in Figure 65, Case 4 demonstrated a ~1 % thermal improvement compared to Case 2.

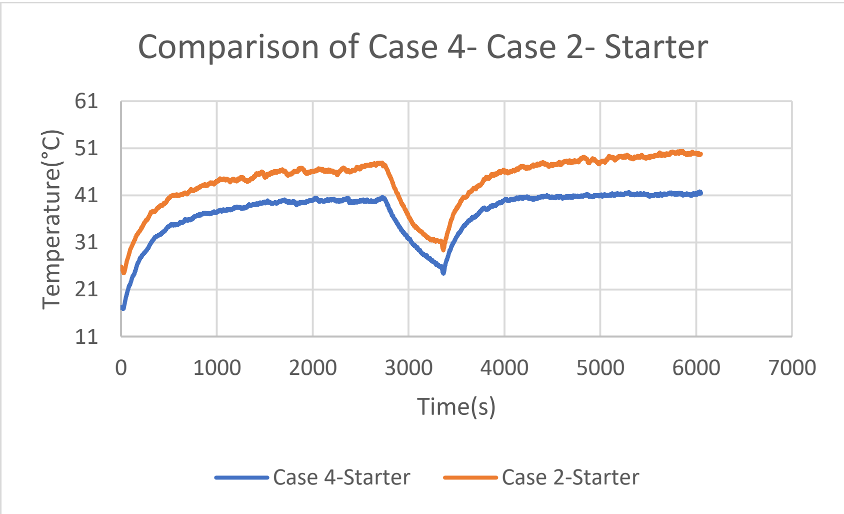


**Figure 65**: Case 4 Starter temperature changes

#### 4.6.3.3.Rubber Hoses Temperature Changes

According to the thermal comparison of the Rubber Hoses in Case 2 and Case 4 shown in Figure 66, Case 4 demonstrated a ~2 % Thermal deterioration compared to Case 2.

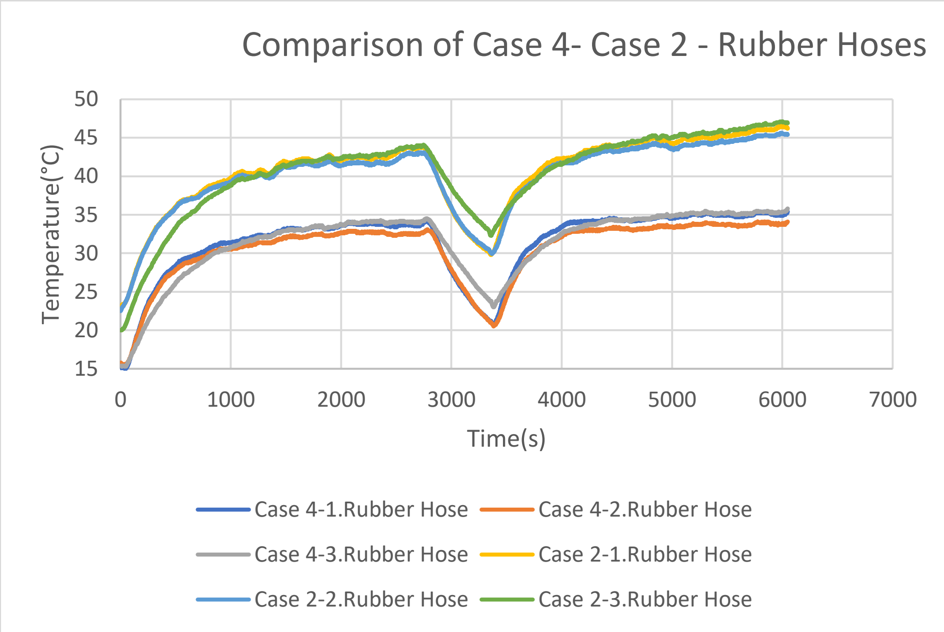


**Figure 66:** Case 4 Rubber Hoses temperature changes

#### 4.6.3.4.Engine Oil Dipstick Temperature Changes

According to the thermal comparison of the Engine Oil Dipstick in Case 2 and Case 4 shown in Figure 67, Case 4 demonstrated a ~2 % Thermal improvement compared to Case 2. Since the measurements were taken in high-precision mode with a 1-second sampling interval, instantaneous peaks in the graphs are normal.

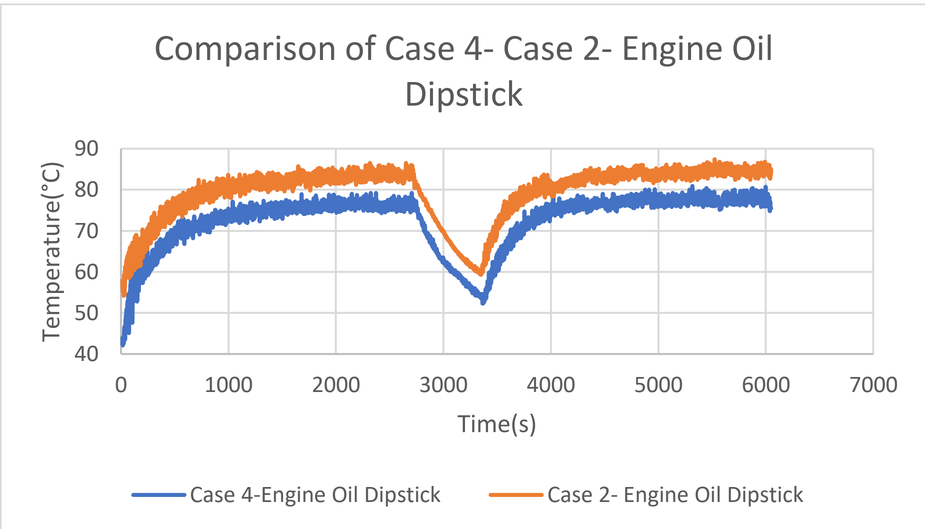


**Figure 67**: Case 4 Engine Oil Dipstick temperature changes

#### 4.6.3.5.Engine Harness Connector Temperature Changes

According to the thermal comparison of the Engine Harness Connector in Case 2 and Case 4 shown in Figure 68, Case 4 demonstrated a ~2 % Thermal improvement compared to Case 2. Since the measurements were taken in high-precision mode with a 1-second sampling interval, instantaneous peaks in the graphs are normal.

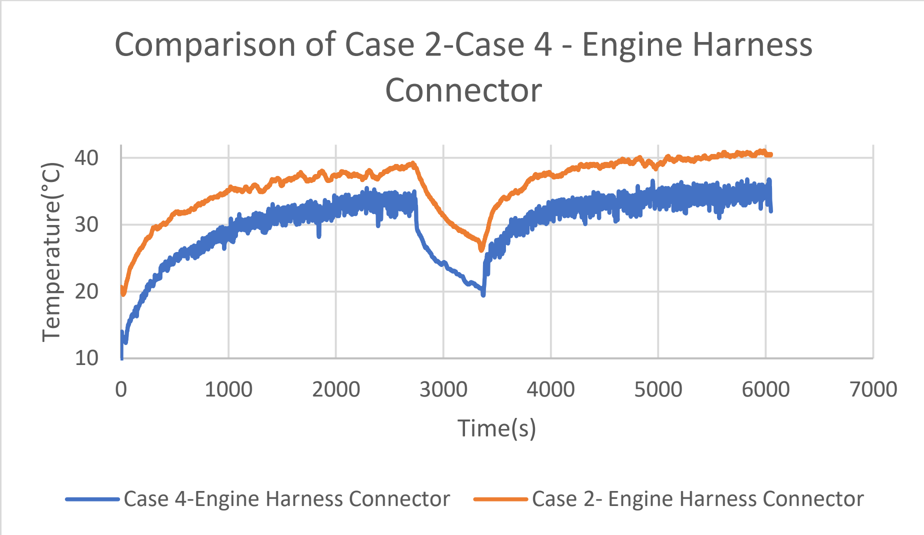


**Figure 68**: Case 4 Engine Harness Connector temperature changes

#### 4.6.3.6.Radiator Temperature Changes

According to the thermal comparison of the Engine Harness Connector in Case 2 and Case 4 shown in Figure 69, Case 4 demonstrated ~2 % Thermal deterioration compared to Case 2.

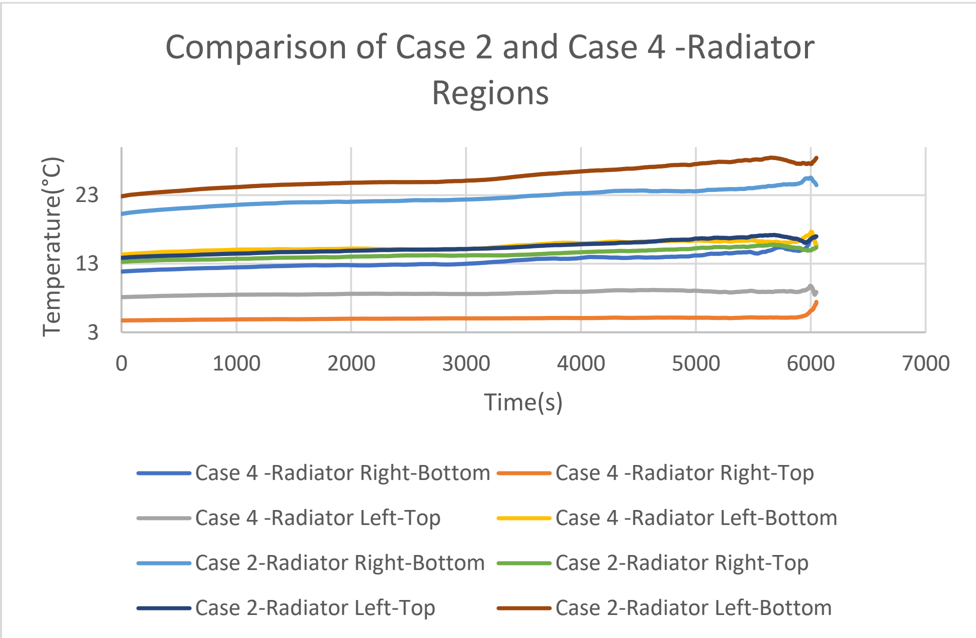


**Figure 69**: Case 4 Radiator temperature changes

Table 15 summarizes the peak temperatures observed for key under-hood components during the cooling performance test, specifically under the Case 1 configuration where all ventilation grilles (P1, P2, and P3) were completely open. The focus of this data is on the localized thermal behavior of parts that are either heat-sensitive or located close to significant heat sources like the exhaust, hydraulic pump, or radiators.

The results confirm that all monitored components stayed within their safe operating temperature limits, as specified by the engine or component manufacturers. Critical elements such as the engine coolant outlet, hydraulic oil, intercooler outlet, and other heat-sensitive parts (e.g., ECM, starter motor, rubber hoses, electrical harness connectors) all maintained safe thermal margins throughout the full-load test cycle.

This positive outcome demonstrates the effectiveness of the open-vent layout in Case 1. It significantly improves under-hood airflow, boosts natural convection, and reduces heat buildup, particularly in areas prone to localized overheating. Furthermore, this ventilation strategy helps protect electrical insulation, mechanical seals, and ensures accurate engine measurements.

Ultimately, the data in Table 15 validates that Case 1 provides the optimal thermal environment, enhancing both component reliability and system stability by preventing any critical temperature excursions.

**Table 15:** Summary of Local Temperature Behaviors in Case 1

| Component / Region | Vent Proximity | Thermal Risk (If Vent Closed) | Benefit of Ventilation | Observed Max Temp | Limit Value |
|---|---|---|---|---|---|
| ECM | Near P2 | Heat accumulation from hydraulic pumps | Stabilized temp improves component life | ~20°C | Under 75°C |
| Starter | Near P1 | Heat buildup from exhaust area | Lower thermal stress on magnetic parts | ~44°C | Under 100°C |
| Rubber Hoses (x3) | Upper side near P1 | Risk of hardening/cracking due to rising hot air | Maintains elasticity and sealing function | ~47°C | Under 150°C |

**Table 15 Cont.**

| Component / Region | Vent Proximity | Thermal Risk (If Vent Closed) | Benefit of Ventilation | Observed Max Temp | Limit Value |
|---|---|---|---|---|---|
| Engine Oil Dipstick | Near P1 | Hot air affects oil readings and degrades oil | Maintains viscosity and measurement accuracy | ~80°C | Not specified (monitored) |
| Engine Harness Connector | Near P2 | Risk of insulation/plastic deformation | Preserves contact force and signal transmission | ~34°C | Under 100°C |
| Radiator Regions | Behind P3 | Limited airflow reduces cooling effectiveness | Enhanced radiator airflow, lower thermal load | ~23°C | Water Out < 95°C |

As data from Table 15 clearly shows, maximum temperatures vary considerably among under-hood components, influenced by their location, material, and closeness to major heat sources. These variations provide valuable insight into the thermal dynamics within the engine compartment under Case 1 conditions.

The engine oil dipstick registered the highest temperature, at around 80°C. Even though the dipstick isn't a direct heat source, its location near the exhaust system and within a relatively enclosed space makes it susceptible to radiant and convective heat buildup, especially during continuous high-load operation. Despite airflow from the P1 vent, the complex geometry and limited localized airflow in this area contribute to its higher thermal exposure. This finding underscores that vent positioning is crucial relative to component geometry, not just the overall airflow.

Conversely, the ECM recorded the lowest maximum temperature, at approximately 20°C. Despite being near the heat-generating hydraulic pumps, the ECM benefits from its shielded mounting and its proximity to the P2 vent, which significantly enhances convective cooling. This relatively low temperature confirms that the Case 1 ventilation strategy is highly effective in this zone, providing excellent thermal protection for electronic components.

Other components, such as the rubber hoses (~47°C) and starter motor (~44°C), experienced intermediate thermal exposure. Their temperature profiles align with their material properties and their location relative to both the P1 vent and the primary heat sources.

These findings highlight that thermal risk isn't just about component sensitivity. It's also about the complex interplay between airflow paths, component geometry, and the proximity of heat sources. The specific open-vent configuration in Case 1 effectively minimizes localized overheating, supporting the long-term reliability of temperature-sensitive components.

### 4.7. RESULTS OF NOISE MEASUREMENT

Construction machinery is subject to various performance and environmental standards due to the demanding conditions in which it operates. One of these is the ISO 6395 Standard, which regulates exterior noise levels emitted by earth-moving equipment under defined test conditions.

In this study, while investigating the under-hood airflow characteristics through experimental methods, noise emissions were also taken into consideration alongside temperature and pressure parameters. This inclusion was necessary because the modifications applied to the engine hood—primarily aimed at improving airflow—have a direct influence on external noise behavior.

The design improvements focus on enhancing the air circulation from the internal compartment to the external environment, which, in turn, affects the propagation of noise generated by the engine, fans, pumps, and other internal components. As airflow pathways are opened or modified, they not only facilitate thermal dissipation but also alter the acoustic transmission path.

To ensure the overall effectiveness of the proposed improvements, it is essential to monitor noise levels concurrently with other regulated parameters. For this reason, noise measurements were systematically performed for all ventilation cases, allowing for a holistic assessment of the system's compliance with thermal, mechanical, and acoustic standards

In Figure 58, under-hood noise level analysis across ventilation configurations is depicted. In these results, Cycle 1-2-3 indicates that the noise measurements were repeated three times for verification purposes.The main findings can be given as follows:

*Case 1 (P1, P2, P3 Open) – Maximum Ventilation*

With all ventilation grilles (P1, P2, and P3) fully open, the sound power level (LWA) was 102.503 dB(A), with a ΔL of 15.4 dB. This configuration resulted in the second highest noise level. While maximum airflow is achieved due to all vents being open, this also facilitates the transmission of internal noise to the exterior. In Case 1, the noise level has deteriorated by approximately 2% compared to Case 2.

*Case 2 (P1 and P2 Closed, P3 Half-Open) – Most Restricted Ventilation*

In Case 2, where P1 and P2 were closed and P3 was half-open, the sound power level was 102.318 dB(A), with a ΔL of 15.1 dB. This is slightly lower than Case 1. The reduced air outflow likely limited the transmission of sound to the outside.

*Case 3 (P1 Closed, P2 Open, P3 Half-Open) – Medium Level Ventilation*

Case 3, with P1 closed and P2 and P3 half-open, yielded the lowest noise level at 102.200 dB(A), and a ΔL of 13.8 dB. The open P2 likely helps mitigate noise from the hydraulic pump area, while the closed P1 effectively dampens noise originating from the exhaust side. In Case 3, the noise level has improved by approximately 1% compared to Case 2.

*Case 4 (P1 and P2 Closed, P3 Half-Closed) – Most Restricted Airflow*

This configuration, with P1 and P2 closed and P3 half-closed, resulted in the second lowest sound power level at 101.578 dB(A), and a ΔL of 15.7 dB. While this provides the most restricted ventilation, thus limiting sound emission, it's important to note that this also leads to reduced cooling performance. In Case 4, the noise level has improved by approximately 7% compared to Case 2.

| Points | Cycle 1 Sound Pressure Level $L_{PA}$ | Cycle 2 Sound Pressure Level $L_{PA}$ | Cycle 3 Measured Sound Pressure Level $L_{PA}$ |
|---|---|---|---|
| 2 | 72,56 | 72,34 | 72,52 |
| 4 | 75,33 | 75,35 | 75,55 |
| 6 | 74,66 | 74,71 | 74,72 |
| 8 | 73,46 | 73,60 | 73,56 |
| 10 | 75,69 | 75,55 | 75,69 |
| 12 | 74,30 | 74,28 | 74,43 |
| $L_{PA}$ | 74,46 | 74,43 | 74,55 |
| $L_S$ | 28,0 | 28,0 | 28,0 |
| $L_{WA}$ | 102,460 | 102,435 | 102,546 |

| Enviromental Noise | |
|---|---|
| Points | Measured Sound Pressure Level $L_{PA}$ |
| 2 | 54 |
| 4 | 53 |
| 6 | 54 |
| 8 | 53 |
| 10 | 57 |
| 12 | 57 |
| $L_{PA}$ | 55,0 |
| $\Delta L$ | 15,4 |

Measured Sound Power Level $L_{WA}$ 102,503

| Points | Cycle 1 Sound Pressure Level $L_{PA}$ | Cycle 2 Sound Pressure Level $L_{PA}$ | Cycle 3 Measured Sound Pressure Level $L_{PA}$ |
|---|---|---|---|
| 2 | 72,48 | 72,52 | 72,60 |
| 4 | 75,32 | 75,39 | 75,24 |
| 6 | 74,49 | 74,72 | 74,52 |
| 8 | 72,73 | 72,53 | 73,37 |
| 10 | 75,43 | 75,50 | 75,54 |
| 12 | 74,14 | 74,13 | 74,06 |
| $L_{PA}$ | 74,25 | 74,30 | 74,34 |
| $L_S$ | 28,0 | 28,0 | 28,0 |
| $L_{WA}$ | 102,245 | 102,297 | 102,339 |

| Enviromental Noise | |
|---|---|
| Points | Measured Sound Pressure Level $L_{PA}$ |
| 2 | 55,2 |
| 4 | 53 |
| 6 | 55,2 |
| 8 | 53 |
| 10 | 56,5 |
| 12 | 56,5 |
| $L_{PA}$ | 55,1 |
| $\Delta L$ | 15,1 |

Measured Sound Power Level $L_{WA}$ 102,318

| Points | Cycle 1 Sound Pressure Level $L_{PA}$ | Cycle 2 Sound Pressure Level $L_{PA}$ | Cycle 3 Measured Sound Pressure Level $L_{PA}$ |
|---|---|---|---|
| 2 | 72,84 | 72,84 | 72,82 |
| 4 | 75,59 | 75,43 | 75,39 |
| 6 | 74,11 | 74,11 | 74,00 |
| 8 | 72,42 | 72,30 | 72,09 |
| 10 | 75,72 | 75,65 | 75,69 |
| 12 | 73,61 | 73,63 | 73,50 |
| $L_{PA}$ | 74,23 | 74,17 | 74,11 |
| $L_S$ | 28,0 | 28,0 | 28,0 |
| $L_{WA}$ | 102,231 | 102,169 | 102,108 |

| Enviromental Noise | |
|---|---|
| Points | Measured Sound Pressure Level $L_{PA}$ |
| 2 | 55,48 |
| 4 | 53,79 |
| 6 | 55,48 |
| 8 | 53,79 |
| 10 | 58,38 |
| 12 | 58,38 |
| $L_{PA}$ | 56,3 |
| $\Delta L$ | 13,8 |

Measured Sound Power Level $L_{WA}$ 102,200

| Points | Cycle 1 Sound Pressure Level $L_{PA}$ | Cycle 2 Sound Pressure Level $L_{PA}$ | Cycle 3 Measured Sound Pressure Level $L_{PA}$ |
|---|---|---|---|
| 2 | 72,32 | 72,26 | 72,30 |
| 4 | 74,78 | 74,77 | 74,75 |
| 6 | 73,26 | 73,21 | 73,07 |
| 8 | 71,52 | 71,46 | 71,37 |
| 10 | 75,36 | 75,24 | 75,48 |
| 12 | 73,12 | 73,19 | 73,02 |
| $L_{PA}$ | 73,60 | 73,55 | 73,56 |
| $L_S$ | 28,0 | 28,0 | 28,0 |
| $L_{WA}$ | 101,597 | 101,555 | 101,560 |

| Enviromental Noise | |
|---|---|
| Points | Measured Sound Pressure Level $L_{PA}$ |
| 2 | 54 |
| 4 | 52,2 |
| 6 | 54 |
| 8 | 52,2 |
| 10 | 54,8 |
| 12 | 54,8 |
| $L_{PA}$ | 53,8 |
| $\Delta L$ | 15,7 |

Measured Sound Power Level $L_{WA}$ 101,578

**Figure 70:** **(a)** Case 1 Noise Measurement **(b)** Case 2 Noise Measurement **(c)** Case 3 Noise Measurement **(d)** Case 4 Noise Measurement

## 4.8.COMPARISON OF RESULTS AND RECOMMENDATIONS

This study thoroughly examined how different hood ventilation setups affect both thermal management and acoustic performance in high-load construction machinery. We tested four distinct grille configurations (Case 1 to Case 4), meticulously monitoring parameters like intercooler pressure drop, exhaust back pressure, air intake pressure, component-level temperature distributions, and external noise levels (in accordance with ISO 6395 standards)[38].

Thermal Performance:

- Thermal performance results clearly showed that Case 1, with all vents (P1, P2, and P3) fully open, provided the most efficient cooling across all critical components. The maximum airflow in this setup led to effective natural convection, resulting in lower temperatures for components such as the ECM, starter motor, rubber hoses, and radiator regions. This configuration successfully prevented heat buildup in high-risk areas, keeping all component temperatures well within their safety limits. Even the engine oil dipstick, which registered the highest temperature at approximately 80°C, remained within an acceptable range.
- However, this superior thermal environment came with a trade-off: increased external noise emission. Case 1 recorded the second highest sound power level at around 102.5 dB(A), which could be an issue in noise-sensitive applications or areas with strict regulatory requirements.
- Case 3 emerged as a more balanced solution. With P2 open and P1 closed, this configuration still achieved acceptable thermal behavior, particularly for components affected by hydraulic pump heat. From an acoustic perspective, it recorded a reasonable external noise level of approximately 102.2 dB(A), which complies with regulatory limits. This demonstrates that targeted ventilation provides sufficient cooling without compromising acoustic comfort, in contrast to fully opening all vents.
- In contrast, Case 4, which had the most restricted airflow, led to elevated localized temperatures, especially around the radiator and within the engine compartment. While this configuration was acoustically favorable, it may not be sustainable for extended high-load operations due to increased thermal risks.
- Case 2, serving as the baseline configuration of the machine, offers an intermediate solution with the P1 and P2 vents closed and P3 partially open. While the noise level remains moderate and the thermal performance is relatively balanced, this configuration fails to outperform Case 3 in terms of either thermal efficiency or noise reduction.

This study highlights the critical importance of multi-parameter optimization in machine design. Ventilation strategies must be evaluated not only for their ability to dissipate heat but also for their acoustic implications, potential effects on material aging, and compliance with regulatory constraints. The findings underscore that:

- Thermal safety and component durability can be maximized by improving airflow in targeted regions, especially near P2 and P3.
- Noise reduction strategies can be achieved by selectively closing vents in areas with high sound emission, particularly near P1.
- An integrated design approach combining Computational Fluid Dynamics (CFD), thermal testing, and acoustic validation is essential for developing next-generation construction equipment that meets performance, comfort, and compliance requirements.

Therefore, the optimal hood design might not be the one with the most open ventilation. Instead, it's likely the configuration that strikes a balance between thermal control and noise mitigation, with Case 3 serving as a prime example of this principle. Also, in Table 11, In the comparative evaluation of different ventilation configurations based on thermal and acoustic performance, each scenario was assessed relative to the baseline configuration, Case 2. Case 1 delivered the highest thermal improvement at 15.3%, making it the best performer in terms of cooling efficiency. However, this benefit came at the cost of a 1.8% increase in noise level, which poses a disadvantage in terms of operator comfort and potential regulatory compliance. On the other hand, Case 4 achieved the greatest noise reduction with a 2.9% improvement, yet offered only a limited thermal gain of 5.4%. In this context, Case 3 stands out as the most balanced configuration, delivering a meaningful thermal improvement of 8.9% while also achieving a modest 0.7% reduction in noise level. This dual benefit indicates that engine compartment temperatures are effectively reduced without compromising—indeed slightly enhancing—acoustic comfort. The ability to improve both criteria simultaneously makes Case 3 not only a technically viable solution but also the most practical for real-world application. Therefore, Case 3 was selected as the optimal configuration to enhance component reliability and overall user experience.

**Table 16:** Thermal and Noise Performance Changes Compared to Standard Configuration(Case 2)

| | **ECM** | **Starter** | **Rubber Hoses** | **Engine Oil Dipstick** | **Engine Harness Connector** | **Radiator Regions** | **Noise Level** |
|---|---|---|---|---|---|---|---|
| **Case 1** | 4% improvement | 8% improvement | 8.5% improvement | 6.5% improvement | 11% improvement | 8.5% improvement. | 2 % Noise deterioration |
| **Case 3** | 3% improvement | 3% improvement | 4% improvement | 18% improvement | 2% improvement | 7% improvement | 1% improvement |
| **Case 4** | 13% improvement | 1% improvement | 2 % Thermal deterioration | 2% improvement | 2% improvement | 2 % Thermal deterioration | 7% improvement |

## 4.9. CONCLUSION

In this thesis, passive ventilation solutions were investigated to reduce thermal accumulation within the engine compartment of excavator-type construction machinery. Accordingly, the effects of different hood vent configurations were experimentally compared and evaluated against the baseline configuration (Case 2) in terms of both thermal performance and acoustic emission.

In compliance with ISO 6395 standards, key performance parameters such as intercooler pressure drop, exhaust back pressure, intake air pressure, component-level temperature measurements, and external sound power levels were monitored. The results showed that Case 1, in which all vents were fully open, provided the highest cooling efficiency. However, it also caused a noticeable increase in noise emissions, which may present a disadvantage in acoustically sensitive environments.

Case 3, in which only the P2 vent was open, successfully maintained acceptable thermal conditions—particularly around components affected by heat from the hydraulic pump—while also minimizing external noise levels. This configuration demonstrated the most balanced outcome in terms of both thermal and acoustic criteria and was identified as the optimal setup.

The findings revealed that maximizing vent area does not necessarily result in the best overall system performance. Instead, directing airflow specifically toward thermally critical zones proves more effective in ensuring component protection without compromising noise regulation compliance. Furthermore, the study emphasizes that ventilation strategies should be evaluated not only for thermal efficiency but also in terms of acoustic comfort and regulatory compliance.

This study provides valuable engineering insights for future machine design processes by highlighting the importance of an integrated development approach combining Computational Fluid Dynamics (CFD), experimental thermal analysis, and acoustic validation. The outcomes lay a foundation for developing next-generation construction equipment with enhanced thermal resilience, regulatory conformity, and reduced environmental noise impact.

# REFERENCES

[1] GRANSBERG D. D., POPESCU C. M. and RYAN R. C. (2006), *Construction Equipment Management for Engineers, Estimators, and Owners*, CRC Press, Boca Raton, FL.

[2] ARBAB M.I., MASJUKI H.H., KALAM M.A., IMRAN A., VARMAN M., ASHRAFUL A.M. and RIZWANUL FATTAH I.M. (2015), “Evaluation of combustion, performance, and emissions of optimum palm–coconut blend in turbocharged and non-turbocharged conditions of a diesel engine”, *Energy Conversion and Management*, Vol. 90, pp. 111–120.

[3] European Union (2016), *Regulation (EU) 2016/1628 of the European Parliament and of the Council of 14 September 2016*, pp. 53–117, Luxembourg..

[4] European Union (1998), *Directive 97/68/EC of the European Parliament and of the Council of 16 December 1997 on the approximation of the laws of the Member States relating to measures against the emission of gaseous and particulate pollutants from internal combustion engines to be installed in non-road mobile machinery*, pp. 1–86, Brussels.

[5] KALIAFETIS P. and COSTOPOULOS Th. (1995), “Modelling and Simulation of an axial piston variable displacement pump with pressure control*”,In, Mechanism and machine theory*, Vol.20, No.4, pp.599-612, Elsevier.

[6] YU H., LIU Y. and HASAN M. S. (2010), “Review of modelling and remote control for excavators”, *International Journal of Advanced Mechatronic Systems*, Vol. 2, No. 1/2, ss. 68–80.

[7] KIM J., JIN M., CHOI W. and LEE J. (2019), “Discrete time delay control for hydraulic excavator motion control with terminal sliding mode control”, *Mechatronics*, Vol. 60, pp. 15–25.

[8] UEDA K., TSUCHIHASHI T., NAKASHIMA H., YAMAGUCHI Z., MASUDA K. and TABUCHI S. (2019), “Evolution and development of iNDr”, *KOBELCO Technology Review*, No. 37, pp. 31–35.

[9] OZTURK I., KOYUNCU A., PENEKLIOĞLU K. and KARAISMAIL E. (2018), "Effect of radiator cooling package alignment on underhood cooling performance of an agricultural tractor", *International Journal of Advances in Automotive Technology*, Vol. 1, No. 1, pp. 47–53.

[10] LJUNGSKOG E. and NILSSON U. (2014), *CFD for Underhood Modeling: Development of an Efficient Method* (Master's Thesis), Chalmers University of Technology, Göteborg.

[11] NORDIN J. (2017), *CFD Study of Optimal Under-hood Flow for Thermal Management of Electric Vehicles* (Master's Thesis), Chalmers University of Technology, Göteborg.

[12] DHUMAL A., AMBHORE N., KORE S., NAIK A., PHIRKE V. and GHUGE K. (2024), "Investigation of the effect of different fins configurations on the thermal performance of the radiator", *Journal of Advanced Research in Fluid Mechanics and Thermal Sciences*, Vol. 116, No. 1, pp. 27–39,

[13] KADIR S. A. and YOUSIF M. S. (2021), "CFD Simulation of Underhood Airflow and Heat Transfer for Automotive Engine Cooling", *International Journal of Automotive Technology*, Vol. 22, No. 3, pp. 591–602.

[14] ZHANG Y., WEI L. and SONG H. (2020), "Numerical Study on the Effect of Engine Cooling Fan on Underhood Flow and Temperature Distribution", *Applied Thermal Engineering*, Vol. 175, p. 115319.

[15] HUSSAIN M. R. and PANDA S. K. (2021), "Thermal–Fluid Numerical Analysis of Underhood Cooling System Using Conjugate Heat Transfer", *International Journal of Heat and Mass Transfer*, Vol. 167, p. 120738.

[16] GOLLIN M. and BJORK D. (1996), "Comparative Performance of Ethylene Glycol/Water and Propylene Glycol/Water Coolants in Automobile Radiators", *International Congress & Exposition*, SAE Technical Paper No. 960372, pp. 115–123, DOI: 10.4271/960372.

[17] ISMAEL T., YUN S. B. and ULUGBEK F. (2016), "Radiator Heat Dissipation Performance", *Journal of Electronics Cooling and Thermal Control*, Vol. 6, pp. 88–96.

[18] UEDA K., TSUCHIHASHI T., NAKASHIMA H., YAMAGUCHI Z., MASUDA K. and TABUCHI S. (2019), "Evolution and Development of iNDr", *KOBELCO Technology Review*, No. 37, pp. 31–35.

[19] MEZARCIOZ S. (2018), "Değişik sürüş şartları altında bir yolcu otobüsünün motor odası sıcaklık dağılımının belirlenmesi", *Mühendis ve Makina*, Vol. 59, No. 693, pp. 54–63.

[20] Kula, S. (2022), *Motor performansını iyileştirmek için gelişmiş motor soğutma sistemi tasarımı* (Doctoral Dissertation), Bursa Uludağ Üniversitesi, Bursa.

[21] RAJPUT R. K. (2007), *Internal Combustion Engine*, 2nd Edition, Laxmi Publications Ltd, New Delhi.

[22] WANG J., ZHANG Y., LIU H. and YANG X. (2025), "Numerical investigation on thermal–hydraulic performance of an intercooler with bionic channel textures", *International Journal of Heat and Fluid Flow*, Vol. 99, Article No. 109744.

[23] BACCAR M., CHTOUROU S. and DJEMEL H. (2022), "Three-dimensional numerical study of a new intercooler design", *International Journal of Thermofluids*, Vol. 17, Article No. 100263.

[24] ALAM M. J. E., DANG N. T. and LEE P. D. (2021), "Experimental Investigation of Underhood Airflow and Cooling Performance in Passenger Cars", *Applied Thermal Engineering*, Vol. 182, p. 116092.

[25] KIM T. S., JUNG S. H. and LEE J. W. (2019), "Experimental Study on Thermal Management of Heavy-Duty Diesel Engine Underhood Flow", *International Journal of Heat and Mass Transfer*, Vol. 142, p. 118585.

[26] ROSSI L., RICCI M. and D'ANGELO F. (2020), "Wind Tunnel Experimental Investigation of Underhood Flow Fields in High-Performance Vehicles", *Experimental Thermal and Fluid Science*, Vol. 109, p. 109882.

[27] ZHANG B., LI X., WANG Y. and LIU Z. (2021), "Numerical simulation of flow field characteristics of the cooling water jacket of a marine diesel engine", *E3S Web of Conferences*, Vol. 261, No. 2, p. 02040.

[28] APAYDIN S. and DONER N. (2024), "Effects of piston cooling gallery geometry on temperature and flow in a heavy-duty diesel engine", *Thermal Science and Engineering Progress*,Vol. 51, Article 102644, DOI:10.1016/j.tsep.2024.102644.

[29] KIM H. R., SEO Y. M., HA M. Y., LEE J. S. and KIM P. Y. (2019), "Numerical study on the engine room cooling performance of a medium size excavator", *Progress in Computational Fluid Dynamics, An International Journal*, Vol. 19, No. 3, ss. 191–203, DOI:10.1504/PCFD.2019.099596.

[30] SEYBOLD L., SMITH J. and JOHNSON M. (2016), "Optimization of an engine coolant radiator for vehicle thermal management", *ASME 2016 International Mechanical Engineering Congress and Exposition*, pp. 1-8, Phoenix.

[31] PARSONS S. R. and HARPER D. R. (1922), "Radiators for aircraft engines", *National Institute of Standards and Technology Technologic Paper T211*, pp. 1-36, Gaithersburg.

[32] WANG Fang, LI Yanjie, ZHANG Zhenyu and LIU Hongwei (2021), "Control design of a hydraulic cooling fan drive for off-road vehicle diesel engine with a power split hydraulic transmission", *IEEE/ASME Transactions on Mechatronics*, Vol. PP, No. 99, pp. 1–13

[33] TRUKHANOV K. (2012), "Mathematical modeling of hydraulic drive of a fan for automotive engine cooling system", *Izvestiya MGTU MAMI*, Vol. 6, No. 1, pp. 84–95.

[34] TORAMAN E. (2013), Modeling, simulation and experimental verification of a hydraulic fan drive system (Master's Thesis), Mechanical Engineering Department, Middle East Technical University, Ankara.

[35] KALYONCU Arif (2022), "Reversible fan drive systems", *IX. Ulusal Hidrolik Pnömatik Kongresi Bildirileri*, pp. 572–581, Ankara

[36] ADDO K. D., DAVIS F., FIAGBE Y. A. and ANDREWS A. (2023), "Machine learning for predictive modelling of the performance of automobile engine operating without coolant thermostat", *Scientific African*, Vol 21, pp. e01802

[37] KO J. S., HUH J. H. and KIM J. C. (2019), "Improvement of energy efficiency and control performance of cooling system fan applied to Industry 4.0 data center", *Electronics*, Vol 8, No 5, pp. 582.

[38] INTERNATIONAL ORGANIZATION FOR STANDARDIZATION (2008), *ISO 6395,2008 – Earth-moving machinery – Determination of sound power level – Dynamic test conditions*, Geneva, Switzerland.

[39] MORAN M. J. and SHAPIRO H. N. (2010), *Fundamentals of Engineering Thermodynamics*, 7th ed., Wiley, Hoboken, NJ, USA.

[40] YAWS C. L. (2009), *Thermophysical Properties of Chemicals and Hydrocarbons*, William Andrew Publishing, Norwich, NY, USA.

[41] HEYWOOD J. B. (1988), *Internal Combustion Engine Fundamentals*, McGraw-Hill, New York, NY, USA.

[42] INTERNATIONAL ORGANIZATION FOR STANDARDIZATION (2010), *ISO 3744,2010 – Acoustics – Determination of sound power levels of noise sources using sound pressure – Engineering method in an essentially free field over a reflecting plane*, Geneva, Switzerland.

[43] ROWE D. M. (2006), *Thermoelectrics Handbook: Macro to Nano*, CRC Press, Boca Raton, FL, USA.